Effects of Environmental Factors on the Deformation of Bridges Supported by Piles and Geosynthetic Reinforced Soils

By

Maximiliano Garnier Villarreal

A dissertation submitted in partial fulfillment of

the requirements for the degree of

Doctor of Philosophy

(Geological Engineering)

at the

UNIVERSITY OF WISCONSIN-MADISON

2016

Date of final oral examination: 05/03/2016

The dissertation is approved by the following members of the Final Oral Committee:

Dante Fratta, Associate Professor, Geological Engineering
James Tinjum, Associate Professor, Geological Engineering
William Likos, Professor, Civil and Environmental Engineering
Michael Oliva, Emeritus Professor, Civil and Environmental Engineering
Carl Martin, Researcher, Engineering Physics
Brock Hedegaard, Assistant Professor, Civil and Environmental Engineering

Acknowledgements

I would like to thank my advisor, Dante Fratta, for giving me the opportunity to further my academic growth through this PhD, for all his insights, guidance, and help throughout my research. I would also like to thank my committee members Mike Oliva, Bill Likos, Jim Tinjum, Carl Martin, and Brock Hedegaard, for their input and help, and specially to Carl Martin for all his help with the numerical modeling aspect of my research.

Special thanks to Jeff Newgard, Joel Bautista, Ben Warren, David Wang, Paulo Florio, and Abdullah Alsabhan for their help and assistance during the field visits to the different sites. Also, thanks to Xiaodong 'Buff' Wang for his help in the field and in the lab. I am also very grateful to all the GLE/CEE friends who made this a fuller experience, and the staff for all their help.

Greatest of thanks to my family, my dad, my mom, my brother, my wife Bridget, and my daughter Hazel, for pushing me, supporting me, and giving me the motivation and strength to complete this big achievement.

Table of Contents

List of Tables

List of Figures

Abstract

This study evaluates the behavior of three bridges supported by piles and one by geosynthetic reinforced soils (GRS) by analyzing the effect of service and environmental loading conditions. The pile-supported bridges are located just northeast of Madison, Dane County, Wisconsin, and have different span lengths, pile lengths, and subsurface conditions, but share similar service and environmental loads. The GRS bridge is located south of Bloomer, Chippewa County, Wisconsin, and has different subsurface and environmental conditions with respect to the pile-supported bridges. The behavior of these bridges was analyzed by monitoring their vertical deformations over time and performing numerical analyses. The pile-supported bridges show general deformation trends similar to the temperature changes, contracting and expanding as temperature falls and rises. The GRS bridge is also affected by temperature changes but in a different way, as this bridge crosses a stream. As temperatures fall below the freezing point, the water present in the foundation soil and embankment freezes, causing the soils and structure to heave. As temperatures rise and the soil thaws, settlement occurs as the shear strength and stiffness in the soil decrease due to water content increase. Service loading conditions are found to have a lesser impact on the general behavior of the structures as the deformation versus time results do not show consistent settlement trends. The results indicate that the bridges are performing adequately but environmental loads should be considered while assessing the design and behavior of highway bridges.

CHAPTER 1: Introduction

1.1 Motivation

Transportation structures, highway bridges among these, must comply with serviceability and strength design specifications throughout their service life, with the serviceability criteria usually being more critical. Because of the importance of the deformation of bridges, monitoring of these over time is critical to evaluate their behavior, determine maintenance operations, and establish service life among other operations needed to manage transportation assets. Monitoring the behavior of foundation systems is an important part of this process. The type of foundation implemented at a bridge site have a big impact on the overall response of bridges. This is important because the response to different loads depends on the combination and response of soils and foundation systems. In this research the deformation over time and due to environmental factors for four bridges in the state of Wisconsin is investigated to determine their behavior.

1.2 Objectives and Hypothesis

The main objective of this research is to evaluate the deformation of bridges supported by different foundation systems such as piles and Geosynthetic Reinforced Soil – Integrated Bridge System (GRS-IBS) under traffic and environmental loads, and to determine if their deformations fall under the design specifications for highway bridges. More specific objectives are the monitoring of the bridges' deformations over time, to determine trends that would correlate with any of the considered loads, and the use of numerical models to generalize their response to different loading scenarios for traffic and environmental loads, and compare these with the monitoring results. To accomplish these objectives, monitoring of their movements over time,

and numerical modeling were performed on three pile-supported bridges north-east of Madison, Wisconsin, and one GRS-IBS bridge southwest of Bloomer and north of Howard in Chippewa County, Wisconsin.

The hypothesis explored in this thesis is that the effects of environmental and seasonal changes (loads), and associated phenomena (temperature, moisture content, etc.) can be more important on the deformation of bridges than just the effects of service (traffic) loads.

1.3 Thesis Organization

This thesis document is organized and presented in the form of draft manuscripts for journal publication submission, and some general chapters summarizing the motivation, objectives and results of this research. Chapter 1 provides a general introduction to the research motivation and objectives, and thesis organization. Chapter 2 is a manuscript focusing on the deformation (from field and numerical data) of three pile-supported bridges. Chapter 3 is a manuscript focusing on the field deformation results for the GRS-IBS bridge. Chapter 4 is a manuscript focusing on the numerical modeling of the GRS-IBS bridge under different traffic and environmental loads. Literature review is presented in the introduction of each of the manuscripts. Chapter 5 summarizes the findings and conclusions of this research. The last section of the thesis contains the appendices, presenting data and supplemental material that were not included in the main body of the document.

CHAPTER 2: Monitoring and Modeling of Deep Foundation Bridges Under Different Subsurface Conditions and Temperature Changes

Maximiliano Garnier-Villarreal[1]; and Dante Fratta[1]

Abstract: This study assesses the performance of three deep foundation bridges located along a 4-km stretch of US Highway 51, northeast of Madison, in south-central Wisconsin. While their design layout and subsurface conditions are different (i.e., different spans, pile lengths supporting the abutments and central columns, and thickness and type of supporting layers); they undergo similar service and environmental loads. Their performance was evaluated by surveying the deformation of several different elements in the bridges and assess their response by numerically modelling the action and responses. Results show that bridges are influenced by temperature changes as the different parts of the bridge structure contract and expand. The deformation monitoring was complemented with a finite element analysis, using ANSYS, to assess the behavior of the studied structures based on their different supporting element lengths, difference in supporting layers, and multiple temperature loading cases. Results from design traffic loads show that the system with longer piles and resting on the stiffer stratum experience less deformation than the system with shorter piles and less stiff stratum. Temperature loads results show a relationship between temperature changes and deformations experienced by the bridges. From the results not only a relationship between deformation and temperature can be observed, but also the measured deformations fall within the AASHTO requirements for serviceability limits.

[1] Geological Engineering. University of Wisconsin-Madison. Madison, WI 53706. USA. Emails: garniervilla@wisc.edu and fratta@wisc.edu.

Keywords: Deep foundations; Temperature change; Finite element analysis; Field monitoring; Deformation

2.1 Introduction

Foundation systems and structural systems experience deformations caused by dead and service loads (including time-dependent effects) and by environmental actions. These deformations include rotation, lateral displacements, and vertical settlements. The design of foundation systems for bridges in transportation structures must comply with serviceability and strength limit states requirements (AASHTO 2012). The AASHTO (2012)'s *LRFD Bridge Design Specifications* provide limits of deformations that must be fulfilled by the in service bridge (i.e., 10 cm for vertical displacements and 5 cm for horizontal displacements). The specifications also provide limits for load capacity based on the Load Resistance Factor Design (LRFD) approach. This design approach gives different weight factors to both acting forces and resistance parameters based on the likelihood of occurrence of the acting forces and on the reliability of the resistance parameters (Salgado 2006). While the reliability of the structural resistance parameters is relatively high, the characterization of mechanical parameters for the foundation soils is often suspect due to poor sampling (e.g., disturbed vs. undisturbed sample – Peck et al. 1974; Rogers 2006), testing protocols (e.g., Standard Penetration Test – Rogers 2006; Mahmoud 2013), data interpretation (e.g., cohesive soils – Santamarina 1997; Schofield 1998), and model of behavior (e.g., small vs. large strain behavior; elastic vs. plastic behavior – Cho et al. 2006; Diaz-Rodriguez et al. 2009). Furthermore, there are few systematic measurements of performance after the structure is complete.

Movements of foundation systems have been monitored and studied by different engineers and researchers. Moulton and Kula (1980) and Moulton et al. (1985) studied the movements of over 300 bridges in 39 different states and the District of Columbia (among these states were Connecticut, Idaho, Indiana, Iowa, Kansas, Maine, Michigan, Minnesota, Missouri, New Jersey, New York, North Dakota, Ohio, Oregon, South Carolina, Utah, Virginia, Washington, Wisconsin, West Virginia and Wyoming). They found that no matter the type of foundation (shallow or deep) movements occur. Shallow foundations tend to experience larger movements than deep foundations, and in general larger deformations happened when the foundation soil comprised mostly of fine-grained materials; the same deformation pattern has been described by other researchers, as follow.

Settlements of shallow foundations can range between less than 1 cm to up to 100 cm in some extreme cases with highly compressible soils (i.e. deltaic fine-grained deposits, peat deposits, and silt and clay foundation soils) with high water content and shallow water tables (< 1 m) (Bauer and Felio 1985; Bertok 1987; Felio and Bauer 1994; Karim et al. 2004; Anderson and LaFronz 2007; Jilin et al. 2007; Tarawneh et al. 2013). Settlement of deep foundations has been reported to be typically less than 3 cm, with the larger deformations occurring when shallow water table and fine-grained soils are present, as in the case of bridges crossing rivers or streams (Aziz and Ma 2012; Chen et al. 2011; Ma et al. 2014; Xue et al. 2011). Moreover, even though bridge abutments might be resting over deep foundations the approach embankments rest over compressible layers and the settlement of the approach embankment can resemble those of shallow foundations (Lin and Wong 1999; Robison and Luna 2004; Sallam and Jammal 2010). In the case of deep foundation systems, settlements are considered to be negligible if the piling system lies over a very dense soil or rock (end bearing pile), but if the piles transmit the loads

mainly through skin friction, minor settlements (< 2.54 cm) are expected to occur (Helwany et al. 2007). Elastic settlement estimations for both end bearing and frictional piles have been proposed by Poulos and Davis (1980) and Poulos (1989) based on factors such as stiffness of the foundation soil, length, diameter and stiffness of the piles.

Environmental loads and conditions (e.g., temperature, water table fluctuation, freezing and thawing, precipitation, etc.) also have an effect on the behavior of foundations and structures they support. In the case of concrete structures these can experience shrinkage and creep during the early stages of their service life (Mehta and Monteiro 2006). Li et al. (2013) found from an experimental program on clay specimens that larger water contents result in larger cumulative deformations under low-level repeated cyclic loading. Moreover, seasonal changes (precipitation, temperature) can affect the shear modulus of the soil (decreasing it as the water content increases), thus affecting deformations in foundation soils, even under constant loads (Kim et al. 2003).

Michal and Urban (2015) found that bridges deform as temperature changes but these deformations have a time delay with respect to the ambient temperature of between 5 to 8 hours. This time delay is required to allow for the heat to diffuse into the foundation soil and structure. Similar observations were made by Cao et al. (2010) who found delays between 5 and 6 hours for the deformation on a bridge in the inner gulf in south China to follow changes in air temperature. Thermal cracking in flexible pavements and concrete surfaces can be another effect of temperature changes, which will happen as the surface expands and contracts due to temperature changes over time (Helwany et al. 2007).

Lateral movements of the abutments are also affected by temperature changes, and in some cases these changes can have a larger effect than just the action of active earth pressures (Lawver

et al. 2000). During the warmer months of the year the lateral displacement of the abutment walls tends to be outwards (away from the backfill), while during the colder seasons the lateral displacement tends to be inwards (towards the backfill). Reported values range from 1.3 cm for expansion to -1.5 cm for contraction. These results are related to wall height, and bridge length, as all the abutments are supported by pile elements. The heights of the reported walls range between 1.8 m to 5.8 m, while their lengths range between 19 to 128 m, with the highest walls and longer bridges, usually, experiencing the largest movements (Lawver et al. 2000; DeJong et al. 2004; Civjan et al. 2004; Shoukry et al. 2008; Davids et al. 2010; Ooi et al. 2010; Kim and Laman 2012; Civjan et al. 2013; Razmi et al. 2014; Huntley and Valsangkar 2013). No studies have been found about the effect of freezing and water expansion on lateral displacements of abutment walls, although these displacements should be expected to be significant.

Moulton et al. (1985) studied tolerable movements under serviceability considerations of highway bridges. These researchers suggested that distortions (settlement over span length) smaller than 0.004 radians (1/250) are considered acceptable. Differential movements occur between different parts and structural elements of a bridge (i.e., deck and approach), and when differential movements reach values of 1.3 cm to 2.5 cm it becomes noticeable, raising concerns about the condition of the system (Wahls 1990; Long et al. 1998). According to AASHTO (2012), rideability and safety should also be taken in consideration when determining the serviceability of a structure, as it has been found to cause discomforts to riders and to create costly maintenance operations for Departments of Transportation (DOTs – Briaud et al. 1997).

Wahls (1990), Long et al. (1998), and White et al. (2007) recapped some of the major causes for differential settlement at the deck and road approach as follows: poor compaction of backfill, erosion of backfill material, poor drainage management in backfill, creep, consolidation of

foundation soil, and poor construction practices. Long et al. (2007) also indicated that embankment heights can be a factor on the development of differential settlement. Taller embankments (i.e., more than 8 m in height) yield greater overburden pressures and are more prone to settlements than shorter embankments (i.e., less than 3 m in height).

The objective of this study is to evaluate the behavior of pile-supported transportation structures by studying their response to design traffic loads and environmental loads. To accomplish this, monitoring of their vertical movements over time, and finite element analysis were performed on three different bridges north-east of Madison, Wisconsin, with the three bridges having differences in their span length, pile lengths, subsurface conditions while they undergo similar service and environmental loads.

2.2 Studied Bridges and Monitoring Approach

2.2.1 Bridges description

The studied bridges are located on United States Highway (USH) 51, northeast of Madison in Dane County, Wisconsin (Figure 2.1). Pictures of the finished bridges are shown in Figure 2.2. The north bound bridges were built over Bear Tree Road, Windsor Road, and Vinburn Road. The bridges over Bear Tree and Windsor roads were opened to traffic on June 23rd, 2013, while the bridge over Vinburn road was opened to traffic on August 29th, 2014. Concrete girders were used for all bridges.

The abutments of the bridge over Bear Tree Road are supported by H-piles 4.6 m long. The deck (superstructure) is 32.5 m long by 13.5 m wide. The subsurface exploration for this bridge (Figure 2.3) shows predominantly sandstone and gravel with a single clay layer 1.3 m thick under the north abutment.

The south and north abutments of the bridge over Windsor Road are supported by H-piles driven to 9.1 m and 12.2 m, respectively. The deck is 49.1 m long by 13.3 m wide. The bridge is supported by abutments at the two ends and a set of three columns at mid-span. The columns are supported by H-piles 4.6 m long under a square pile cap of 2.74 m per side and 0.76 m thick. The columns are 5.9 m apart from each other (center-to-center), and are 4.8 m tall. Subsurface exploration for this bridge (Figure 2.4) shows the presence of a clay/sandy clay layer at depths between 0.6 m and 2.1 m, with the rest of the soil profile corresponding to sand, gravel and sandstone. All of the piles for this bridge are supported by the underlying sandstone layer.

The south and north abutments of the bridge over Vinburn Road are supported by H-piles 10.7 m and 7.6 m long respectively. The bridge deck is 34 m long by 13.3 m wide. Similar to the bridge over Bear Tree Road, the subsurface layers consist predominantly of sand and gravel, with sparse clay layers around 1 m thick (Figure 2.5).

The studied bridges are located in an area of Wisconsin that has experienced glaciation (Mickelson 1983), therefore the foundation soils in the area should be considered to be dense or overconsolidated. This observation agrees with the SPT values presented in the soil exploration studies and results by studies presented by Peck et al. (1974) and Terzaghi et al (1996), classifying the soils in the area as medium to dense.

2.2.2 Monitoring approach

Conventional surveying techniques were implemented to monitor the deformation of all the bridges over different driving seasons. Total station, prism, and reflecting surveying targets were used. The slope-distance, vertical and horizontal angles were measured using a total station. The accuracy of the instrument is given by (modified from GLM-Laser, 2015):

$$\delta = \pm(0.005\ m + 3 \cdot 10^{-6} \cdot D) \tag{2.1}$$

where D is the total station-prism horizontal distance.

The location and layout of the surveying points for the bridges are documented in Figure 2.6. The surveying points on the deck are approximately 0.5 m from the edge of the deck, and the middle one at the midpoints along each side of the deck bridge decks. The surveying points on the approaching road start 1.8 m from the edge of the deck, and are 5 m apart from each other. A bench mark was installed for each bridge to use as reference.

2.3 Field Monitoring of Deep Foundation Bridges

2.3.1 Bridge over Bear Tree Road

The results from the deformation monitoring are shown in Figure 2.7. The data summarize the vertical deformation of the abutment walls, which show a clear downward trend, with a maximum deformation of less than 1.6 cm. The results for the deck and road are shown in Appendix A.

A simple estimation of elastic settlement for a single friction (floating) pile, and assuming homogeneous conditions, can be performed (Poulos 1989):

$$s = \frac{P}{d \cdot E_S} I \qquad\qquad I = f(L, d, E_P, E_S) \tag{2.2}$$

where P is the applied load, d is the diameter of the pile, E_S is the soil's elastic modulus, and *I* is the settlement factor that depends on the length and diameter of the pile, the stiffness of the pile (E_P), and the stiffness of the soil.

Using a load of 160 kN (Davids et al. (2010) estimated that a single pile can carry up to 25% of a two truck load, with a total load of 640 kN), a length of 4.6 m, a diameter of 0.26 m

(approximate diameter of H-pile), a elastic modulus of the foundation soil ranging between 22-70 MPa (From average SPT values and correlations for sands from Kulhawy and Mayne (1990), and Bowles (1997)), and a pile with stiffness 1000 times greater than the stiffness of the foundation soil, the estimated settlement of a single pile range between 0.1 and 0.32 cm. This value appears to explain, in part, the measured deformation after the bridge was opened to traffic (~ 0.6 cm – Figure 2.7).

The wall deformations show that after the bridge was open to traffic the settlement became more noticeable (Figure 2.7), suggesting that for this bridge the traffic loads had an effect on the deformations after it was opened to traffic. As shown by Poulos and Davis (1980), Poulos (1989), and Li and Zhang (2009), under the same load shorter piles experience larger deformations than longer piles. Thus this bridge, as the one with the shortest piles of the three, would be more susceptible to deform under the same service loading conditions than other bridges supported by longer piles, as it is the case for the other two bridges in this stretch of USH 51. If the subsurface were only comprised of sand and gravel the settlement due to service loads would be expected to be immediate, but since there was about 5 months until the bridge reaches a steady settlement, it could be inferred that there might be small pockets or lenses of fine-grained material that consolidated over this period of time, as shown by the subsurface exploration data on the southeastern wall. Also, the presence of a clay layer would explain that the southern wall settlement is approximately 0.5 cm larger than the northern wall, if this layer were to be present not only at the location of the boring, and were to be more spread out through the site.

Thermal related loads are also considered to affect the behavior of the structure, as the deformation of the bridge emulates the temperature trend. Once the bridge reached a steady

settlement the temperature effects are not as predominant, but there is still some correlation between the temperature change and the deformations experienced by the bridge. As this bridge is supported by the shorter piles, the expansion and contraction of these due to temperature changes would be expected to be less than for longer piles as their volume is smaller than that of the longer piles, thus the lesser effect of temperature loads.

2.3.2 Bridge over Windsor Road

The results from the monitoring of the deformation of the abutment walls are shown in Figure 2.8 (The results for the deck and road are shown in Appendix A). The main difference for this bridge is that the piles reach the sandstone bedrock (Figure 2.4), which is a much stiffer material than the sand and gravel layers where the piles are supported under the other two bridges. The reported Young's modulus for sandstone lies between 10 and 58 GPa, with most of the reported values around 20 GPa (i.e., Chen 2007; Ko 2008; Walsri 2009; Fintland 2011; Hassanzadegan et al. 2012).

A similar estimation for the settlement can be performed for this bridge, using equation 2.3 from Poulos and Davis (1980):

$$s = \frac{P}{d \cdot E_s} I \qquad I_b = I_0 R_K R_b R_v \tag{2.3}$$

where P = axial load (kN), d = pile diameter (m), E_s = soil's Young's modulus (kPa), and I = settlement influence factor for an end-bearing pile (I_b), and depends on the factor for incompressible pile in a semi-infinite mass (I_0), pile's compressibility (R_K) Poisson's ratio (R_v), and stiffness of bearing layer (R_b). Using the same values from equation 2.2 for P, d, E_S and E_P, but pile lengths of 9 and 12 m and a Poisson's ratio of 0.3, the expected settlement would range between 0.03 and 0.08 cm.

This bridge does not show a downward trend as the one over Bear Tree Road (Figure 2.7) once it was open to traffic (Figure 2.8). The bridge shows a settlement of approximately 0.8 cm right after being open to traffic. After the initial deformation the bridge shows and up and down behavior that resembles the temperature record when compared to it. This behavior could be the response of the steel piles expanding and contracting, since they are resting in the sandstone they can not easily deform (expand or contract) at their base, thus their thermal deformation would tend to push or pull into and from the bottom of the abutment walls when expanding or contracting. Also, since the piles here are longer than at the other two bridges, their volumetric change would be more, thus requiring to accommodate more deformation.

2.3.3 Bridge over Vinburn Road

The results from monitoring the abutment walls are shown in Figure 2.9 (The results for the deck and road are shown in Appendix A). As the piles supporting this bridge are longer than the ones at the bridge over Bear Tree Road, and the foundation soils are similar in this this bridge to the foundation soils under the bridge over the Bear Tree Road, the expected settlement would be less. Using pile lengths of 7.6 m and 10.7 m in equation 2.2, the resulting settlement would range between 0.06 and 0.25 cm. When comparing the temperature record to the deformation results over time (Figure 2.9), the two records follow similar trends. These results show that long term deformation experienced by this bridge is mainly controlled by environmental loads, in particular by temperature changes; as these piles are longer their volumetric expansion would be more, resulting in larger deformations due to temperature loads.

For all these bridges temperature is considered the predominant environmental factor, as deformation does not follow precipitation trends. Figure 2.10 shows the vertical deformation for the NE surveying point for each of the three bridges versus rain, cumulative amount over the past

month, previous to the field visit. This would indicate that the effects of matric suction and water table changes are less than like the effects of temperature.

2.4 Pile Modelling and Finite Element Analysis Validation

An elastic validation was implemented to validate the use of the general purpose finite element package ANSYS and to confirm the proper modeling of pile elements to be used in the finite element analysis of the bridges on Highway 51. The validation was carried out using the ANSYS, using the analytical solution from Poulos and Davis (1980) to compare with our results. Equation 2.4 is used to calculate the settlement of a single pile, as shown below:

$$s = \frac{P}{d \cdot E_s} I \qquad I_f = I_0 R_K R_h R_v \qquad I_b = I_0 R_K R_b R_v \tag{2.4}$$

where P = axial load (kN), d = pile diameter (m), E_s = soil's Young's modulus (kPa), and I = settlement influence factor for either a floating pile (I_f) or an end-bearing pile (I_b), and depends on the factor for incompressible pile in a semi-infinite mass (I_0), pile's compressibility (R_K), depth of the layer (R_h), Poisson's ratio (R_v), and stiffness of bearing layer (R_b).

Different cases where analyzed for a floating pile, using different loads (64-320 kN – Figure 2.11) and different diameters (0.2-2.5 m – Figure 2.12). The values used for the analysis were P = 320 kN (approximate truck load, when changing diameter), length of 5 m, diameter of 0.2 m (when changing load), pile stiffness of 60 GPa, and soil stiffness of 60 MPa (typical value for sands and gravels).

The approach that yielded the best results to model the pile-soil interaction was to have the pile and soil share nodes at their interface (Results shown in Figures 2.11 and 2.12), as this approach resulted in the best agreement with the proposed solution by Poulos and Davis (1980).

The use of contact elements between the pile and soil was analyzed but yielded larger settlement values than the expected ones and than the node-sharing approach.

2.5 Deep Foundation Bridges Modeling

Three bridges with different designs and subsurface conditions were modeled and analyzed using the finite element package ANSYS. The finite element model was a 3D linear elastic transient model, as the properties of the materials are not well known (estimated from correlations or general known values). The model consists of 8-node brick elements with 3 translational degrees of freedom (dof) for the regular shape solid bodies, 10-node brick elements with 3 translational dof for the irregular shape solid bodies, 2-node beam elements with 6 dof (rotational and translational) for the girders, and contact elements to model the interaction between the different parts and elements. A section was defined for the girders to match their geometry and take full advantage of the beam elements.

The deck was modeled with the 8-node brick elements and a bonded contact was used between the deck and girders. A bonded contact was also used between the top of the piles and bottom of the abutment walls. The rest of the contacts in the model were frictional with a friction coefficient μ=0.5. The piles were modeled as cylinder elements with a diameter of 0.26 m (i.e., the approximate equivalent diameter of the H-pile in the bridges on USH 51). The interaction between pile and soil was modeled with the pile and soil sharing nodes at their interface, as this was the approach that yielded the best results during the pile modeling validation analysis.

All of the models' base was put at 14 m below the abutment wall (~ 4 m in height), this was done so all the models would have similar geometries, with the difference between them being

the length and width of the deck, the length of the piles, and the thickness of the sand and gravel, and sandstone layers.

The foundation soils and bedrock were constrained at their bottom on the vertical direction, and normal to its sides on the lateral directions; for the beam elements their rotation was constrained (rotation equals zero) on the direction perpendicular to the abutment walls. The foundation soils and bedrock are modeled as homogeneous, as the subsurface data are very localized and the presence of fine-grained soil layers could be in the form of lenses and not extended layers. The loads for service and temperature are described in their respective sections. The material parameters used in the models are shown in Table 2.1.

One of the major differences between the three bridges is the pile length used under their abutment walls, and also that the foundation piles in the bridge over Windsor Road are resting on sandstone while the other two bridges are being supported by floating piles in sand and gravel. The bridges are subjected to service (i.e., traffic) loads and environmental loads (only temperature effects are considered), to study the response of the foundation and structures of the bridges to different types of loads.

2.5.1 Service (Traffic) loading

An overall uniform load of ~10^3 kN (250 kip) was applied uniformly to the nodes on the bridge deck as this corresponds to the largest design load (Wisconsin Standard Permit Vehicle) according to WisDOT's bridge manual (WisDOT 2015). This load was the same for all three bridges, resulting in pressures of 2.52 kPa, 1.68 kPa, and 2.34 kPa, for the bridges over Bear Tree, Windsor, and Vinburn roads respectively. The results from applying the service (traffic) load to the bridge's deck are shown in Table 2.2, showing the vertical deformation at the NE abutment wall, yielding larger deformation values for the bridge with shorter piles and smaller

deformation values for the bridge with longer piles and supported by a stiffer layer, showing the relationship between pile length and deformation (Numerical model results are shown in Appendix B).

2.5.2 Thermal validation

A transient heat transfer model validation was performed to confirm accurate modeling of heat transfer problems. The validation corresponded in simulating the result from example 2.11 from Kreith et al. (2011). The problem asks to find the depth at which the temperature will be 0 °C, when the soil has a uniform temperature of 20 °C and the ground surface has been exposed to a temperature of -15 °C for 60 days. The thermal properties of the soil are: ρ=2050 kg/m3, k=0.52 W/m-K, and c=1840 J/kg-K. The solution by Kreith et al. (2011) for this example is given as 0.68 m below the ground surface.

To model this problem a 2D transient heat transfer model was implemented using ANSYS, with the given thermal properties, and employing a 4-node thermal plane element with temperature as its dof. The step size used was 1 day (86400 s), with a total duration of 60 days (5184000 s). As mentioned in the example, a uniform temperature of 20 °C was applied to the entire soil area, and a temperature boundary condition of -15 °C was applied to the top of the model. The result of this analysis is shown in Figure 2.13, where the arrow on the right points to the 0 °C isotherm at a depth of 0.68 m, same as the analytical solution by Kreith et al. (2011), thus showing the ability of ANSYS to solve for this type of problem.

2.5.3 Temperature loading

For the temperature loads two identical models were used for each of the bridges: first, one transient heat transfer analysis and second, a structural analysis. The transient heat transfer

analysis' results (heat distribution) were used as input for the structural analysis. The temperature over time for each node is determined by the heat transfer analysis, this nodal temperature is then assigned to the corresponding node for the structural analysis as a loading condition. To account for the transient thermal effects density, specific heat and thermal conductivity were used as material properties. For the models a time step of one day (86400 s) was used. For all of these bridges an initial uniform temperature of 9.7 °C was applied to the entire model, representing a time when the air temperature and soil temperature were the same. This value (9.7 °C) represents an average ground temperature at approximately 18 m below the surface (bottom of the models) for this area of Wisconsin (WGNHS 2016). The thermal properties used in the analysis are shown in Table 2.3. Temperatures, based on times when field measurements were taken, were then used as boundary conditions for the outer areas of the model (top of deck, girders, abutment walls, top of road) to simulate the effect of air temperature changes over time, ranging from -13 °C to 31 °C.

To reduce computer time just a few points from all the visits to the field were chosen to be modeled to obtain a general idea of the behavior of the structures at different temperatures. A total of 12 temperatures (approximately one month apart each) were used to represent an annual thermal cycle of the temperatures experienced by the structures. Figures 2.14 to 2.16 show the comparison between the vertical field deformations and the results from the finite element model as function of temperature for the NE walls for each of the three bridges (The results for the deck and road are summarized in Appendix B). From these results it can be interpreted that the deformations experienced by the bridges are related to changes in temperature, as the field and model deformations have similar trends. Average day temperatures (from a nearby weather station – Madison Airport) were used for the comparison. It is important to consider the

limitations of using average day temperatures. Cao et al. (2010) and Michal and Urban (2015) showed in their research, that the deformation due to temperature changes usually manifests itself with a delay between 5 to 8 hours from the maximum or minimum temperatures, thus the field measurements presented here may or may not be capturing this behavior. The intent of the modeling presented in this paper is to show seasonal variations in the deformation and not hourly or even daily changes. The different scales in the measurements added noise to the modeling results and to the scatter behavior of the field measurements.

2.6 Modeling and Response Discussions

Foundation Soils. As shown by the figures comparing the field deformations versus the model deformations (Figures 2.14 to 2.16), the general trend of these deformations seems to agree in part with the effects of temperature changes. The up and won behavior of the modeled results is attributed to the transient effects of temperature changing over time, transitioning from hot to cold and from cold to hot. The field deformations when plotted against time (Figures 2.7 to 2.9) do not seem to follow the seasonal temperature cycle, with Figure 2.7 showing little seasonal variation and Figures 2.8 and 2.9 showing a higher frequency in the displacements as compared to the temperatures. This difference in phase between the two data sets could be a factor of measurement error for some of the measurements, other factors rather than just temperature are affecting the behavior of the structures, and also the lack of measurements during several periods of time do not help in the comparison as more evenly distributed measurements would show a clearer pattern.

The deformation of structures can be affected by other factors, including environmental conditions. Concrete structures will experience shrinkage due to loss of water and creep due to

constant applied stress (Mehta and Monteiro 2006). Other factors such as changes in moisture content in the soil and cyclic deformations cause changes in the shear strength and stiffness of the foundation soils (Kim et al. 2003; Okur and Ansal 2007), which will have an effect on the deformation the soil experiences. Also, soil heterogeneity and the presence of fine-grained soil layers can cause the system to deform non-uniformly, as fine-grained soils are more susceptible to changes in water content (Mitchell and Soga 20015; Li et al. 2013), and can also give place to larger and differential deformations when present in the foundation soils (Moulton and Kula 1980; Moulton et al. 1985; Wahls 1990; Long et al. 1998; White et al. 2007).

The presence and/or fluctuation of moisture at the field sites is not well characterized, making difficult to take this in consideration when analyzing the field results. Both of the factors mentioned above are difficult to account for in the finite element models. However, these effects of moisture decrease with increasing confinement. This is because strength and stiffness in soils is controlled by both net stresses (caused by self-weight) and matric suction (caused by moisture); as depth increases net stresses increase because the weight of the soil column increases and matric suction decreases (as the moisture of the soil decreases).

Given the very localized subsurface explorations and uncertainty on how the layers extend laterally, the soils in the models were idealized as homogeneous. This generalization and the uncertainty on the properties of the soils could be a reason for the discrepancy between the finite element results and the field measurements.

Surveying factors. There are several factors in the field that can have an effect on the surveying measurements. The assumption that the reference points used in the field is not moving might not be completely accurate, as these can also be experiencing slight deformations due to changes in temperature and moisture, thus carrying an error into the field measurements or

exaggerating the measurements. Also, as pointed by Kavanagh (2009) as the vertical angle between the surveying equipment and the target increases a slight error in the measurement can be introduced. As the vertical angle between the total station and the different surveying points was not the same (ranging between 4-40 degrees) a slight error could be affecting the measured deformations. Beshr and Elnaga (2011) and Elhassan and Ali (2011) described how the accuracy of the measurements depends on the distance between the equipment and the target, decreasing with distance, as shown by equation 2.1. Beshr and Elnaga (2011) also studied the effects of surveying towards (front) and against (back) the sun, battery capacity, inclination of target, and reflecting surface. They found that surveying against the sun results in more accurate readings; as the battery capacity decreases the accuracy of measurements decreases; the inclination of the target surface decreases the accuracy. All of the factors mentioned here can add up to errors in the field measurements, consequently these factors could be affecting the measurements presented in this study.

2.7 Conclusions

From the field monitoring and numerical modelling of the deep foundation bridges on H51 the following conclusions can be made:

- The bridge over Bear Tree Road appears to be the one affected by both traffic loads and temperature loads, as this bridge is being supported by the shortest piles, giving place to larger deformations due to service loads.
- All three surveyed bridges show a deformation pattern that can be linked or explained by the changes in temperature between measurements, as one of the major factors affecting the behavior of the bridges.

- The pile length is a factor affecting the deformation due to temperature changes, as the longer piles experience a larger volumetric change for the same temperature change than shorter piles.
- Factors such as moisture changes and presence of fine-grained soils could explain deformations that are not fully explained by the temperature changes. The difficulty to account for both of these in the field measurements and the finite element model results can be a reason for the behavior of some of the recorded deformations. Other factors like concrete creep and shrinkage could also account for part of the deformations.
- The assumption that the reference point is static and not affected over time might not be realistic, this combined with other several factors can add up to errors while taking field measurements, thus affecting the results from the surveying campaign.

Acknowledgments

We would like to thank Mr. Jeff Newgard, Mr. Joel Bautista, Mr. Ben Warren, Mr. David Wang, Mr. Paulo Florio, and Mr. Abdullah Alsabhan for helping with field surveying, Mr. Xiaodong Wang (Buff) for helping with the installation of the equipment, and Carl Martin (Engineering Physics – UW-Madison) for his help on the numerical modeling aspects of this research. The Wisconsin Department of Transportation through the Wisconsin Highway Research Program provided funding for this project.

References

AASHTO (2012). *AASHTO LRDF Bridge Design Specifications*, American Association of State Highway and Transportation Officials, Washington, D. C.

Anderson, S.A., and LaFronz, N.J. (2007). "Rockfill embankment settlement - Sugarloaf

Mountain Bridge abutment and Hoover Dam Bypass (US-93)." *Transport. Res. Rec.*, 2016, 3-12.

Aziz, H.Y., and Ma, J.-l. (2012). "Deep Foundation Numerical Analysis Using Modified Compression Modulus." *Open Civ. Eng. J.*, 65-86.

Bauer, G.E., and Felio, G.Y. "Movements of a Bridge Abutment." *Proc., Ground Movements and Structures, Proceedings of the 3rd International Conference.*, Pentech Press, 581-593.

Bertok, J. (1987). "Settlement of embankments and structures at Vancouver International Airport." *Can. Geotech. J.*, 21(1), 72-80.

Beshr, A.A.A., and Abo Elnaga, I.M. (2011). "Investigating the accuracy of digital levels and reflectorless total stations for purposes of geodetic engineering." *Alexandria Eng. J.*, 50(4), 399-405.

Bowles, J. (1997). *Foundation Analysis and Design*, McGraw-Hill Companies, Inc., New York.

Briaud, J.-L., Maher, S.F., and James, R.W. (1997). "Bump at the end of the bridge." *Civ. Eng.*, 67(5), 68-69.

Cao, Y., Yim, J., Zhao, Y., and Wang, M.L. (2010). "Temperature effects on cable stayed bridge using health monitoring system: a case study." *Struct. Health Monit.*, 10(5), 523-537.

Chang, S.P., Kim, S., Lee, J., and Bae, I. (2008). "Health monitoring system of a self-anchored suspension bridge (planning, design and installation/operation)." *Struct. Infrastruct. Eng.*, 4(3), 193-205.

Chen, Y.-p. (2007). "Strength and elastic properties of sandstone under different testing conditions." *J. Cent. South Univ. T.*, 14(2), 210-215.

Chen, Z.-J., Zhang, N.-N., and Zhang, X.-W. (2011). "Settlement monitoring system of pile-group foundation." *J. Cent. South Univ.*, 18(6), 2122-2130.

Cho, G.C., Dodds, J., and Santamarina, J.C. (2006). "Particle shape effects on packing density, stiffness, and strength: Natural and crushed sands." *J. Geotech. Geoenviron. Eng.*, 132(5), 591-602.

Civjan, S.A., Breña, S.F., Butler, D.A., and Crovo, D.S. (2004). "Field monitoring of integral abutment bridge in Massachusetts." *Transport. Res. Rec.*, 1892, 160-169.

Civjan, S.A., Kalayci, E., Quinn, B.H., Breña, S.F., and Allen, C.A. (2013). "Observed integral abutment bridge substructure response." *Eng. Struct.*, 56, 1177-1191.

Davids, W.G., Sandford, T., Ashley, S., DeLano, J., and Lyons, C. (2010). "Field-Measured Response of an Integral Abutment Bridge with Short Steel H-Piles." *J. Bridge Eng.*, 15(1), 32-43.

DeJong, J., Howey, D.S., Civjan, S.A., Brena, S.F., Butler, D.S., Crovo, D.S., Hourani, N., and Connors, P. (2004). *Influence of daily and annual thermal variations on integral abutment bridge performance*, Amer Soc Civil Engineers, New York.

Diaz-Rodriguez, J.A., Martinez-Vasquez, J., and Santamarina, J.C. (2009). "Strain-Rate Effects in Mexico City Soil." *J. Geotech. Geoenviron. Eng.*, 135(2), 300-305.

Elhassan, I.M., and Ali, A.S. (2011). "Comparative study of accuracy in distance measurement using: Optical and digital levels." *J. King Saud Univ. Eng. Sci.*, 23(1), 15-19.

Felio, G.Y., and Bauer, G.E. "Settlement and deformation response of a bridge footing on a sloped fill." *Proc., Proceedings of the Conference on Vertical and Horizontal Deformations of Foundations and Embankments*, Publ by ASCE, 1071-1081.

Fintland, T.W. (2011). "Measurements of Young's Modulus on Rock Samples at Small Amplitude and Low Frequency." M.Sc. Thesis, Norwegian University of Science and Technology.

GLM-Laser (2015). "The Total Station SET 4 made by Sokkisha." <http://www.glm-laser.com/glm/452-1-Sokkisha-SET-4.html>. (Jan. 5, 2016).

Hassanzadegan, A., Bloecher, G., Zimmermann, G., and Milsch, H. (2012). "Thermoporoelastic properties of Flechtinger sandstone." *Int. J. Rock Mech. Min. Sci.*, 49, 94-104.

Helwany, S.M.B., Koutnik, T.E., and Ghorbanpoor, A. (2007). "Evaluation Bridge Approach Settlement Mitigation Methods." University of Wisconsin-Milwaukee, Milwaukee, WI, 280.

Hirai, H., Yanagisawa, E., and Satake, M. (1984). "Elastic-Plastic Constitutive Models For The Behavior Of Sand." *Proc. Japan Soc. Civ. Engineers*, 1984(343), 255-265.

Huntley, S.A., and Valsangkar, A.J. (2013). "Field monitoring of earth pressures on integral bridge abutments." *Can. Geotech. J.*, 50(8), 841-857.

Jilin, Q., Yu, S., Jianming, Z., and Zhi, W. (2007). "Settlement of embankments in permafrost regions in the Qinghai-Tibet Plateau." *Norwegian J. Geog.*, 61(2), 49-55.

Karim, U.F.A., van Meekeren, H., and Feenstra, R. (2004). "Settlement of a bridge embankment on soft soils." *Proc. Inst. Civil Eng.-Geotech. Eng.*, 157(1), 9-12.

Kavanagh, B. (2009). Surveying with Construction Applications, Prentice Hall.

Kim, D.-S., Seo, W.-S., and Kim, M.-J. (2003). "Deformations characteristics of soils with variations of capillary pressure and water content." *Soils Found.*, 43(4), 71-79.

Kim, W., and Laman, J.A. (2012). "Seven-Year Field Monitoring of Four Integral Abutment Bridges." *J. Perform. Constr. Facil.*, 26(1), 54-64.

Ko, T.Y. (2008). "Subcritical crack growth under mode I, II, and III loading for Coconino Sandstone." Ph.D. Dissertation, University of Arizona.

Kreith, F., Manglik, R.M., and Bohn, M.S. (2011). *Principles of Heat Transfer*, Cengage Learning.

Kulhawy, F.H., and Mayne, P.W. (1990). *Manual on Estimating Soil Properties For Foundation Design*, Electric Power Research Institute, Palo Alto, California.

Lawver, A., French, C., and Shield, C.K. (2000). "Field performance of integral abutment bridge." *Transport. Res. Rec.*, 1740, 108-117.

Li, F.-R., and Zhang, Z. (2009). "Numerical analysis of settlement of bridge pile group foundation." *Electron. J. Geotech. Eng.*, 14 M(2009), 1-9.

Li, Q.-l., Ling, X.-z., Wang, L.-n., Zhang, F., Wang, J.-h., and Xu, P.-j. (2013). "Accumulative strain of clays in cold region under long-term low-level repeated cyclic loading: Experimental evidence and accumulation model." *Cold Reg. Sci. Technol.*, 94, 45-52.

Lin, K.Q., and Wong, I.H. (1999). "Use of deep cement mixing to reduce settlements at bridge approaches." *J. Geotech. Geoenviron. Eng.*, 125(4), 309-320.

Long, J.H., Olson, S.M., Stark, T.D., and Samara, E.A. (1998). "Differential Movement at Embankment–Bridge Structure Interface in Illinois." *Transport. Res. Rec.*, 1633, 53-60.

Ma, J.-l., Aziz, H.Y., Su, C.-h., and Shi, C. (2014). "Settlement prediction and behaviour of pile foundations in deep clayey soil deposits." *J. Cent. South Univ. T.*, 21(4), 1554-1564.

Mahmoud, M.A.A.N. (2013). "Reliability of using standard penetration test (SPT) in predicting properties of silty clay with sand soil." *Int. J. Civ. Struc. Eng.*, 3(3), 545-556.

Mamlouk, M.S., Witczak, M.W., Kaloush, K.E., and Hasan, N. (2005). "Determination of thermal properties of asphalt mixtures." *J. Test. Eval.*, 33(2), 118-126.

Mehta, P.K., and Monteiro, P.J.M. (2006). *Concrete: Microstructure, Properties, and Materials*, McGraw-Hill, New York.

Michal, O., and Urban, R. (2015). "Temperature effects on the bridge structure during the all-day monitoring." *Geoinformatics FCE CTU*, 14(1), 79.

Mickelson, D.M. (1983). "A guide to the glacial landscapes of Dane County, Wisconsin." Wisconsin Geological and Natural History Survey, Madison, Wisconsin.

Mitchell, J.K., and Soga, K. (2005). *Fundamentals of Soil Behavior*, John Wiley & Sons, Inc., Hoboken, New Jersey.

Moulton, L.K., GangaRao, H.V.S., and Halverson, G.T. (1985). "Tolerable movement criteria for highway bridges." *Report No. FHWA/RD-85/107*, Federal Highway Administration, U.S. Department of Transportation, Washington, DC.

Moulton, L.K., and Kula, J.R. (1980). "Bridge Movements and Their Effects." *Public Roads*, 44(2), 62-75.

Okur, D.V., and Ansal, A. (2007). "Stiffness degradation of natural fine grained soils during cyclic loading." *Soil Dyn. Earthq. Eng.*, 27(9), 843-854.

Ooi, P.S.K., Lin, X.B., and Hamada, H.S. (2010). "Field Behavior of an Integral Abutment Bridge Supported on Drilled Shafts." *J. Bridge Eng.*, 15(1), 4-18.

Peck, R.B., Hanson, W.E., and Thornburn, T.H. (1974). *Foundation Engineering*, Wiley & Sons, New York.

Poulos, H.G. (1989). "Pile behavior -- theory and application." *Geotechnique*, 39(3), 365-415.

Poulos, H.G., and Davis, E.H. (1980). *Pile foundation analysis and design*, Wiley, New York.

Razmi, J., Ladani, L., and Aggour, S.M. (2014). "Finite element simulation of pile behaviour under thermo-mechanical loading in integral abutment bridges." *Struct. Infrastruct. Eng.*, 10(5), 643-653.

Robison, J.L., and Luna, R. (2004). "Deformation analysis of modeling of missouri bridge approach embankments." *Geotechnical Engineering for Transportation Projects: Proceedings of Geo-Trans 2004*, American Society of Civil Engineers, Geotechnical

Engineering for Transportation Projects: Proceedings of Geo-Trans 2004, 2020-2027.

Rogers, J.D. (2006). "Subsurface Exploration Using the Standard Penetration Test and the Cone Penetrometer Test." *Env. Eng. Geosc.*, XII(2), 161–179.

Salgado, R. (2006). *The Engineering of Foundations*, McGraw-Hill Education.

Sallam, A.M., and Jammal, S.E. (2010). "Case History: Finite Element Analysis of Time Dependent Settlement of Lake Jessup Bridge Embankment in Central Florida." *GeoFlorida 2010: Advances in Analysis, Modeling and Design Conference*, American Society of Civil Engineers (ASCE), West Palm Beach, FL, United states, 2182-2191.

Santamarina, J.C. (1997). "Cohesive Soil: A Dangerous Oxymoron." *Electron. J. Geotech. Eng. - Magazine*, <https://egel.kaust.edu.sa/Documents/Papers/Santamarina_1997nn.pdf>. (Feb. 19, 2016).

Schofield, A.N. (1998). "Mohr Coulomb error correction." *Ground Eng.*, 31(8), 30-32.

Shoukry, S.N., William, G.W., and Riad, M.Y. "Response of an Integral Abutment Bridge to Temperature Variations." *Proc., Structures Congress 2008: Crossing the Borders*, American Society of Civil Engineers, 1801 Alexander Graham Bell Drive, Reston, VA 20191-4400, United States.

Skinner, B.J. (1966). "Thermal expansion." *Handbook of Physical Constants*, S. P. J. Clark, ed., Geological Society of America, 75-96.

Tarawneh, B., Masada, T., and Sargand, S. (2013). "Estimated and Measured Settlements of Shallow Foundation Supporting Bridge Substructure." *Jordan J. Civ. Eng.*, 7(2), 224-235.

Tarefder, R.A., Zaman, A.M., and Uddin, W. (2010). "Determining hardness and elastic modulus of asphalt by nanoindentation." *Int. J. Geomech.*, 10(3), 106-116.

Terzaghi, K., Peck, R.B., and Mesri, G. (1996). *Soil Mechanics In Engineering Practice*, John

Wiley & Sons, New York, NY.

Thomas, L.C. (1992). *Heat Transfer*, Prentice Hall, New Jersey.

Wahls, H.E. (1990). "NCHRP Synthesis of Highway Practice 159: Design and Construction of Bridge Approaches." National Cooperative Highway Research Program, Transportation Research Board, National Research Council, Washington, D.C.

Walsri, C. (2009). "Compressive Strength of Sandstone Under True Triaxial Stress States." M.Sc. Thesis, Suranaree University of Technology.

WGNHS (2016). "Geophysical logs available by request from the Wisconsin Geological and Natural History Survey data collections." WGNHS (Wisconsin Geological and Natural History Survey), Madison, WI.

White, D.J., Mekkawy, M.M., Sritharan, S., and Suleiman, M.T. (2007). "“Underlying” Causes for Settlement of Bridge Approach Pavement Systems." *J. Perform. Constr. Facil.*, 21(4), 273-282.

Xue, F., Ma, J., and Yan, L. (2011). "Three-dimensional FEM Analysis of Bridge Pile Group Settlement in Soft Soils." 2011 GeoHunan International Conference - Advances in Pile Foundations, Geosynthetics, Geoinvestigations, and Foundation Failure Analysis and Repairs, American Society of Civil Engineers (ASCE), Hunan, China, 135-143.

Tables

Table 2.1. Material properties used for the service (traffic) loading models.

Section	Young's modulus [MPa]	Poisson's ratio
Road (Asphalt) [1]	$2 \cdot 10^3$	0.2
Piles (Steel) [2]	$200 \cdot 10^3$	0.3
Walls, deck and girders (Concrete) [2]	$25 \cdot 10^3$	0.2
Backfill [3]	70	0.3
Foundation soil (Sand and gravel) [4]	60	0.3
Bedrock (Sandstone) [5]	$20 \cdot 10^3$	0.3

[1] From Tarefder et al. (2010)

[2] From Razmi et al (2014)

[3] Value for dense sands from Bowles (1997)

[4] From SPT correlations and typical Poisson's ratio for soils

[5] From Chen (2007), Ko (2008), Walsri (2009), Fintland (2011), and Hassanzadegan et al. (2012)

Table 2.2. Summary of vertical deformations from service (traffic) loads.

Bridge	Subsurface conditions	Pile length [m]	Vertical deformation on NE wall [cm]
Bear Tree	Sand and gravel	4.6	-0.91
Windsor	Sand and gravel, and sandstone	9 to 12	-0.57
Vinburn	Sand and gravel	7.6 to 10.7	-0.86

Table 2.3. Material properties used for the temperature loading models.

Section	Density [kg/m^3]	Specific heat [J/(kg °K)]	Thermal conductivity [W/(m °K)] [1]	Thermal expansion coefficient [1/°K]
Road (Asphalt)	2100 [1]	920 [3]	0.75	$4 \cdot 10^{-5}$ §
Piles (Steel)	7800 [1]	460 [1]	14	$1.2 \cdot 10^{-5}$ †
Walls, deck and girders (Concrete)	2300 [1]	880 [1]	1.2	$1 \cdot 10^{-5}$ †
Backfill	1937 [2]	830 [1]	0.7	$3 \cdot 10^{-5}$ ‡
Foundation soil (Sand and gravel)	1937 [2]	830 [1]	0.7	$3 \cdot 10^{-5}$ ‡
Bedrock (Sandstone)	2200 [1]	710 [1]	1.8	$1.2 \cdot 10^{-5}$ ¶

[1] From Thomas (1992)

[2] Based on unit weight value of 19 kN/m^3 fro sands and gravels from Bowles (1997)

[3] Chadbourn et al. (1996)

§ From Mamlouk et al. (2005)

† Modified from Razmi et al (2014)

‡ From Mitchel and Soga (2005) and Thomas (1992)

¶ From Skinner (1966)

Figures

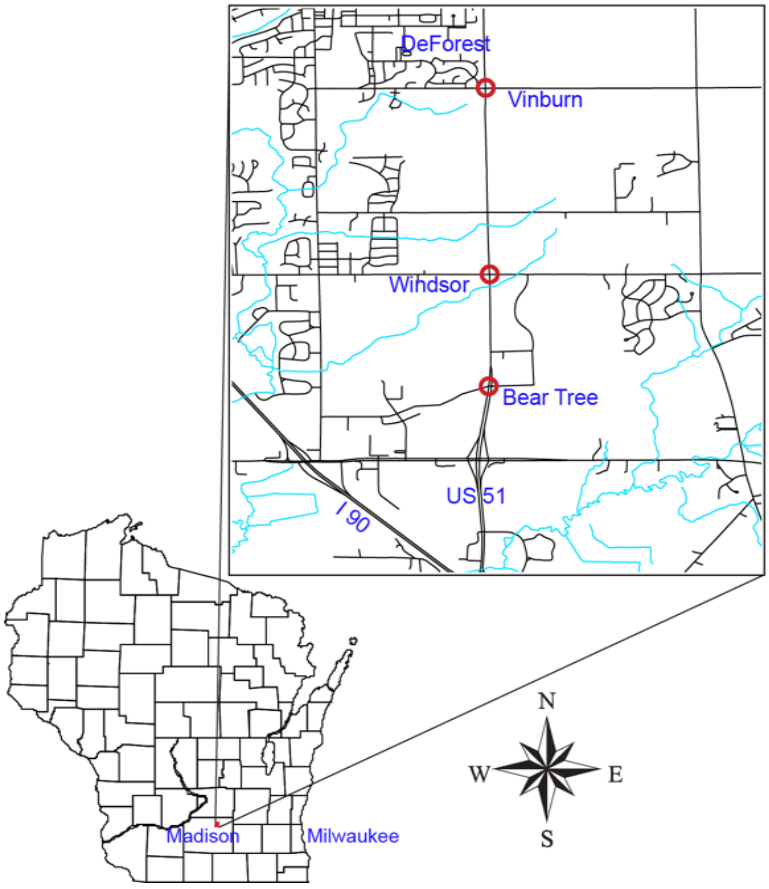

Figure 2.1. Location of the deep foundation bridges. The red circle indicates the location of the bridges.

(a)

(b)

(c)

Figure 2.2. Pictures of the finished bridges on USH51: (a) Bridge over Bear Tree Road, (b) Bridge over Windsor Road, and (c) Bridge over Vinburn Road.

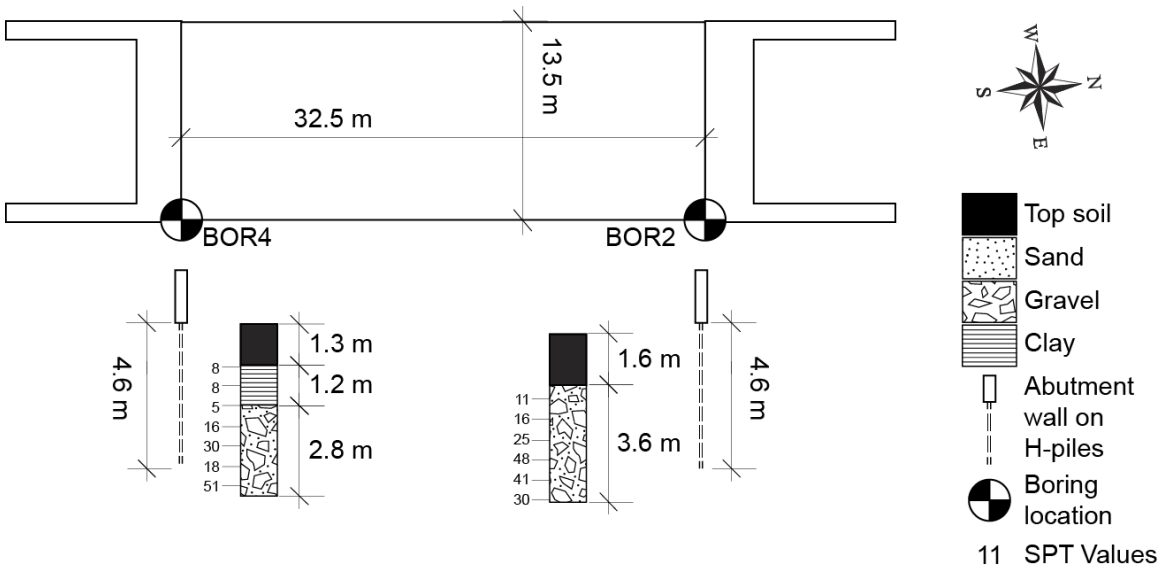

Figure 2.3. Subsurface exploration data for the bridge over Bear Tree road.

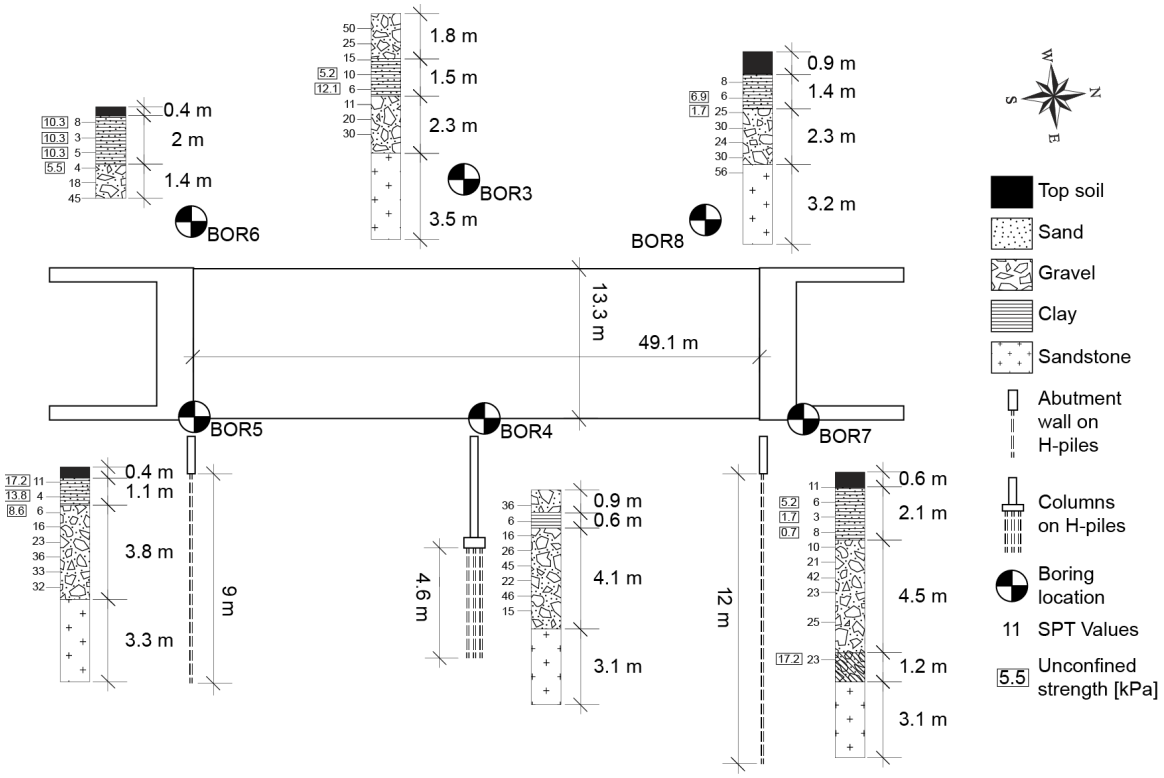

Figure 2.4. Subsurface exploration data for the bridge over Windsor road.

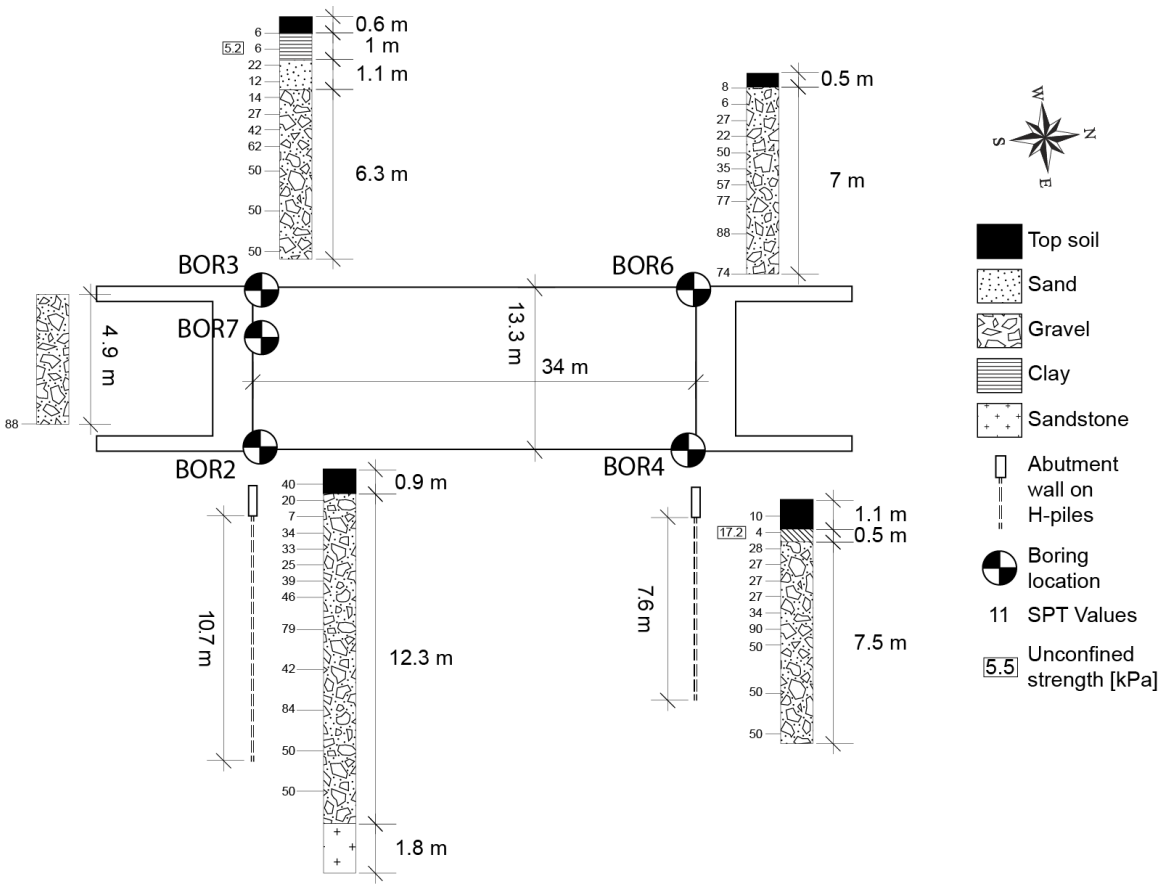

Figure 2.5. Subsurface exploration data for the bridge over Vinburn road.

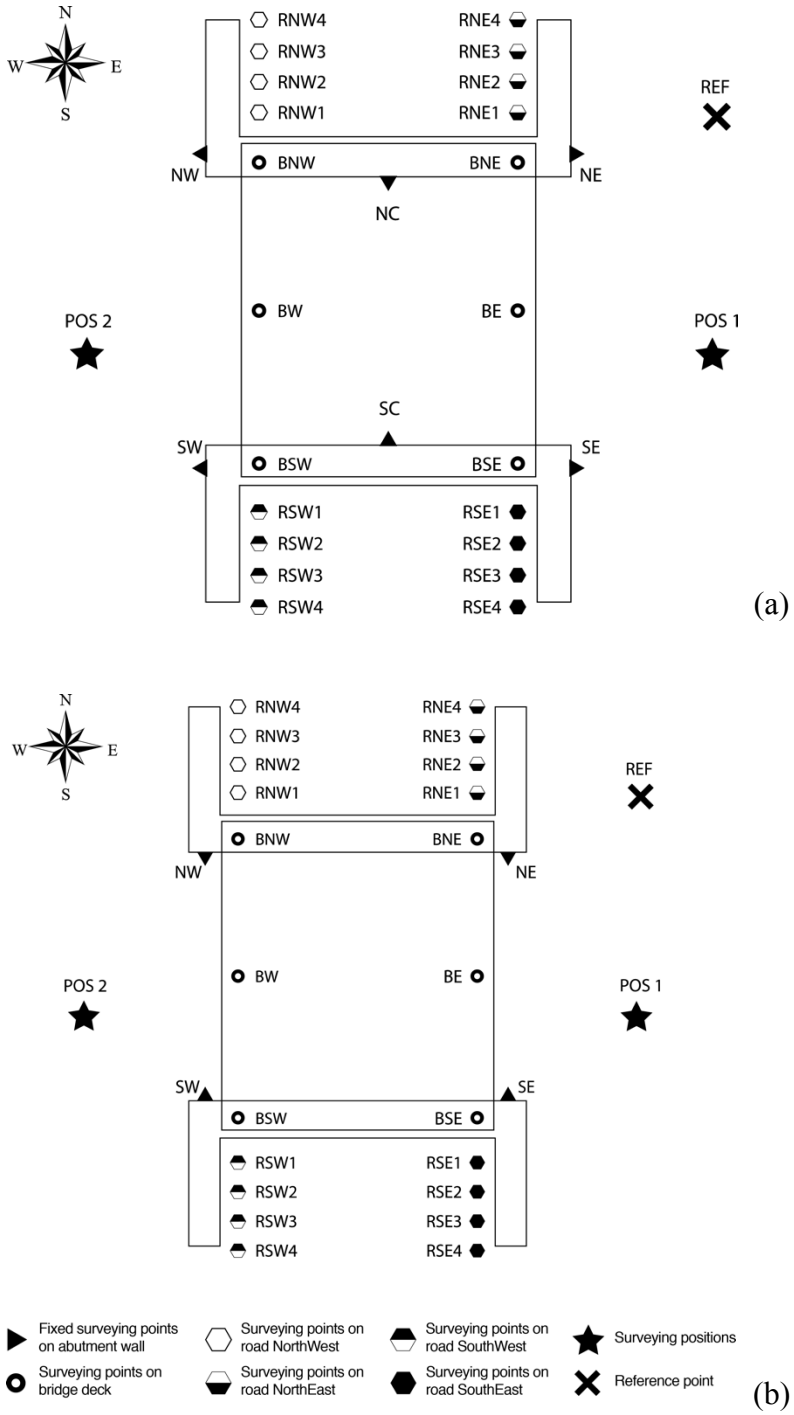

Figure 2.6. Relative location of the surveying points at (a) Bridge over Bear Tree Road and Bridge over Windsor Road bridges and (b) Bridge over Vinburn Road.

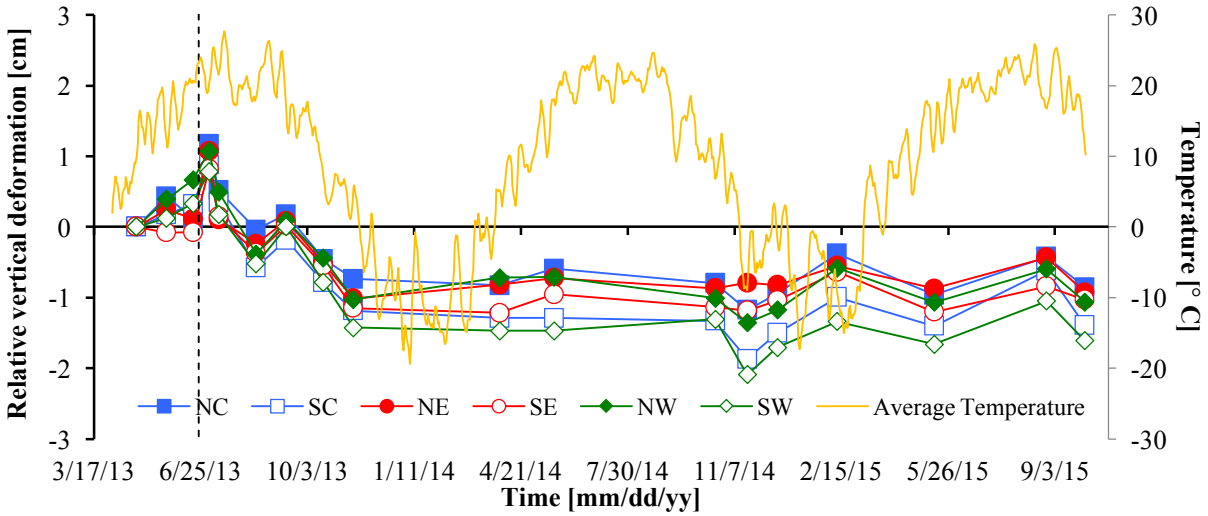

Figure 2.7. Bridge over Bear Tree Road. Relative vertical deformation on the abutment walls with respect to the reference point. Positive values correspond to upward movement. Vertical dashed line corresponds to the opening date to traffic.

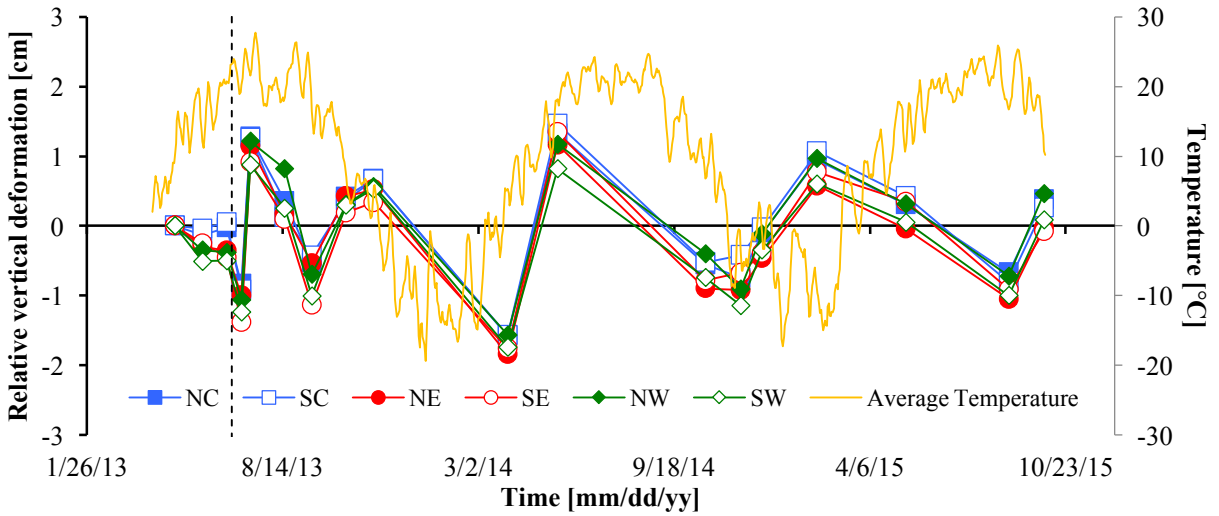

Figure 2.8. Bridge over Windsor Road. Relative vertical deformation on the abutment walls with respect to the reference point. Positive values correspond to upward movement. Vertical dashed line corresponds to the opening date to traffic.

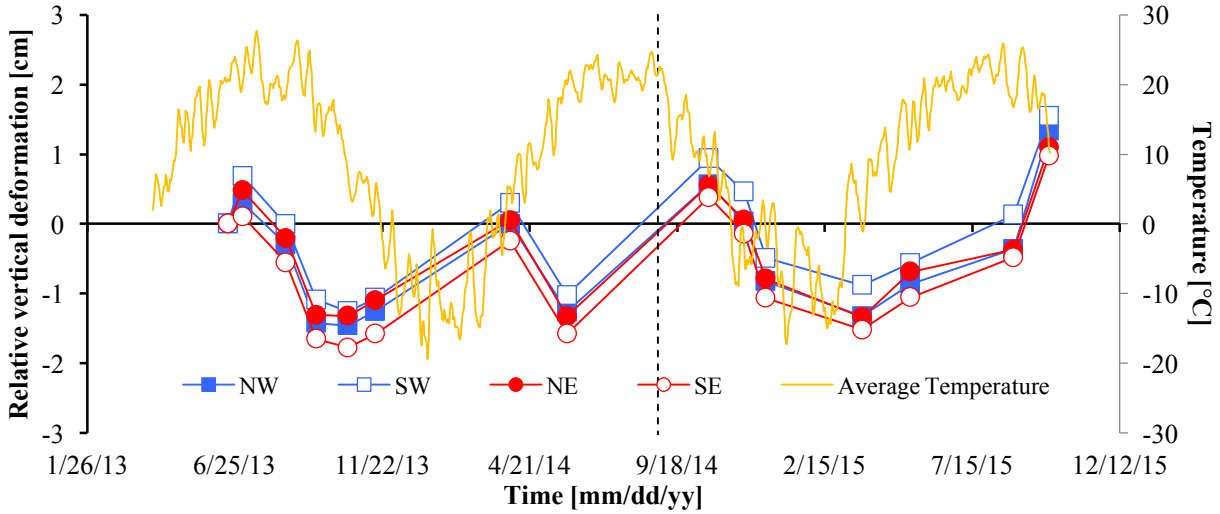

Figure 2.9. Bridge over Vinburn Road. Relative vertical deformation on the abutment walls with respect to the reference point. Positive values correspond to upward movement. Vertical dashed line corresponds to the opening date to traffic.

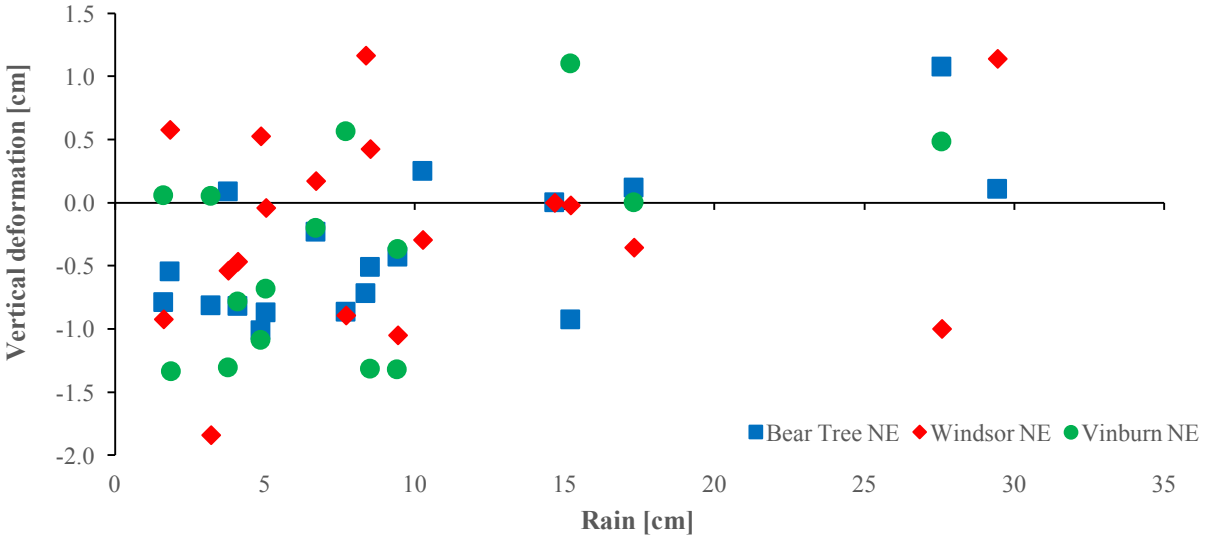

Figure 2.10. Vertical deformation versus rain for the NE surveying point for all three bridges.

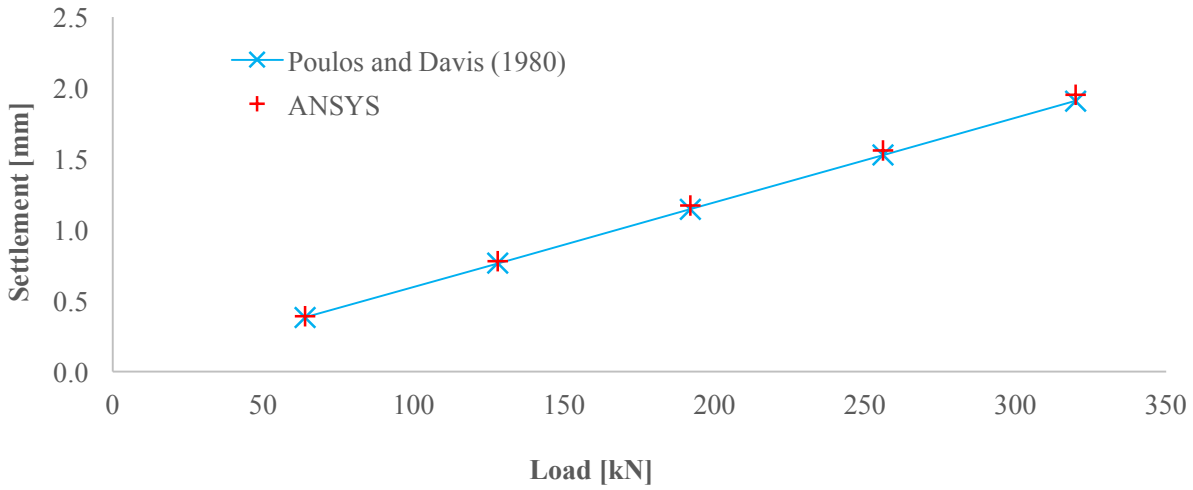

Figure 2.11. Settlement of a pile under different axial loads, comparing the finite element results to the analytical solution from Poulos and Davis (1980).

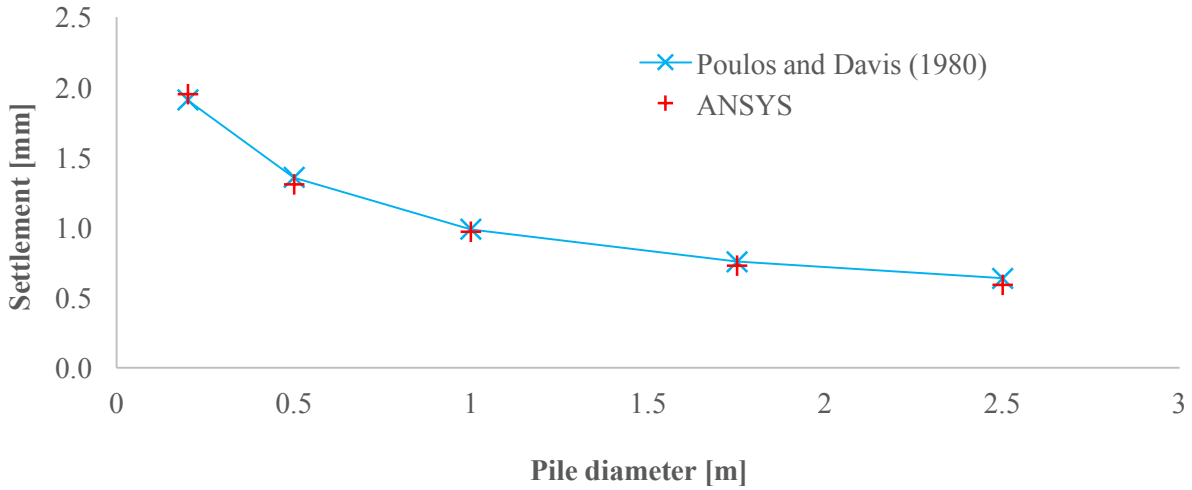

Figure 2.12. Settlement of a pile under different pile diameters, comparing the finite element results to the analytical solution from Poulos and Davis (1980).

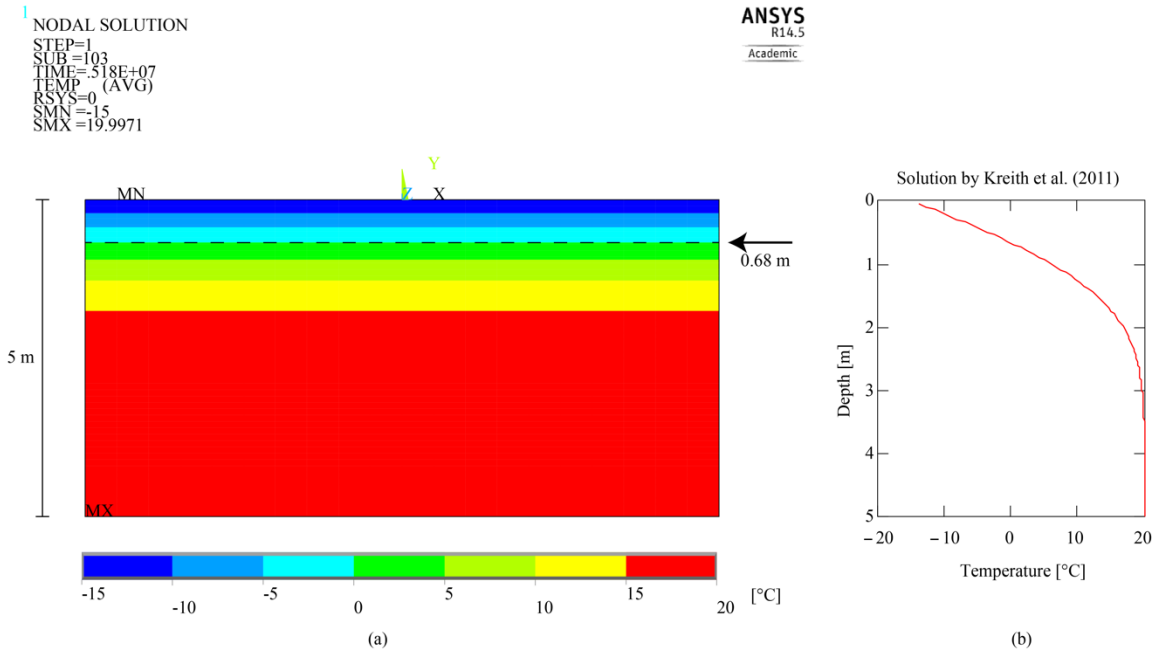

Figure 2.13. (a) Transient heat transfer model results for example 2.11 from Kreith et al. (2011). The arrow on the right and black dashed line represent the 0 °C isotherm at 0.68 m below the ground surface, same as the analytical solution. (b) Solution by Kreith et al. (2011) as function of depth.

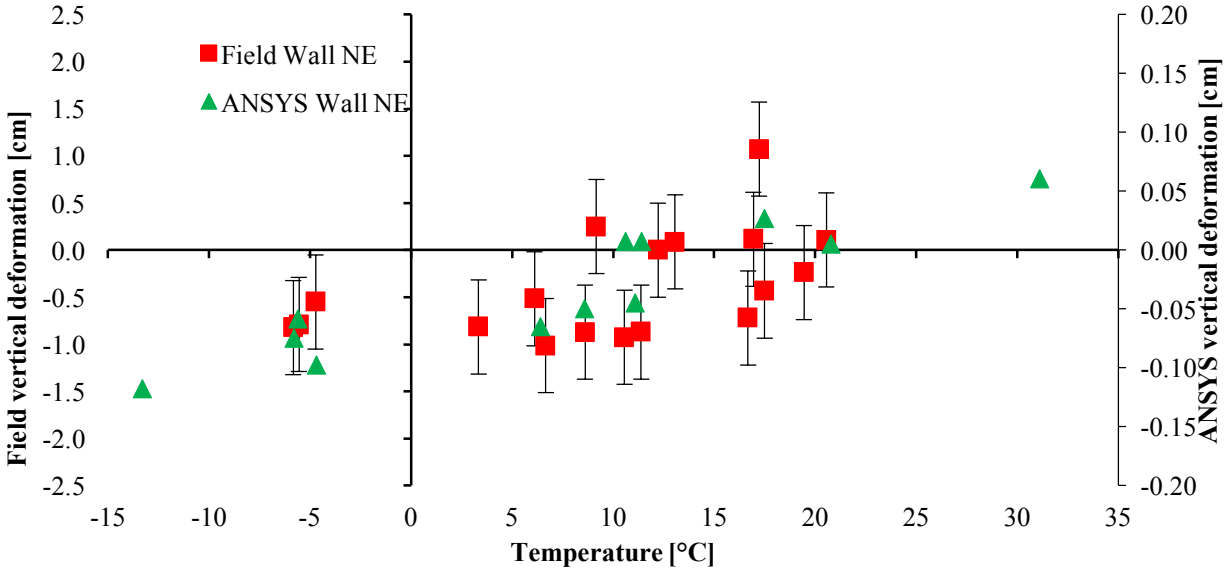

Figure 2.14. Bridge over Bear Tree Road. Comparison between field measurements and finite element model results for the NE wall. Error bars are +- 0.5 cm instrument accuracy.

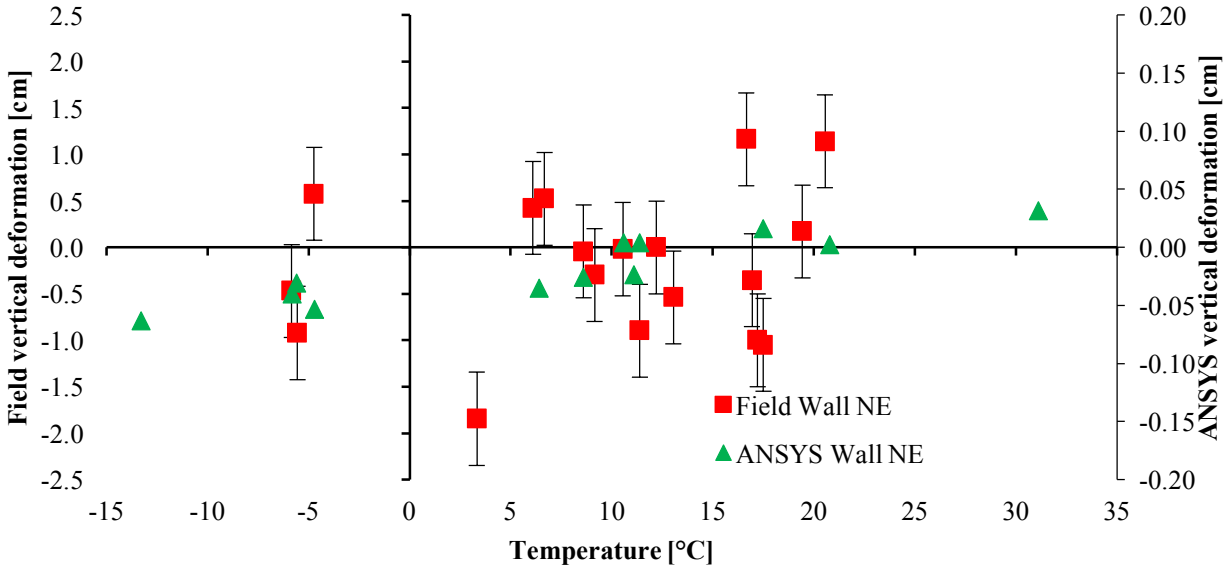

Figure 2.15. Bridge over Windsor Road. Comparison between field measurements and finite element model results for the NE wall. Error bars are +- 0.5 cm instrument accuracy.

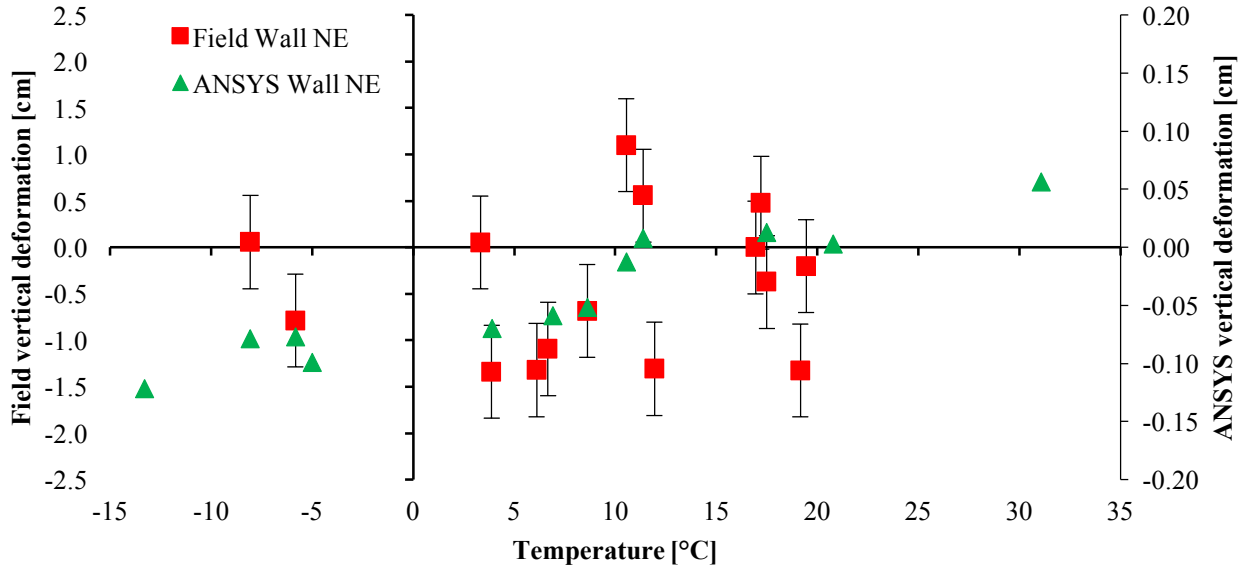

Figure 2.16. Bridge over Vinburn Road. Comparison between field measurements and finite element model results for the NE wall. Error bars are +- 0.5 cm instrument accuracy.

CHAPTER 3: Geosynthetic-Reinforced Soil Bridge Deformation due to Environmental Loading - From Field Monitoring

Maximiliano Garnier-Villarreal[1]; Dante Fratta[2]; and Michael Oliva[3]

Abstract: This study documents the performance of a Geosynthetic Reinforced Soil – Integrated Bridge System (GRS-IBS) located in Chippewa County, Wisconsin. This type of bridge construction system possesses some advantages over conventional, rigid foundation systems as it alleviates differential settlement between road embankment and bridge deck; reduces construction times; and is cost effective for small, rural bridges. Under operation, the bridge in our study was influenced by environmental loads much more than service loads. Observations in this study show that different sections of the structure undergo seasonal temperature contraction and expansion and also experience frost heave and thawing deformations. When temperatures fall below the freezing point, the deformation is controlled by heaving as water in the pores turns to ice. When the temperatures rise above freezing point, the deformations are controlled by settlement due to a decrease in the stiffness of the soil, and an increase in effective stresses as pore pressure dissipates. The study shows that the performance of the bridge is acceptable but designers and transportation officials should consider environmental loads to assess and control accumulation of deformations. Also, designer must follow design specifications, as in this case a

[1] Graduate Student. Geological Engineering. University of Wisconsin-Madison. Madison, WI 53706. USA. Email: garniervilla@wisc.edu.
[2] Associate Professor. Geological Engineering. University of Wisconsin-Madison. Madison, Wisconsin 53706. Email: fratta@ wisc.edu.
[3] Emeritus Professor. Civil and Environmental Engineering. University of Wisconsin-Madison. Madison, Wisconsin 53706. Email: oliva@engr.wisc.edu.

joint-sealing layer was not implemented here, resulting in differential settlements between road and deck due to frost heave as water infiltrated into the backfill.

Keywords: GRS-IBS; Shallow foundation; Temperature changes; Frost-heave; Field monitoring; Deformation.

3.1 Introduction

Movements of foundation systems can be rotational, lateral and/or vertical (settlement). These movements can be caused by dead, service and/or environmental loads. The design of foundation systems for bridges in transportation structures should comply with serviceability and strength limit states requirements. (AASHTO 2012). Serviceability requirements for bridges require deformation limits to be less than 10 cm (3.94 in) for vertical displacements and 5 cm (1.97 in) for horizontal displacements (Moulton et al. 1995; Wahls 1990).

Differential settlement between the bridge deck and approaching road has been found to cause discomfort to riders and to create costly maintenance operations for Departments of Transportation (DOTs – Briaud et al. 1997). This problem is also known as the "bump at the end of the bridge." When the differential displacement reaches 1.3-2.5 cm (0.5-1 in.) it is considered to become noticeable (Wahls 1990; Long et al. 1998). According to AASHTO (2012), rideability and safety should also be taken in consideration when determining the serviceability of a structure. Moulton et al. (1985) studied tolerable movements of highway bridges under serviceability considerations, proposing that a distortion (differential settlement over span length) smaller than 0.004 radians (1/250) may be considered acceptable.

Briaud et al. (1997) reported that approximately 25% of the bridges around the United States have suffered differential settlements, and the cost to repair and maintain these bridges was estimated to be $100 million per year. Long et al. (1998) found that around 27% of the inspected bridges showed differential settlement. This problem also affects up to 50% of the railway bridges (Nicks and Briaud 2007).

Some of the major causes for differential settlement in transportation structures as follow (Figure 3.1a - Wahls 1990; Long et al. 1998; and White et al. 2007): poor compaction of backfill, erosion of backfill material, poor drainage management in backfill, creep, consolidation of foundation soil, and poor construction practices. Long et al. (2007) also indicated that embankment height can be another cause of differential settlement, as taller embankments (i.e., more than 8 m - 26.25 ft in height) generate greater pressures and are more prone to deform than shorter embankments (i.e., less than 3 m - 9.84 ft height).

To prevent some of these problems in small, rural road bridges, the FHWA has been implementing a new construction methodology: Geosynthetic Reinforced Soil – Integrated Bridge System (GRS-IBS). This type of bridge is a support system that merges the approaching road with the bridge deck. The system is built to create a jointless boundary between approach road, abutment and the bridge deck, as the deck rests directly on top of the abutment.

3.1.1 Deformation of Bridge Foundations: Mechanical and Environmental Causes

For bridges supported by shallow foundations, settlements usually control the serviceability design (Lambe and Whitman 1969). Foundation settlement has three stages: immediate or elastic, primary consolidation, and secondary compression or creep. Immediate or elastic settlement happens soon after construction. For coarse-grained foundation soils the elastic deformation correspond to most of the settlement (Helwany et al. 2007). Primary consolidation

refers to the process settlement caused by the dissipation of excess pore water over time. Finally, secondary compression refers to the deformation under constant loading (creep). Both primary consolidation and secondary compression comprise most of the settlement for fine-grained soils (Helwany et al. 2007). The long-term impacts are controlled by relative ratio of live over dead loads and the rate of excess pore pressure dissipation during dynamic loading conditions (Helwany et al. 2007).

Environmental conditions (e.g., temperature, precipitation, water table changes, freezing and thawing, etc.) can also have an effect on the behavior of foundations and structures they support. Ma et al. (2011) studied the behavior of embankments with respect to ground temperatures. When the mean annual ground temperature was -1.5 °C (29.3 °F) or less, embankments experienced frost heave during the colder seasons and settlement during the warmer seasons.

Li et al. (2013) studied the effect of freeze-thaw cycles, cyclic stress amplitude, confining pressure, moisture content, and number of loading cycles on the strain of clays under low stress level (< 0.3 MPa) repeated mechanical cyclic loading conditions. Li and co-workers found that the larger deformation occurs after the first freeze-thaw cycle, however this effect is reduced with consecutive cycles. They also found that larger water contents result in larger cumulative strains. Also, heaving of soils with a nearby water supply (i.e., creeks, streams, etc.) will occur when the soil reaches 90% saturation. When soils are not near a water supply, localized heaving can occur due to lenses in the soil mass (Shoop and Bigl 1997).

Freezing and thawing of soils is a transient heat-moisture process, as liquid water transforms into solid ice while giving up heat (i.e., latent heat effect). Two types of frozen soil fabrics can form: homogenous, layered (ice lenses), or both (Farouki 1981). The homogenous fabric occurs when the freezing rate is fast, not allowing for water migration, thus only the water present in the

pores gets frozen (Farouki 1981). The layered fabric occurs when the freezing rate is slow, allowing for water to migrate to form the ice lenses (Farouki 1981; Shoop and Bigl 1997; Mitchell and Soga 2005; Holts et al. 2011; Ming and Li 2016).

Ice lens formation and frost heave can occur under the following conditions: frost-susceptible soil, freezing temperatures, and water supply (Mitchell and Soga 2005; Holts et al. 2011). Soils with more than 3 percent of fine-grained particles are considered to be frost susceptible. The thickness of the ice lenses can range between millimeters to centimeters (Mitchell and Soga 2005), and the lenses tend to become thicker and more separated with depth (Farouki 1981; Mitchell and Soga 2005).

In coarse-grained soils all water is frozen and this occurs over a small temperature range, while in fine-grained soils (typically more frost susceptible) not all water freezes, some remain as thin films on the grains surface, and freezing occurs over a large temperature range (Farouki 1981; Mitchell and Soga 2005; Zhang and Michalowski 2015; Bao et al. 2016). Ice lens formation occurs as it is easier to draw water to ice than to propagate ice through the pore space (Mitchell and Soga 2005). Desiccation at the freezing front causes a suction effect due to remaining water films, this suction and the thermal gradient at the freezing front is what causes water to migrate towards the freezing zone (Farouki 1981; Mitchell and Soga 2005). As the water supply below the freezing front becomes more limited the freezing front moves downward until it can start forming new lenses (Farouki 1981; Mitchell and Soga 2005). The soil thermal properties get affected by temperature changes; as the soil freezes and ice forms the soil's thermal conductivity increases and its heat capacity decreases (Farouki 1981; Bao et al. 2016).

Frost heave happens as water freezes ice forms and expands (~ 9%), resulting in an increase of the void space and thus the porosity of the soil (Farouki 1981; Mitchell and Soga 2005; Özgan

et al. 2015; Zhang and Michalowski 2015). As the mechanical, hydraulic and thermal properties of the soil are affected by freezing and thawing (Farouki 1981; Qi et al. 2008; Mitchell and Soga 2005; Özgan et al. 2015; Wang and Liu 2015; Zhang and Michalowski 2015), the ice-bonding effect makes the soil experience an increase in stiffness and a reduction in its compressibility and permeability below the freezing point (Wang and Liu 2015; Zhang and Michalowski 2015).

Freezing and thawing cycles can have either a cumulative heave effect on the deformation of the soils or add to the settlement of the soils experiencing these cycles. If the soils comprise mostly of fine-grained particles or have large over-consolidation ratios they would tend to have a cumulative heave effect (Ma et al. 2011; Li et al. 2013; Zhang and Michalowski 2015), but if the soils are mostly coarse-grained or normally consolidated they would tend to experience extra settlement (Özgan et al. 2015; Zhang and Michalowski 2015).

Thaw settlement occurs as temperatures rise, this increase in temperature causes the ice and lenses to melt, increasing the water content of the soil, resulting in a weaker soil with increased permeability (larger voids). Under constant load and drained conditions the thawed soil may be re-arranged into a denser state than before freezing (Farouki 1981; Kim et al. 2003; Md. Noor et al. 2008; Qi et al. 2008; Mitchell and Soga 2005; Holtz et al. 2011; Özgan et al. 2015; Shahriar et al. 2013; 2015; Zhang and Michalowski 2015).

Helwany et al. (2007) also shows that volumetric changes due to freeze/thaw cycles could cause the soil to deform, increasing the stress on the pavement of approaching roadways and abutment walls. Another effect of temperature changes can be the generation of thermal cracking in flexible pavements and concrete surfaces; cracking can happen as a response to thermal gradients occurring in the structure due to repeated contraction and expansion as temperature changes. Thermal changes can happen in matter of hours, as Michal and Urban (2015) reported,

bridges deforms as the temperature changes but with a delay between 5 to 8 hours after the maximum or minimum temperature, allowing for the heat to diffuse into the structure and foundation soils.

Water table changes can also affect the behavior of foundation soils. As water level declines the pore pressure decreases thus the effective stress felt at a certain point below the water table increases. This increase in effective stress causes the pore space to decrease, resulting in settlement or subsidence (Md. Noor et al. 2008; Anochikwa et al. 2012; Loáiciga 2013). Deformation over time will depend on the water content, as soils with higher water contents will take longer time for the pore pressure to dissipate, thus deformation will occur over a longer period of time (Kim 2000; Qi et al 2013; Wang and Liu 2015). Settlement due to water table rise has also been discussed in relation to the soil stiffness, as water table rises and water contents increase the stiffness of the soil decreases, affecting the soil deformation (Kim et al. 2003; Md. Noor et al. 2008; Shahriar et al. 2013; 2015).

3.1.2 Geosynthetic Reinforced Soil – Integrated Bridge System

In this type of bridges, the structure comprises of reinforced abutment, foundation, and approach roadway. The reinforced abutment consists of layers of compacted backfill between layers of geosynthetic reinforcement and provides the support to the bridge deck. The reinforced foundation increases the bearing capacity of the foundation system. When GRS-IBS is used over waterways, the use of scour protection is required to avoid erosion at its bottom of the abutment-foundation system (Adams et al. 2011- Figure 3.1b).

GRS-IBS systems have been used since the late 1990s, offering some advantages over the more conventional rigid foundations (i.e., shallow and deep foundation systems). These advantages include cost effective construction (up to 30% savings), rapid and easy construction,

and good seismic performance. Also, GRS-IBS systems can be implemented in remote areas, may be used to reconstruct bridges after natural disasters, and can be built on top of stiff to soft soils as the unit behaves as a whole distributing the load in a uniform way (Adams et al. 1999; Abu-Hejleh et al. 2002; Helwany et al. 2003; Keller and Devine 2003; Mohamed et al. 2011).

One of the main disadvantages of GRS-IBS is the susceptibility of erosion on the face and footing of the abutment, thus mitigation techniques, such as embedment, riprap, cellular confinement system, or segmental blocks, should be implemented to avoid scouring of the foundation (Mohamed et al. 2011). Another disadvantage is that GRS-IBS can only be used in small bridges (span less than about 40 m – Adams et al. 1999). Abu-Hejleh et al. (2002) emphasize that with the use of GRS-IBS in a bridge, supported on claystone bedrock, this bridge did not suffer differential settlement even after three years of surveying, with the majority of the settlement happening the first year.

Viswanadham and König (2009) used a centrifuge experiment to study the behavior of a GRS system on a yielding foundation. They observed that even at larger differential settlements (1 m over 18 m - 3.3 ft over 59 ft - in length, in prototype dimensions) the reinforced embankment does not reach failure and its lateral deformation is approximately 1.6% of the slope height. The effect of a yielding foundation was also studied by Skinner and Rowe (2005), finding that the yielding of the foundation can cause or add to the differential settlement on an abutment, but its effect can be reduced by the use of the GRS system, especially by increasing the length and stiffness of the bottom most reinforcement layer.

The specifications for the implementation of GRS-IBS were proposed by Adams et al. (2011). They specified a height of less than 9.1 m (30 ft), a deck span less than 42.6 m (140 ft), a bearing stress less than 191.5 kPa (27.8 psi), and a separation of the geosynthetic reinforcement

of 30 cm (12 in) or less. GRS-IBS perform better with shorter reinforcement separation and less tensile strength in comparison with higher tensile strength and larger reinforcement separation (Adams et al. 1999).

The objective of this study is to evaluate the behavior of a GRS-IBS system by studying their response to design traffic loads and environmental loads. To accomplish this, monitoring of its movements over time, and finite element analysis were performed on a bridge in Bloomer, Wisconsin.

3.2 Studied bridge and monitoring approach

3.2.1 Bridges description

The studied Geosynthetic Reinforced Soil – Integrated Bridge System (GRS-IBS) is located on State Highway (STH) 40, southwest of the City Bloomer and north of the Town of Howard in Chippewa County, Wisconsin, and it crosses over Hay Creek (Figure 3.2). The deck is 12.2 m (40 ft) long by 11.7 m (38.4) wide. The bridge deck is directly supported by the geosynthetic reinforced backfill. The geosynthetic used as reinforcement for the soil is a biaxial woven polypropylene with a wide width tensile strength of 70 kN/m (4800 lb/ft), with layers spaced 20 cm (7.87 in) near the bottom and 10 cm (3.94 in) near the top. The length of the reinforcing layers' ranges between 1.8 to 4.3 m (5.9 to 14.1 ft), from bottom to top. Also, riprap protection was used to prevent scouring, and masonry-facing elements were used to protect the reinforced soil abutment. The structure was founded on the natural soil. Subsurface exploration shows that the soil consists predominantly of sand layers with some traces of clay and silt (Figure 3.3). This area hosts sand quarries to produced silica sand used in shale hydraulic fracturing operations. Thus a great portion of the traffic correspond to trucks transporting sand for this purpose (maximum allowed weight is 355 kN - 80 kip – AASHTO 2012). Due to this added traffic,

WisDOT have been required to upgrade maintenance operations in rural roads in the country and region. The GRS-IBS bridge was built to replace an old bridge that was supported on timber piles. Because of the presence of a previous structure and that glaciers covered this area thousands of years ago (Syverson 2007), the foundation soils in this area can be considered to be either dense or over-consolidated.

3.2.2 Monitoring approach

Conventional surveying techniques were implemented to monitor the deformation of the bridge, using a total station, with the accuracy of the instrument given by (GLM-Laser, 2015):

$$\delta = \pm(0.005m + 3 \cdot 10^{-6} \cdot D) \quad (3.1)$$

where D is the total station-prism horizontal distance.

The location and layout of the surveying points for the bridges is shown in Figure 3.4. The surveying points on the deck, close to its edge, are approximately 0.5 m (16 ft) from the edge of the deck, and the middle ones at the midspan of the deck. The surveying points on the approaching road start 1.8 m (5.9 ft) from the edge of the deck, and are 5 m (16.4 ft) apart from each other. Settlement plates have been used to monitor the deformation of the foundation. On the north abutment wall these are connected to a rebar encased in pipe, while on the south abutment wall there are no rebars. A benchmark was installed to use as reference far from the bridge site but within the right of way.

There are several factors that can have an effect on the surveying measurements in the field. First, the assumption that the reference point used in the field is not moving might not be completely accurate, as this point, as the rest of the surveying points, can also be experiencing slight deformations due to changes in temperature (heaving and compression during summer and winter seasons), carrying an error into the field measurements or exaggerating them. Second, as

far as the instrumentation goes it has been reported that the accuracy of the measurements depends on the distance between the equipment and the target, decreasing with distance (Equation 1 - Beshr and Elnaga 2011; Elhassan and Ali 2011). Lastly, other factors such as the effects of surveying towards (front) and against (back) the sun, battery capacity, inclination of target, and reflecting surface also affect the accuracy of the measurements. Beshr and Elnaga (2011) report that surveying towards the sun, with a battery with lower capacity, a larger inclination of the target surface, and darker targets, results in less accurate measurements.

3.3 Geosynthetic Reinforced Soil-Integrated Bridge System Deformations

The results from monitoring the vertical deformation of the bridge are shown in Figures 3.5 to 3.8 (The rest of the monitoring results are shown in Appendix C). Figure 3.5 summarizes the vertical deformation of the settlement plates over time and versus temperature. In general, the foundation has experienced slight deformation, 0.5 cm (1.6 in) or less. Given that the foundation soils in the area are likely dense or over-consolidated, the induced traffic load imposed on the system might be less than what the maximum effective stresses the soils have experienced before. Such effect has been documented in bridges in colder environments than Wisconsin (Ma et al. 2011). A hypothesis on what could cause these deformations is that the environmental conditions (mostly temperature) might be controlling the deformation for the structure.

Figure 3.6 shows the vertical deformation of the abutment walls over time and versus temperature. The fact that all the displacement trends are closely together indicates that the abutment walls are moving uniformly as a unit, meaning that no section is undergoing more or less deformation than any other. The data indicate a general upward trend, with some periods of downward movement. This trend could be due in part to environmental factors; as the

temperature and moisture content changes, the structure could be showing a response to these changes. The structure and soils can expand and contract during hot and cold periods, but also the soils can experience heave due to freezing of water in the pore space, with a general effect of cumulative deformation due to freezing and thawing (Ma et al. 2011; Li et al. 2013).

Figure 3.7 shows the vertical deformation on the bridge deck over time and versus temperature. The figure presents a general downward trend with respect to temperature. The general deformations could be due in part to the system's response to environmental (i.e., temperature) changes. Moreover, as for the design of GRS-IBS bridges the deck is resting directly on the reinforced backfill, the deformation could also be a result of poorly compacted backfill (White et al. 2007), due to the loss of the strength in the backfill due to the infiltration of water (Li et al. 2013; Kim et al. 2013), or due to the use of a geosynthetic with not enough strength and stiffness.

Figures 3.8 describes the vertical deformation of the South and North approaching roads over time and versus temperature. The behavior of these points shows an upward trend during the winter season, a downward trend during the transition to and from winter, and a more or less steady behavior the rest of the time. These deformations could be attributed to the effect of frost heave and then thawing on the soil underneath the road.

To assess the potential effect of frost-heave the following scenario can be considered. A fine-grained soil under a foundation is expected to freeze 1 m (3.3 ft) below the foundation. The soil is saturated and has a void ratio of 0.6. The volume of voids (and water as S=100%) can be found using equation 3.2:

$$V_V = \frac{eV_T}{1+e} \tag{3.2}$$

where V_V is the volume of voids, V_T is total volume, and e is the void ratio of the soil.

Assuming a total volume of 1 m^3 that the volume of water before freezing occurs is 0.38 m^3; then after freezing occurs the volume of ice becomes 0.42 m^3 (density of ice = 0.9 kg/m^3), resulting in a frost-heave of 4 cm (1.6 in). Ma et al. (2011) and Li et al. (2013) mention that frost heave could have a larger cumulative effect than the settlement or deformation due to thawing, which could explain the upward trend shown by the approaching roads. A more comprehensive and general explanation of the observed deformations is presented in the Section 3.5 Field Monitoring Response Discussion later in this chapter.

Visual inspection of the deck and approaching road in March 2013 revealed a relative displacement of -1.2 cm (-0.5 in.) and -3 cm (-1.2 in) between the bridge deck and the approaching road level, in between the traffic lanes. At the corners of the deck no deformation was observed. During the April and May 2013 visits, visual inspection revealed that the deck and approaching road were at the same level, no difference was observed at the joint of these two sections, but a crack (25.5 cm – 10 in long) was observed on the southeast section of the road (Figure 3.9a). In March of 2013 the southeast traffic lane section of the deck was 3 cm (1.2 in) below the roadway, while the other three traffic lane sections were 2 cm (0.8 in.) or less. The crack could have been formed as a response of the pavement/embankment to the temperature change between March and April, and the leveling of the deck and approaching road during this period of time, as mentioned by Helwany et al. (2007) thermal cracking on pavements and concrete surfaces can happen due to temperature changes.

During June 2013 the southwest and northeast sections of the deck moved up approximately 2 cm (0.8 in.), with respect to the approach road and since the previous month visit (May 2013), while the southeast and northwest traffic lane sections stayed level. This behavior has remained the same between July 2013 and March 2014. The last set of measurements, May and August

2014, indicates that all the approaching road corners, in between the traffic lanes, have moved up with respect to the bridge deck. In March 2014 another crack (31.4 cm – 12.4 in long) was observed (Figure 3.9b) next to the one that first appeared in May 2013, probably due to the same factors as the first crack, changing temperature during the transition between seasons.

During the winter months, snow accumulated on the bridge deck and approaching roadway. As the temperature rose and the snow melted away, the resulting water ponded around the deck and approaching road joint. The general GRS-IBS design specification (Adams et al. 1999) calls for a layer of pavement on top of the deck and approaching road to create a continuous and smooth surface and a jointless transition. The pavement layer was not implemented on this bridge, leaving a joint between the deck and road exposed, thus allowing for water to infiltrate and accumulate inside the reinforced backfill, making this joint exposed to environmental conditions and the corresponding effects on the structure. The implementation of the pavement layer could have diminished the environmental effects and improve the behavior of the system.

As discussed by Wahls (1990), deformations are expected to occur on shallow foundations. As a response to these deformations the GRS-IBS system is expected to deform and match these deformations instead of resisting them. As soils are not homogeneous they can deform in a non-uniform way and this deformation can be transferred to the structure being supported by the soil, thus causing differential deformations.

3.4 Freeze-Thaw Experiment on Sand-Silt Mixtures

To provide a better understanding of the behavior of sand and silt mixtures under freezing and thawing cycles, two samples were subjected to freezing and thawing. The two samples comprise of sand and silt with different percentages: sample A had 90% sand and 10% silt, and

sample B had 50% sand and 50% silt. The samples were consolidated to 100 kPa (14.5 psi) and then unloaded to 25 kPa (3.6 psi) to create dense, over-consolidated soil specimens, with these two stages taking a total time of 48 hours. The freezing and thawing cycles were started after the loading-unloading of the samples, with each cycle lasting 48 hours (24 hours for freezing, 24 hours for thawing), keeping the vertical pressure constant at 25 kPa (3.6 psi), and the samples saturated at all times. The displacement of the samples was recorded using a Linear Variable Displacement Transducer (LVDT) and the temperature of each sample was recorded using a thermocouple placed at the middle of the sample. The samples were placed inside an open chest freezer for the loading-unloading part of the test. To freeze the samples, the freezer turned on and closed, and to thaw the samples the freezer was turned off and open. A set up of the experiment is shown in Figure 3.10a. Based on the setup of the experiment (fast freezing rate and continuous water supply) and the soils' composition (more than 3% of fine grained soil) a homogeneous freezing fabric would be expected to occur.

Figure 3.10b shows the results of the freeze and thaw experiment. It can be seen that the soil sample with a higher content of silt (sample B) experienced larger compression during the loading-unloading stage, with sample A changing height by 1% and sample B changing height by 3.5%. This behavior would be expected as a soil with higher content of fine-grained particles is more compressible than a soil with a higher content of coarse-grained particles (Mitchell and Soga 2005). After 16 freeze-thaw cycles both samples have experienced extra compression, once again with sample B recording a larger deformation. Sample A has changed (reduced height) 0.43%, while sample B has changed (reduced height) 0.63%. Similar observations were made by Özgan et al. (2015), reporting consolidation test results of clayey sand samples after 30 freeze-thaw cycles resulted in an increase of 23% in the compression of the soil with respect to samples

before freezing and thawing. Their results are consistent with the remarks from Zhang and Michalowski (2015), stating that coarse-grained soils or normally consolidated soils tend to experience extra compression due to the effects of freezing and thawing.

Figure 3.10c shows the change in height for each freeze-thaw cycle, showing how the magnitude of the deformation for each cycle remains pretty much the same for sample A (90% sand), but for sample B (50% sand) the magnitude of the deformation increases as the number of cycles increase, resulting in a cumulative effect of the freezing and thawing for the sample with higher fine particles content, as previously reported by Ma et al. (2011), Li et al. (2013), and Zhang and Michalowski (2015).

The tests results indicate that the soil composition will not only have an effect on the initial compression due to added load, fine-grained soils will compress more, but will also have an effect on the response to freezing and thawing, with fine-grained soils being more susceptible to freezing and thawing effects than coarse-grained soils.

3.5 Field Monitoring Response Discussion

Foundation Soils. The deformation of structures can be affected by environmental factors, other than temperature changes, such as changes in moisture content and cyclic loading, causing changes in the shear strength and stiffness of the soil (Kim et al. 2003; Okus and Ansal 2007). Additionally, soil heterogeneity and the occurrence of fine-grained soil layers can cause the system to deform in a non-uniform way. Fine-grained soils, in particular clays, are more predisposed to changes in moisture content (Mitchell and Soga 20015; Li et al. 2013), resulting in larger deformations when present in foundation soils (Moulton and Kula 1980; Moulton et al. 1985; Whals 1990; Long et al. 1998; White et al. 2007).

The presence and/or fluctuation of moisture in the field is not known, making difficult to account for this effect when analyzing the field results; with the only exception of the reinforced foundation, which can be assumed to be saturated as the bridge crosses a creek. Given the very localized subsurface explorations and uncertainty on how the layers extend laterally and specific percentages of the different particle fractions, the response of the soils based on their composition can only be generalized and speculated. As shown by the freezing and thawing experiment results, the soils composition has a direct impact on the response of these to the different loading conditions.

Conceptual model for deformations. As water in the pore space freezes ice forms and expands, causing the soil to heave, resulting in an increase of the void space and thus the porosity of the soil (Farouki 1981; Mitchell and Soga 2005; Özgan et al. 2015; Zhang and Michalowski 2015). As the properties of the soil are affected by freezing and thawing (Farouki 1981; Qi et al. 2008; Mitchell and Soga 2005; Özgan et al. 2015; Wang and Liu 2015; Zhang and Michalowski 2015), the foundation experiences an increase in stiffness and a reduction in its compressibility below the freezing point due to ice-bonding. Because of this behavior, frost heave is considered to be the driving mechanism for the deformation of the foundation soils below freezing temperatures, as captured by the field results from the different surveyed sections. The long-term behavior of the bridge shows cumulative heave effect, which would indicate that the foundation soils have a significant fraction of fine-grained soils and/or are heavily over-consolidated, and this behavior has been described under similar conditions by other researchers (Ma et al. 2011; Li et al. 2013; Zhang and Michalowski 2015).

As temperature rises the ice present in the voids starts to melt, thus increasing the water present in the soil, weakening the soil and resulting in thaw settlement or shrinkage. As water

migrates (this can contribute to the lowering of the water table) pore pressure starts to dissipate, as pore pressure dissipates the effective stresses increase, and the void space starts to shrink (Md. Noor et al. 2008; Anochikwa et al. 2012; Ming et al. 2012; Loáiciga 2013). As the field results show, when plotted against temperature (Figures 3.5-3.8), there is a downward deformation trend with increasing temperature; this trend is attributed to the lowering of the water table as the soils dry with an increase in temperature, leading to an increase on the effective stress and therefore resulting in settlement or shrinkage of the soils.

As an example of this mechanism, a quick estimation of settlement, on an over-consolidated or dense soil, can be performed using the following equation:

$$\delta = \frac{H}{1+e_0} \cdot C_r \cdot \log\left(\frac{\sigma'_{vf}}{\sigma'_{vi}}\right) \tag{3.3}$$

where δ is settlement, H is thickness of the soil, e_0 is initial void ratio, C_r is the re-compression index, σ_{vf}' is final effective vertical stress, and σ_{vi}' is initial effective vertical stress.

Assuming H = 5 m (16.4 ft), e_0 = 0.6, C_r = 0.05, γ_{dry} = 18 kN/m^3 (114.6 lb/ft^3), γ_{sat} = 20 kN/m^3 (127.3 lb/ft^3), initial water table at 2 m (6.6 ft) below the surface, and final water table at 3 m (9.8 ft) below the surface, the estimated settlement due to a 1 m (3.3 ft) lowering of the water table is 0.75 cm (0.3 in), which is in the same order of magnitude that the field results show. This calculation shows that lowering of the water table could contribute to the settlement of the foundation soils as these become drier as temperatures rise. Furthermore, the settlement may be even higher as the matric suction increases during the lowering of the water table.

3.6 Conclusions

From the field monitoring of the GRS-IBS bridge in Bloomer the following conclusions can be made:

- The bridge at Bloomer has experienced deformations due predominantly to environmental factors, such as temperature and water content changes, as these factors have been known to affect the properties of the soils (stiffness, compressibility, etc.).
- During winter when temperatures fall below freezing, the soils freeze and experience heaving, transferring this effect to the structure. The deformations show a general upward trend, as the cumulative effect of frost heave seems to be greater than settlement from thawing.
- As temperatures rise above freezing, ice starts to melt and the water content increases the soils become weaker, yielding to thaw settlement. Settlement can also be affected by a decline in the pore pressure, resulting in an increase of the effective stresses.
- Differential settlement has occurred between the approaching road and deck, the main reason for this being probably the lack of the joint-sealing layer over the structure, as water is believed to infiltrate into the backfill, giving room for erosion and the generation of ice lenses.
- Soil composition plays a significant factor on the soil's response to freezing and thawing, as the laboratory test showed, a soil with higher content of coarse-grained particles does not seem to be affected as much as a soil with higher content of fine-grained particles, as the soil with higher fine-grained content experiences larger deformations.

Acknowledgments

We would like to thank Mr. Jeff Newgard, and Mr. Joel Bautista, for helping with field surveying, and Mr. Xiaodong Wang (Buff) for helping with the installation of the equipment and laboratory testing. The Wisconsin Department of Transportation provided funding for this project.

References

AASHTO (2012). *AASHTO LRFD Bridge Design Specifications*, American Association of State Highway and Transportation Officials, Washington, D. C.

Abu-Hejleh, N., Zornberg, J.G., Wang, T., and Watcharamonthein, J. (2002). "Monitored displacements of unique geosynthetic-reinforced soil bridge abutments." *Geosynth. Int.*, 9(1), 71-95.

Adams, M., Ketchart, K., Ruckman, A., DiMillio, A.F., Wu, J., and Satyanarayana, R. (1999). "Reinforced soil for bridge support applications on low-volume roads." *Transport. Res. Rec.*, 1652, 150-160.

Adams, M., Nicks, J., Stabile, T., Wu, J., Schlatter, W., and Hartmann, J. (2011). "Geosynthetic Reinforced Soil Integrated Bridge System, Synthesis Report." *Report No. FHWA-HRT-11-027*, Federal Highway Administration, U.S. Department of Transportation, Washington, DC.

Anochikwa, C.I., van der Kamp, G., and Barbour, S.L. (2012). "Interpreting pore-water pressure changes induced by water table fluctuations and mechanical loading due to soil moisture changes." *Can. Geotech. J.*, 49(3), 357-366.

Bao, H., Koike, T., Yang, K., Wang, L., Shrestha, M., and Lawford, P. (2016). "Development of an enthalpy-based frozen soil model and its validation in a cold region in China." *J Geophys Res-Atmos*.

Beshr, A.A.A., and Abo Elnaga, I.M. (2011). "Investigating the accuracy of digital levels and reflectorless total stations for purposes of geodetic engineering." *Alexandria Eng. J.*, 50(4), 399-405.

Briaud, J.-L., Maher, S.F., and James, R.W. (1997). "Bump at the end of the bridge." *Civ. Eng.*, 67(5), 68-69.

Elhassan, I.M., and Ali, A.S. (2011). "Comparative study of accuracy in distance measurement using: Optical and digital levels." *J. King Saud Univ. Eng. Sci.*, 23(1), 15-19.

Farouki, O.T. (1981). "Thermal Properties of Soils." *Report No. CRREL Monograph 81-1*, United States Army Corps of Engineers, Hanover, New Hampshire.

GLM-Laser (2015). "The Total Station SET 4 made by Sokkisha." <http://www.glm-laser.com/glm/452-1-Sokkisha-SET-4.html>. (Jan. 5, 2016).

Helwany, S.M.B., Koutnik, T.E., and Ghorbanpoor, A. (2007). "Evaluation Bridge Approach Settlement Mitigation Methods." University of Wisconsin-Milwaukee, Milwaukee, WI.

Helwany, S.M.B., Wu, J.T.H., and Froessl, B. (2003). "GRS bridge abutments - an effective means to alleviate bridge approach settlement." *Geotext. Geomembranes*, 21(3), 177-196.

Holtz, R.D., Kovacs, W.D., and Sheahan, T.C. (2011). *An introduction to geotechnical engineering*, Prentice Hall, New Jersey.

Jilin, Q., Yu, S., Jianming, Z., and Zhi, W. (2007). "Settlement of embankments in permafrost regions in the Qinghai-Tibet Plateau." *Norwegian J. Geog.*, 61(2), 49-55.

Keller, G.R., and Devin, S.C. (2003). "Geosynthetic-reinforced soil bridge abutments." *Transport. Res. Rec.*, 1819, 362-368.

Kim, D.-S., Seo, W.-S., and Kim, M.-J. (2003). "Deformations characteristics of soils with variations of capillary pressure and water content." *Soils Found.*, 43(4), 71-79.

Kim, J.-M. (2000). "A fully coupled finite element analysis of water-table fluctuation and land deformation in partially saturated soils due to surface loading." *Int. J. Numer. Meth. Eng.*, 49(9), 1101-1119.

Lambe, T.W., and Whitman, R.V. (1969). *Soil Mechanics*, John Wiley & Sons, Inc., New York.

Li, Q.-l., Ling, X.-z., Wang, L.-n., Zhang, F., Wang, J.-h., and Xu, P.-j. (2013). "Accumulative strain of clays in cold region under long-term low-level repeated cyclic loading: Experimental evidence and accumulation model." *Cold Reg. Sci. Technol.*, 94, 45-52.

Loáiciga, H.A. (2013). "Consolidation Settlement in Aquifers Caused by Pumping." *J. Geotech. Geoenviron. Eng.*, 139(7), 1191-1204.

Long, J.H., Olson, S.M., Stark, T.D., and Samara, E.A. (1998). "Differential Movement at Embankment–Bridge Structure Interface in Illinois." *Transport. Res. Rec.*, 1633, 53-60.

Ma, W., Mu, Y., Wu, Q., Sun, Z., and Liu, Y. (2011). "Characteristics and mechanisms of embankment deformation along the Qinghai–Tibet Railway in permafrost regions." *Cold Reg. Sci. Technol.*, 67(3), 178-186.

Md. Noor, M.J., Mat. Jidin, R., and Hafez, M.A. (2008). "Effective stress and complex soil settlement behaviour." *Electron. J. Geotech. Eng.*, 13 H, 1-13.

Michal, O., and Urban, R. (2015). "Temperature effects on the bridge structure during the all-day monitoring." *Geoinformatics FCE CTU*, 14(1), 79.

Ming, F., and Li, D.-q. (2016). "A model of migration potential for moisture migration during soil freezing." *Cold Reg. Sci. Technol.*, 124, 87-94.

Ming, F., Li, D.Q., and Zhang, K. (2012). "Theoretical study on thaw settlement of saturated frozen soil." *2012 International Conference on Civil, Architectural and Hydraulic Engineering, ICCAHE 2012*, Trans Tech Publications, 155-162.

Mitchell, J.K., and Soga, K. (2005). *Fundamentals of Soil Behavior*, John Wiley & Sons, Inc., Hoboken, New Jersey.

Mohamed, K., Abouzakhm, M., and Elias, M. (2011). "Applications and Performance of Geosynthetic-Reinforced Soil Abutments on Soft Subsurface Soil Conditions." *Transport. Res. Rec.*, 2212, 74-81.

Moulton, L.K., GangaRao, H.V.S., and Halverson, G.T. (1985). "Tolerable movement criteria for highway bridges." *Report No. FHWA/RD-85/107*, Federal Highway Administration, U.S. Department of Transportation, Washington, DC.

Moulton, L.K., and Kula, J.R. (1980). "Bridge Movements and Their Effects." *Public Roads*, 44(2), 62-75.

Nicks, J.E., and Briaud, J.-L. (2007). "Preliminary evaluation of the bump at the end of the railway bridge." 2007 ASME/IEEE Joint Rail Conference and the ASME Internal Combustion Engine Division, Spring Technical Conference, JRCICE 2007, American Society of Mechanical Engineers, 227-240.

Özgan, E., Serin, S., Ertürk, S., and Vural, I. (2015). "Effects of Freezing and Thawing on the Consolidation Settlement of Soils." *Soil Mech. Found. Eng.*, 52(5), 247-253.

Qi, J., Ma, W., and Song, C. (2008). "Influence of freeze–thaw on engineering properties of a silty soil." *Cold Reg. Sci. Technol.*, 53(3), 397-404.

Qi, J., Yao, X., and Yu, F. (2013). "Consolidation of thawing permafrost considering phase change." *KSCE J. Civ. Eng.*, 17(6), 1293-1301.

Shahriar, M.A., Sivakugan, N., Das, B.M., Urquhart, A., and Tapiolas, M. (2015). "Water Table Correction Factors for Settlements of Shallow Foundations in Granular Soils." *Int. J. Geomech.*, 15(1), 06014015.

Shahriar, M.A., Sivakugan, N., Urquhart, A., Tapiolas, M., and Das, B.M. (2013). "A Study on the Influence of Ground Water Level on Foundation Settlement in Cohesionless Soils." *Proceedings of the 18th International Conference on Soil Mechanics and Geotechnical Engineering*, International Society for Soil Mechanics and Geotechnical Engineering (ISSMGE), 953-956.

Shoop, S.A., and Bigl, S.R. (1997). "Moisture migration during freeze and thaw of unsaturated soils: Modeling and large scale experiments." *Cold Reg. Sci. Technol.*, 25(1), 33-45.

Skinner, G.D., and Rowe, R.K. (2005). "Design and behaviour of a geosynthetic reinforced retaining wall and bridge abutment on a yielding foundation." *Geotext. Geomembranes*, 23(3), 234-260.

Syverson, K.M. (2007). "Pleistocene Geology of Chippewa County, Wisconsin." Wisconsin Geological and Natural History Survey.

Viswanadham, B.V.S., and König, D. (2009). "Centrifuge modeling of geotextile-reinforced slopes subjected to differential settlements." *Geotext. Geomembranes*, 27(2), 77-88.

Wahls, H.E. (1990). "NCHRP Synthesis of Highway Practice 159: Design and Construction of Bridge Approaches." National Cooperative Highway Research Program, Transportation Research Board, National Research Council, Washington, D.C.

Wang, S., and Liu, F. (2015). "A Hypoplasticity-Based Method for Estimating Thaw Consolidation of Frozen Sand." *Geotech. Geol. Eng.*, 33(5), 1307-1320.

White, D.J., Mekkawy, M.M., Sritharan, S., and Suleiman, M.T. (2007). "“Underlying” Causes for Settlement of Bridge Approach Pavement Systems." *J. Perform. Constr. Facil.*, 21(4), 273-282.

Zhang, Y., and Michalowski, R. (2015). "Thermal-Hydro-Mechanical Analysis of Frost Heave

and Thaw Settlement." *J. Geotech. Geoenviron. Eng.*, 141(7), 04015027.

Figures

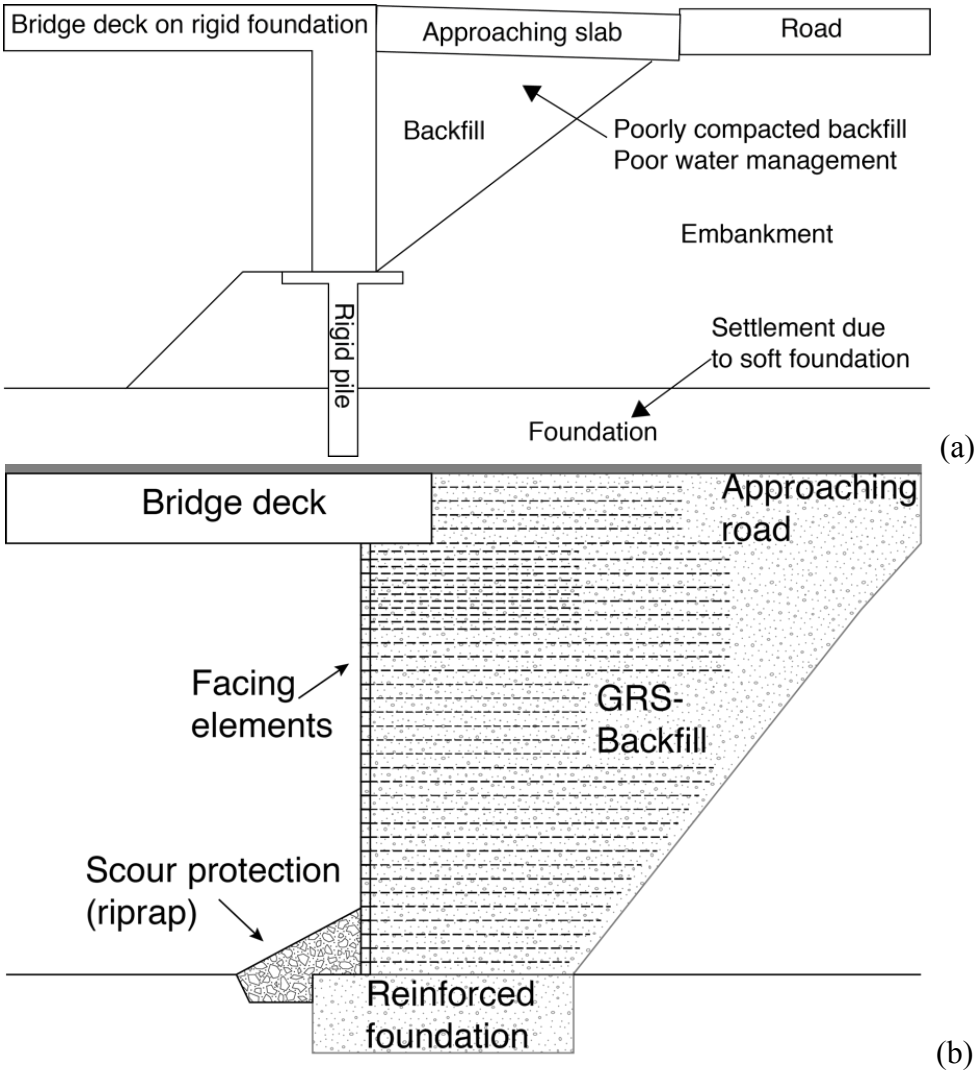

Figure 3.1. (a) Typical cross-section of a deep foundation system and causes for differential settlement. (b) Typical cross-section of a Geosynthetic Reinforced Soil-Integrated Bridge System (GRS-IBS).

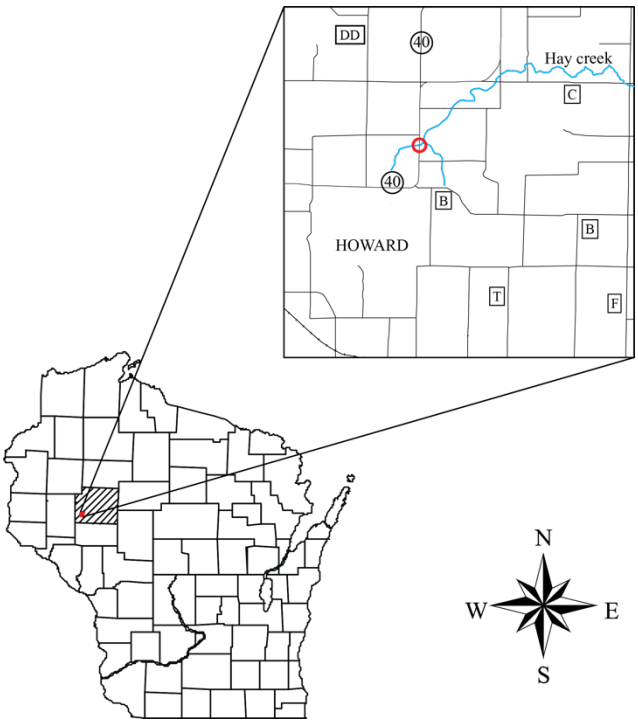

(a)

(b)

Figure 3.2. (a) Location of the GRS-IBS bridge. The red circle indicates the location of the bridge. (b) Picture of the GRS-IBS bridge.

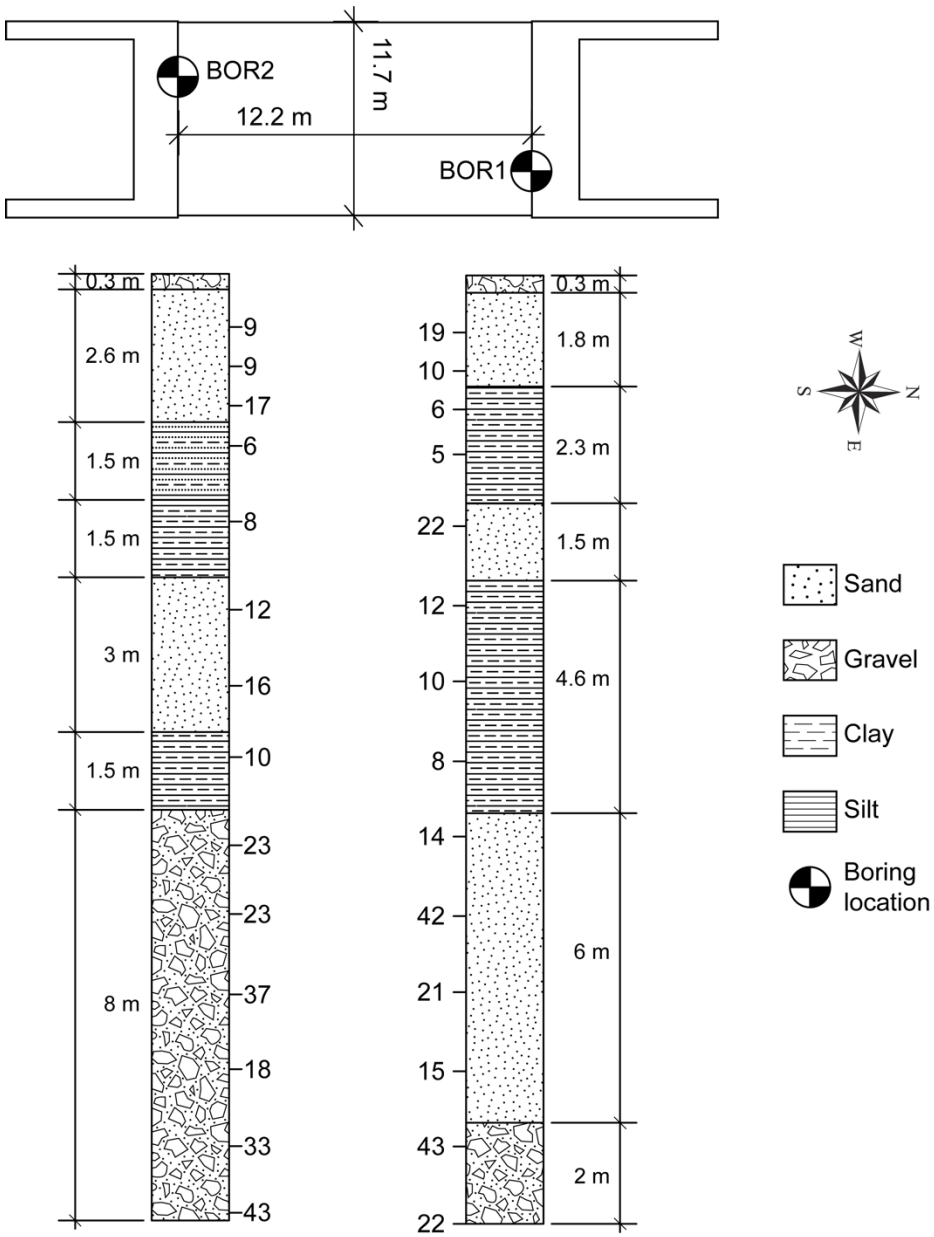

Figure 3.3. Subsurface exploration data for the GRS-IBS bridge at Bloomer

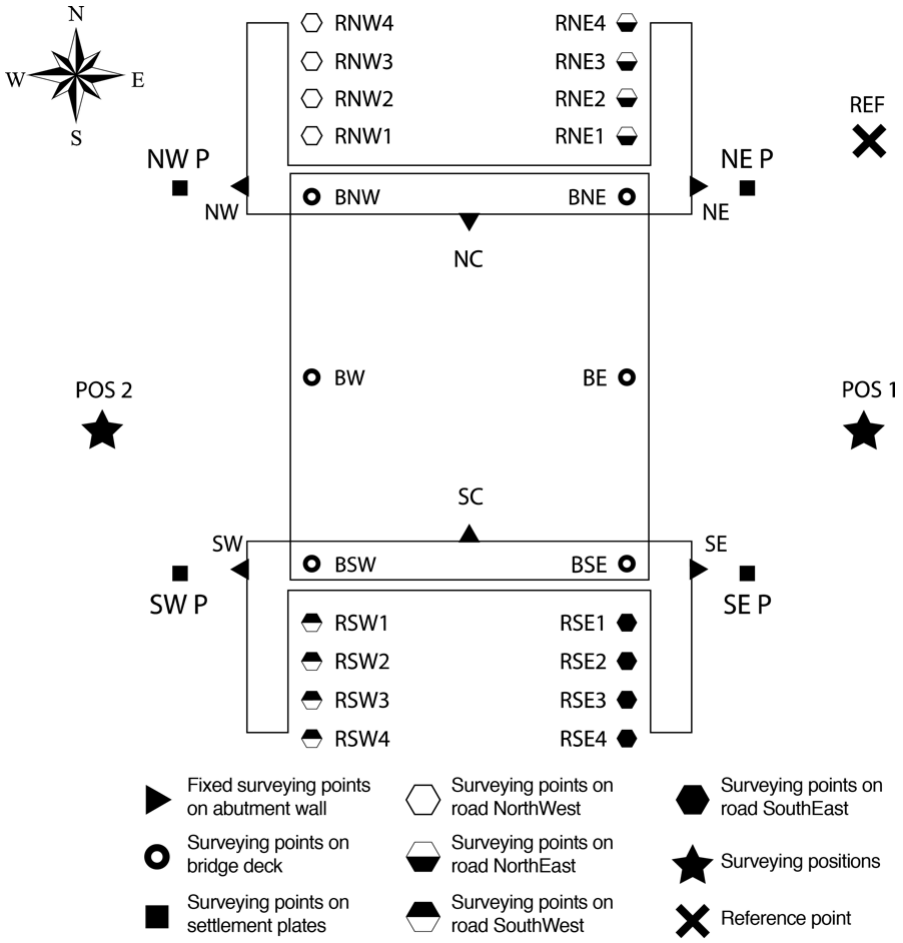

Figure 3.4. Location of the surveying points at the bridge in Bloomer.

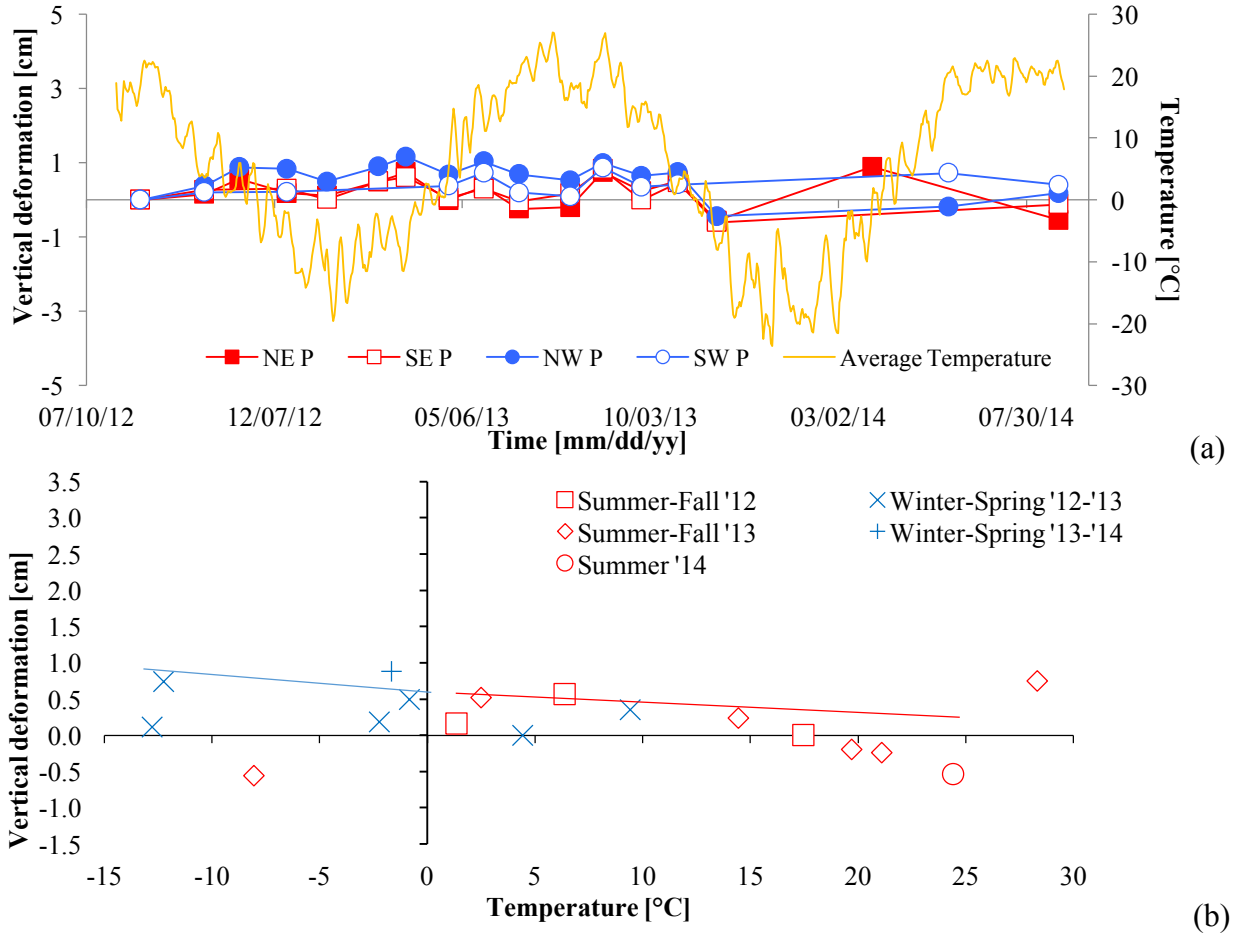

Figure 3.5. (a) Relative vertical deformation of settlement plates with respect to the reference point. Positive values correspond to upward movement. (b) Vertical deformation of NE settlement plate versus temperature, separated by temperature cycles. Warm periods correspond to minimum temperatures above zero and cold periods are the opposite.

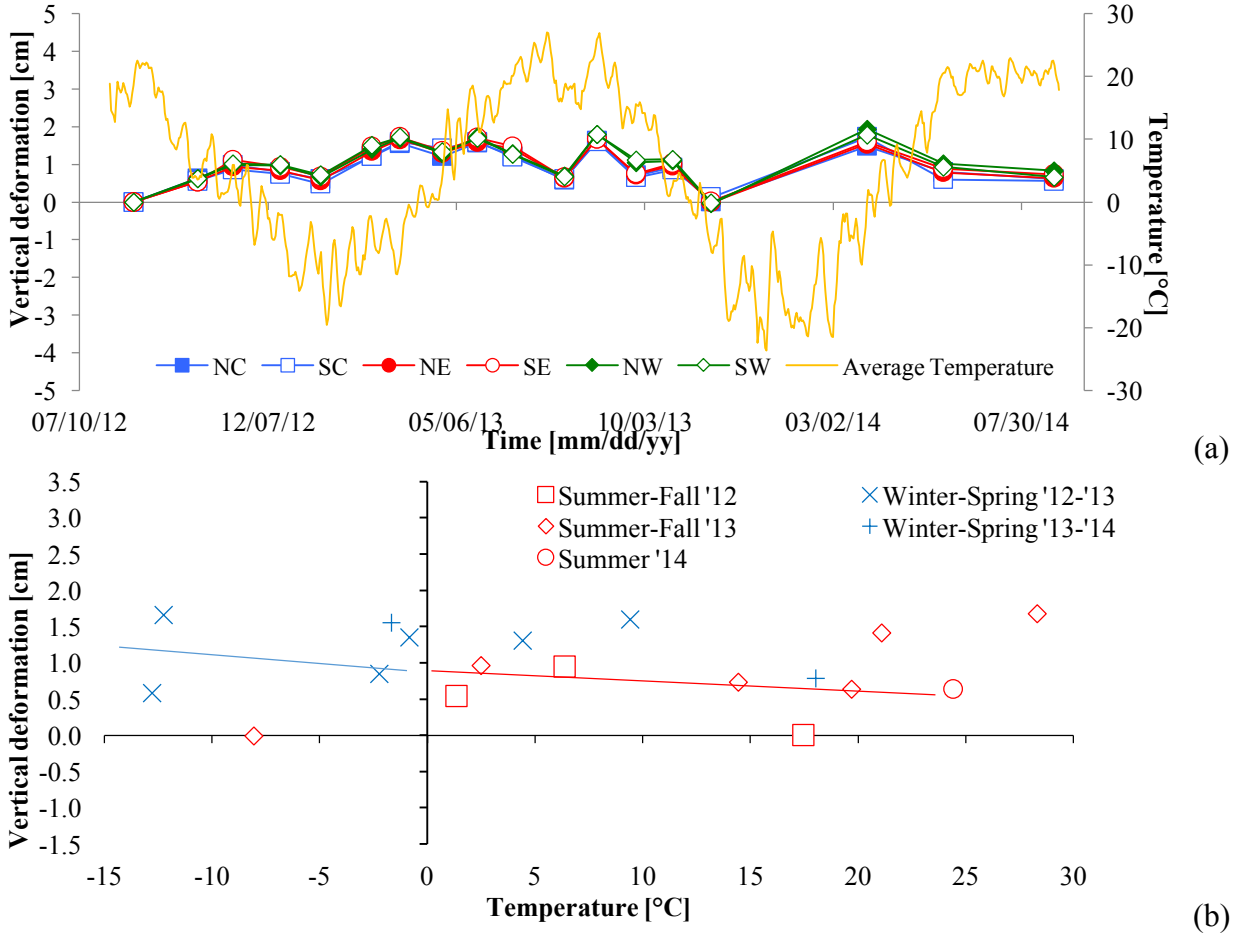

Figure 3.6. (a) Relative vertical deformation on the reinforced abutment walls with respect to the reference point. Positive values correspond to upward movement. (b) Vertical deformation of NE wall versus temperature, separated by temperature cycles. Warm periods correspond to minimum temperatures above zero and cold periods are the opposite.

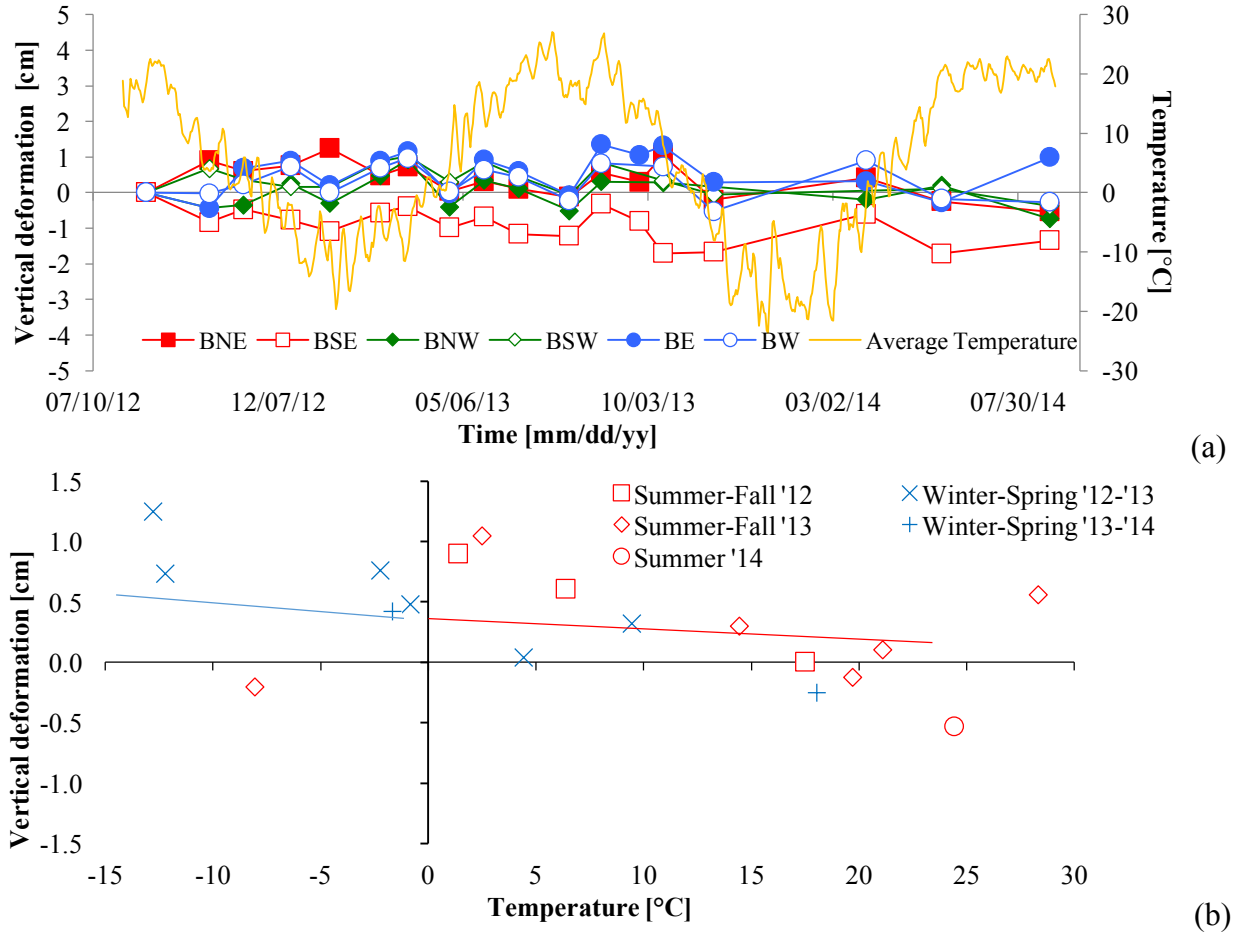

Figure 3.7. (a) Relative vertical deformation on the bridge deck with respect to the reference point. Positive values correspond to upward movement. (b) Vertical deformation of NE deck versus temperature, separated by temperature cycles. Warm periods correspond to minimum temperatures above zero and cold periods are the opposite.

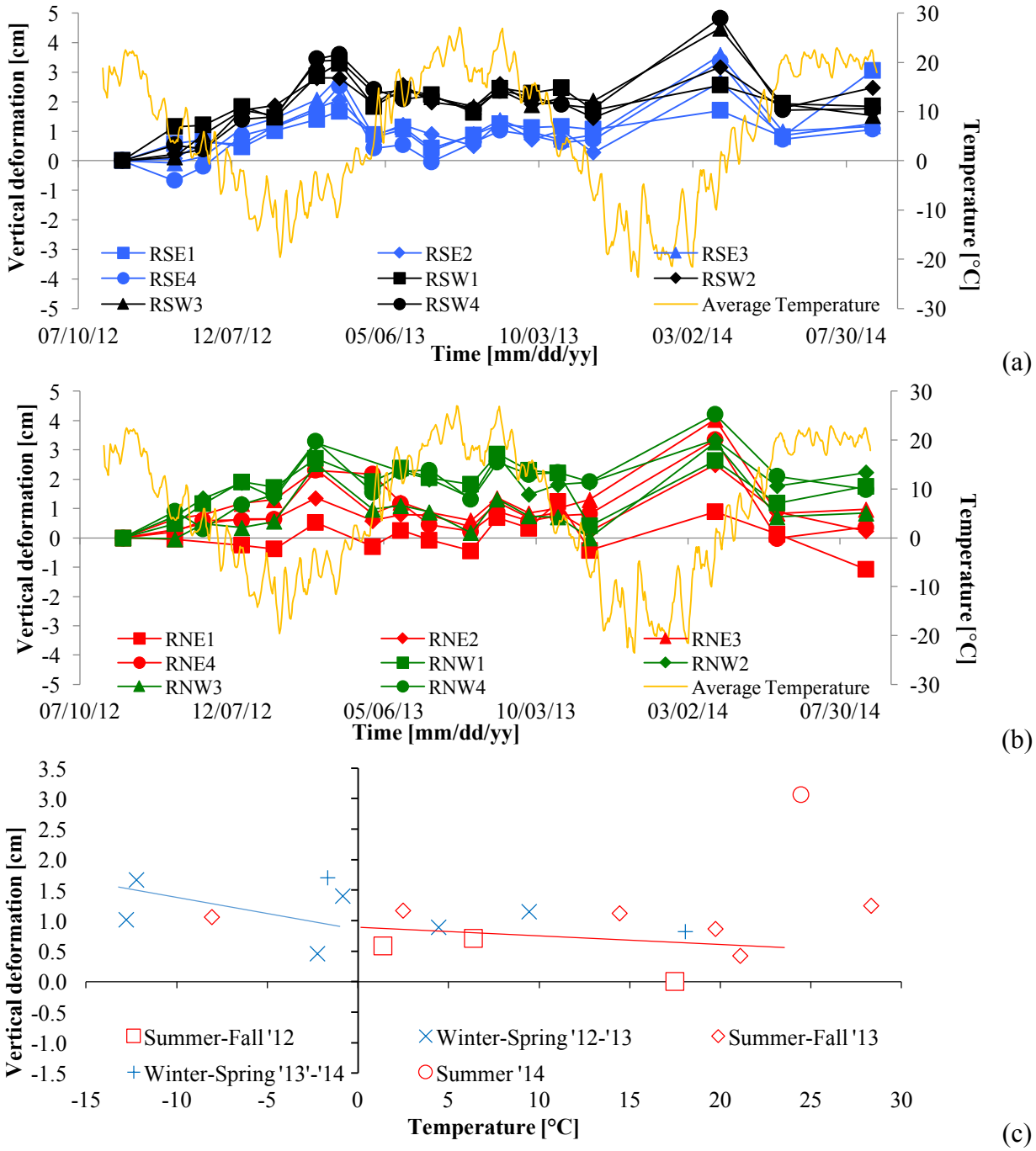

Figure 3.8. Relative vertical deformation on the (a) south approaching road and (b) north approaching road with respect to the reference point. Positive values correspond to upward movement. (c) Vertical deformation of SE road versus temperature, separated by temperature cycles. Warm periods correspond to minimum temperatures above zero and cold periods are the opposite.


(a)


(b)

Figure 3.9. (a) Crack observed in May of 2013 at the edge between the deck (bottom) and approaching road (top) at the south-east end. (b) New crack observed in March 2014 right next to the old one.

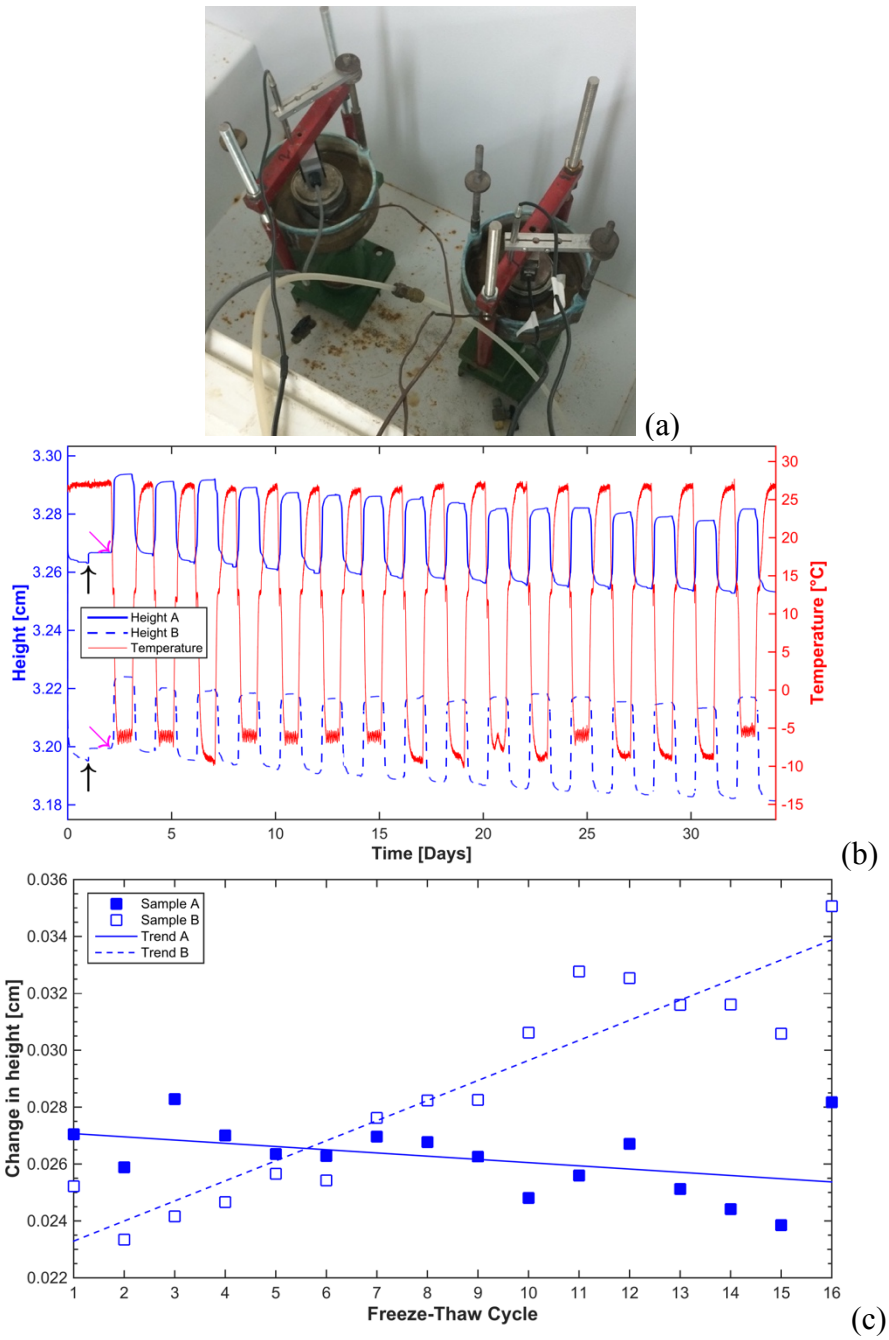

Figure 3.10. (a) Set up for the freezing and thawing experiment. (b) Results of the freezing and thawing experiment on two different sand-silt mixtures, sample A is 90% sand and 10% silt and sample B is 50% sand and 50% silt. Black arrow marks the end of unloading, magenta arrow marks end of unloading and start of freeze-thaw cycles. The 32 days of measurements correspond to the 16 freeze-thaw cycles on Figure 3.10c. (c) Change in height for each freeze-thaw cycle for both samples, with the 16 cycles corresponding to the 32 days of measurements on Figure 3.10b.

CHAPTER 4: Finite Element Modeling of a Geosynthetic-Reinforced Soil Bridge – Service and Temperature Loads

Maximiliano Garnier-Villarreal[1]; Dante Fratta[2]; and Michael Oliva[3]

Abstract: Geosynthetic Reinforced Soil systems have been implemented in different types of structures to improve their performance regarding deformations and bearing capacity. Geosynthetic Reinforced Soil – Integrated Bridge System (GRS-IBS) has been specifically implemented in transportation structures as an alternative to costlier, time consuming typical deep foundations. GRS-IBS helps to alleviate the issue with differential settlements between road and deck. This study focuses on the numerical modeling of a short span GRS-IBS bridge that replaced an old bridge going over a seasonal creek. The numerical modeling considers several loading scenarios, including different traffic and thermal loads, looking also at the structural integrity of the deck for cracking. The results of the traffic load analyses show that none of the considered scenarios would cause a deformations or stresses large enough that would reach the specified limits for critical deformation or stress. The thermal load analyses show how the structure is affected by temperature as it experiences frost heave when the water in the pore space freezes, but mechanical and hydrological mechanisms are expected to control the deformations as temperatures rise. In conclusion, the structure shows good response to traffic loads and seems to be influenced by environmental factors as temperature changes.

[1] Graduate Student. Geological Engineering. University of Wisconsin-Madison. Madison, WI 53706. USA. Email: garniervilla@wisc.edu.
[2] Associate Professor. Geological Engineering. University of Wisconsin-Madison. Madison, Wisconsin 53706. Email: fratta@ wisc.edu.
[3] Emeritus Professor. Civil and Environmental Engineering. University of Wisconsin-Madison. Madison, Wisconsin 53706. Email: oliva@engr.wisc.edu.

Keywords: GRS-IBS; Shallow foundation; Temperature; Frost-heave; Finite element analysis.

4.1 Introduction

Geosynthetic Reinforced Soils (GRS) have been used in different types of structures to improve their performance, including reinforced flexible pavements, soils supporting structures with shallow foundations, and abutment and embankments for highway structures (Erickson and Drescher 2001; Skinner and Rowe 2003; Siriwardane et al. 2008; Al-Azzawi 2012; Belal et al. 2015). More specifically Geosynthetic Reinforced Soil – Integrated Bridge Systems (GRS-IBS) have been used in transportation structures to alleviate the differential settlement issue between road and deck, known as the "bump at the end of the bridge". These systems also offer advantages over more conventional supporting systems, including cost, construction time, and ease of implementation in remote areas (Adams et al. 1999; Abu-Hejleh et al. 2002; Helwany et al. 2003; Keller and Devine 2003; Mohamed et al. 2011). Main disadvantages include the small size of these structures (spans less than 42.6 m (140 ft)) and the need of special consideration for prevent erosion of the reinforced soils when the structures run across creeks or small rivers. Adams et al. (1999) provide the rest of the specifications needed for implementing this type of construction on bridges, including a height of less than 9.1 m (30 ft), a separation of the geosynthetic reinforcement of 30 cm (12 in) or less, a deck span less than 42.6 m (140 ft), and a bearing stress less than 191.5 kPa (27.8 psi).

Figure 4.1a shows a typical cross section for a GRS-IBS system. In general, the system consists of a reinforced abutment, foundation, and approach roadway. The design also creates a jointless transition between the approaching roadway, abutment, and bridge deck. The deck is

supported by the reinforced abutment, which consists of lifts of compacted backfill with layers of geosynthetic reinforcement in between. The foundation is sometimes also reinforced with geosynthetic to provide a higher bearing capacity for the system. Both surface scour and internal erosion has to be considered and taken care of when the system is to go over small rivers or creeks (Adams et al. 1999).

Finite element analysis has been used to model GRS structures to try to understand and extrapolate the behavior of the reinforced soil as part of the IBS structure. Emphasis was placed on how reinforcement relates to design properties (i.e., geosynthetic spacing and length) and material parameters (i.e., geosynthetic, backfill, and facing stiffness) and how design parameters influence the behavior of bridge.

As mentioned by Adams et al. (1999) the use of small separation between geosynthetic layers has a more significant effect than using fewer layers with stiffer geosynthetic layers. This statement has been corroborated by other researchers (Helwany et al. 2007; Liu et al. 2009; Belal et al. 2015), finding that decreasing the separation between reinforcement layers reduces the deformations of the system (Helwany et al. 2007). Also, it has been presented that increasing the length or width of the reinforcing layers improves the performance of the system, by reducing the deformations and increasing the bearing capacity, but only up to a certain point. When the embedment length reaches 75% of the embankment span the deformation becomes constant (Ling et al. 1995; Liu et al. 2009; Belal et al. 2015).

The properties of other materials (e.g., soils, wall facing elements, pavement), not only the geosynthetic, also have an important impact on the behavior of the system. As the stiffness of the different materials (e.g., backfill and facing blocks) increase, the deformations experienced by the system overall decrease. Similar to the length of the reinforcement, there is a point that

increasing the stiffness, specially of the geosynthetic material result in minimal return in the decrease of the deformations (Ling et al. 1995; Wathugala et al. 1996; Erickson and Drescher 2001; Han and Gabr 2002; Skinner and Rowe 2005; Helwany et al. 2007; Huang et al 2009; Liu et al 2009; Belal et al 2015). Another property that has been consider of lesser importance, until recent studies, is the creep of the reinforced soil. In some cases, especially for fine-grained soils, soil creep can control the long-term deformation of the system, even more than the creep of the reinforcement. Therefore, when dealing with fine-grained soils creep has to be considered (Helwany and Wu 1995; Liu et al. 2009).

The effects of the foundation soil supporting these structures have been investigated by Skinner and Rowe (2003; 2005) and Viswanadham and König (2009). The researchers studied specifically the effects of yielding (soft, viscous) foundations. Their results show that when a structure is resting on a yielding foundation differential settlements tend to occur, but the use of reinforcement layers can help decrease the magnitude of these deformations and also avoid failure of the foundation.

Environmental factors also influence the deformation of foundation soils and the structures these support (e.g., temperature, moisture content changes, freezing and thawing, etc.). The effect of temperature changes and the resulting freezing and thawing on foundation soils has been documented and studied by several researchers. Freezing and thawing cycles can affect the arrangement and density of soils, densifying loose soil and loosening dense soils (Qi et al. 2008). Frost heaving can happen as water in the pore space freezes causing the soils to expand, and once the ice melts and thaws the soil will experience settlement or shrinkage (Ma et al. 2011; Ming et al. 2012; Zhang and Michalowski 2015). Depending on the composition and particle distribution of the soil, foundations behave differently under freezing and thawing. Fine-grained soil can

experience a cumulative heave over time, as they are more susceptible to water content changes (Mitchell and Soga 2005), while coarse-grained soils may experience settlement over time (Ma et al. 2011; Li et al. 2013; Özgan et al. 2015; Zhang and Michalowski 2015). Moreover, these temperature changes can also affect the properties of soils, making them stronger, stiffer, and less permeable as freezing of the pore fluid occurs, and the changes of these properties are reverse as the ice melts and thaws (Özgan et al. 2015; Qi et al. 2008; Wang and Liu 2015; Zhang and Michalowski 2015).

The objective of this study is to systematically evaluate the behavior of the structural and geotechnical elements of a GRS-IBS system by modelling their response to design traffic loads and environmental (i.e., temperature) loads, making use of the general purpose finite element package ANSYS, and compare some of the numerical results with field data.

4.2 Studied bridge

The studied bridge is located near the City of Bloomer, Chippewa County in the State of Wisconsin (Figure 4.2). The road serves the farming community in the area and recently is being used by large trucks hauling silica sand used in fracking operations in the oil patch. The design traffic for this bridge is HL-93 (AASHTO 2012) and Wisconsin Standard Permit (WisDOT 2015). The deck is 12.2 m (40 ft) long by 11.7 m (38.4) wide, and it is supported by a geosynthetic reinforced soil. The reinforced soil acts as the abutment for the bridge deck. The geosynthetic layers are a biaxial woven polypropylene with a wide width tensile strength of 70 kN/m (4800 lb/ft), spaced 20 cm (7.87 in) near the bottom and 10 cm (3.94 in) near the top, with different lengths (1.8 to 4.3 m or 5.9 to 14.1 ft), not covering the whole area of the backfill (see Figure 4.1b). Foundation soils comprise mostly of sandy soils with presence of clay and silt

mixed with the sand or as separate layers (Figure 4.3). The foundation soils in the area are considered as dense or over-consolidated, as this new structure is replacing an old bridge and the area was covered by most recent glaciation (Syverson 2007).

4.3 Validation of Finite Element Analysis

The finite elements analysis package ANSYS was used in this study to analyze the response of the bridge to a number of different loading and design condition scenarios. However, before a full analysis was performed, a validation was used to determine if the results obtained using the general purpose finite element software ANSYS are in agreement with analytical solutions of known elastic problems commonly used in geotechnical problems.

4.3.1 Elastic problem to analyze

The problem to solve corresponded to a case presented by Poulos et al. (1972) in relation to the deformation that a homogeneous embankment experience due to self-weight loading. Poulos et al. (1972) present dimensionless solutions for five different cases, going from a lift height (h) to final height (H) ratio equal to 0.2 to h/H equal to 1, which would represent a triangular embankment; these solutions use an assumption of a slope angle equal to $\beta=30°$, and a Poisson's ratio equal to $\nu=0.3$. For each case Poulos et al. (1972) present solutions for displacements in the horizontal and vertical directions. The case of h/H=0.6 was chosen as the one to replicate using ANSYS. The solutions for the chosen case are shown in Figure 4.4 for a set of properties presented in Table 4.1.

4.3.2 Finite element analysis validation

The finite element model, as well as the analytical solutions, make use of symmetry, thus only half of the embankment was modeled. The selected finite element consists of 8-node quadrilateral elements with 2 degrees of freedom (dof), horizontal and vertical translation, with the plane strain option. The boundary conditions were defined as a horizontal constrain at the right and bottom edges and a vertical constrain at the bottom edge this to simulate the rough rigid base assumed by Poulos et al. (1972) in their solutions. The applied loads correspond to the self-weight of the structure.

The results from the analysis and their comparison with the analytical solutions are shown in Figures 4.5 and 4.6 as nodal solutions and contour plots comparison. The analytical solutions from Poulos et al. (1972) are compared to the ANSYS solution at nodal locations (Figures 4.5a and 4.6a). For the vertical displacement case nodal solutions at the center of the embankment (right boundary) were taken where the analytical contour plots intersect with the boundary. For the horizontal displacement case nodal solutions where the analytical contour plots intersect at mid-height and across the length of the embankment were taken. Also, by superimposing the analytical contour plots on top of our ANSYS solutions (Figures 4.5b and 4.6b) a general comparison can be drawn. From this finite element analysis, it can be concluded that both analytical and numerical solutions, the nodal solution at the model boundaries and the contour plots, show good agreement for the specific case presented by Poulos et al. (1972). The results from this validation analysis shows that ANSYS can provide good approximate solutions for known problems with the understanding that an error would usually be associated with any numerical simulation solution.

4.4 Geosynthetic-Reinforced Soil Bridge Modeling

The finite element model used in this study is a 3D linear elastic model of the geosynthetic-reinforced bridge. The different elements of the finite element model consist of 8-node brick elements with 3 translational degrees of freedom (dof) for the solid bodies, 4-node shell elements with 6 dof (rotational and translational) for the geosynthetic layers, and surface-to-surface frictional contact elements to model the interaction between the different parts and elements, with a friction coefficient μ=0.5. The membrane option was chosen to model the shell elements, resulting in elements with only 3 translational dof, as rotation is not expected to play a significant role in the deformations. The backfill and foundation soil are modeled as homogeneous elements. The model is constrained vertically at its bottom and laterally at its ends. The properties of the materials used in this study are shown in Table 4.2. The first part of the analysis focuses in the backfill-geosynthetic interaction and the effect of the geosynthetic properties and friction angle of backfill soil. Finally, the full model is analyzed under different loading cases (traffic and temperature) to study the behavior of the whole system.

4.4.1 Effect of geosynthetic elastic properties

To understand the effect of the stiffness of the geosynthetic layers on the deformations, a small model was setup, and different stiffness values were assigned to the geosynthetic layers, using a friction coefficient of μ=0.5 between the backfill soil and geosynthetic layers. The model was vertically constrained at its bottom and fully constrained at its back. A uniform load of 1100 kN (250 kips) was used as the design load and applied uniformly to the nodes at the top of the model. Four different stiffness values were analyzed (0.49 GPa, 7 GPa, 70 GPa, and 700 GPa). The first value corresponds to the stiffness of the geosynthetic used at the bridge in Bloomer. According to the geosynthetic specification sheet, the tensile stress of the geosynthetic at

different strain levels were plotted and fitted using a linear regression (R^2=0.992). The slope of this fit corresponds to the tensile modulus (T = 983.98 kN/m (67 400 lb/ft)). The Young's modulus (E = 492 MPa (71.3 ksi)) was obtained using Equation 4.1, for an assumed geosynthetic thickness of t = 2 mm (0.08 in).

$$E = \frac{T}{t} \tag{4.1}$$

The last three stiffness values that are analyzed correspond to 100, 1000, and 10000 times the stiffness of the backfill material (70 MPa (10.1 ksi)). A summary of the results is shown in Figure 4.7a. The numerical results show that by increasing the geosynthetic stiffness, from the stiffness used in the field, both vertical and horizontal deformations decrease. For the highest geosynthetic stiffness analyzed here the vertical and horizontal deformations decreased by 12% and 32% respectively. These results show the effect of increasing the stiffness of the geosynthetic. As the objective of adding reinforcements is to alleviate or reduce the deformations on the backfill (to reduce differential settlement) it is important to establish the necessary properties to address the desired problem. Please note that these results indicate that greatly increasing stiffness only marginally decrease the deformation indicating that there is point of diminishing return.

4.4.2 Effect of friction angle and shear intercept

The effects of the backfill's friction angle and shear intercept (cohesion) were analyzed to evaluate the stability of the system. When using friction angle as a material property a shear intercept must be used in the analysis (it can not be zero) to provide stability during the numerical modelling. When changing the friction angle a shear intercept of 5 kPa was used during the analysis while the friction angle was varied between 25 and 60 degrees. When

changing the shear intercept a friction angle of 40 degrees was used while the shear intercept was varied between 3 and 20 kPa. A friction coefficient of μ=0.5 was used between the backfill soil and geosynthetic layers, and the model was vertically constrained at its bottom and fully constrained at its back. The geosynthetic had a stiffness of 492 MPa, corresponding to the value used at the bridge in Bloomer.

Figures 4.7b and 4.7c show the results of varying the friction angle and shear intercept. The friction angle and shear intercept should not affect the deformation of the system, as deformation depends only on Young's modulus and Poisson's ratio, but they can have an effect on the stability of the system, as these are strength parameters. Therefore, the larger deformations at the lower friction angles and shear intercepts probably indicate that the system was in an unstable condition. The results indicate that for the applied load a friction angle of 30 degrees or more and a shear intercept of 6 kPa or more would be necessary for the system to be in a stable condition. Helwany et al. (2007) studied the effect of backfill soil type, using different soils with different friction angles and different stiffness, correlating stiffer soils with higher friction angles. As they changed both properties the effect of friction angle can not be singled out, but as it would be expected the soil they assigned the higher stiffness and friction angle experiences lesser deformations.

4.4.3 Service (Traffic) loading

Different service (traffic) loading cases were analyzed to study the behavior of the structure under such different conditions. The traffic loading cases were: uniform load distribution, induced differential settlement, truck load, and truck load plus induced differential settlement. The analyses were performed by comparing the resulting stresses in the superstructure (deck) to the cracking stress of the concrete. The calculated cracking stresses for concrete was 3.3 MPa

(475 psi), modified after ACI (2011) specifications (Equation 4.2). The results were used to compare the integrity of the deck under the loading cases. This study was performed because the road right next to the deck of the bridge in Bloomer experienced cracking and it was important to evaluate if the crack was not related to traffic loads. A summary of the results from the different loading cases is shown in Table 4.3. The results of the different loading cases are shown in the figures in Appendix D.

$$\sigma_{crack} = 0.0623 \text{ MPa} \sqrt{\frac{10 \cdot f_c}{P_a}} \quad (4.2)$$

where f_c is the compressive strength of concrete, Pa is the reference pressure and is taken equal to the atmospheric pressure of 0.1 MPa.

For the first case, a uniform load of 1100 kN (250 kips) was applied to the nodes of the deck, as this corresponds to the design traffic load (Wisconsin Standard Permit Vehicle - WisDOT 2015). This loading condition was achieved by calculating the equivalent pressure for the area of the deck, which turned out to be 7.68 kPa (1.1 psi). Results show that the largest vertical deformation happens at the middle of the deck as it would be expected for a simple supported beam.

Next, differential settlement, under the foundation, was simulated using what ANSYS calls "kill" elements (Figure 4.8a). "Killed" elements are assigned a low stiffness factor (e.g., 10^{-6} Pa) to simulate a soft spot or completely remove their effect in the analysis. By "killing" just some elements at the bottom of the foundation and by leaving the rest as active elements the effect of differential settlement can be simulated. As the location and dimensions of soft spots or layers can vary, the chosen number of "killed" elements and size of the removed patch represent a possible scenario, in this case approximately one-third of the length of the foundation and the bottom most elements. Two locations were chosen to simulate differential settlement: South-East

corner and North-East corner. For this loading case the load was kept uniformly distributed on the deck.

After simulating the differential settlements, the maximum deformations, granted that these occur at different locations, yielded larger values than when no differential settlement was induced. These results show that depending on the location of a soft spot the maximum deformations will happen at or near where the soft spot was located, and these deformations will result in not only localized deformations but also their magnitude will be greater.

Lastly, a truck load of 355 kN (80 kips) was applied over and area of approximately 6.1 m by 2.4 m, based on the truck design used by AASHTO (2012) and maximum allowable weight for Wisconsin (WisDOT 2015). This is strictly a static loading and the dynamic effects were ignored. Differential settlements were also simulated for one of the cases. The load was positioned at different locations on the deck (Figure 4.8b). In general, when the truck loads (355 kN per truck) were located at the corners of the deck the deformation was smaller than for previous cases, which could be expected as the load was less than the full, uniformly distributed design traffic load. The largest deformation and stress happened for the case where settlement was induced with two trucks close to the center of the deck (Figure 4.9), with the largest vertical deformation happening where the settlement was induced, as the stiffness of this area is smaller than any other are in the model.

In summary, none of the loading cases yielded signs that the deck would suffer from cracking due to traffic loads, as the largest deviatoric stress experienced by the structure was smaller than the cracking stress by a factor of 3 (3.3 MPa/1.08 MPa = 3.1). Additionally, the maximum vertical deformation experienced by the system, for the studied cases and conditions,

was less than 1.3 cm (0.5 in), which is considered a threshold for differential settlement to start becoming a problem (Wahls 1990).

4.4.4 Thermal validation

A transient heat transfer model validation was performed to confirm accurate modeling of heat transfer problems. The validation corresponded in simulating the result from example 2.11 from Kreith et al. (2011). The problem asks to find the depth at which the temperature will be 0 °C, when the soil has a uniform temperature of 20 °C and the ground surface has been exposed to a temperature of -15 °C for 60 days. The thermal properties of the soil are: ρ=2050 kg/m3, k=0.52 W/m-K, and c=1840 J/kg-K. The solution by Kreith et al. (2011) for this example is given as 0.68 m below the ground surface.

To model this problem a 2D transient heat transfer model was implemented using ANSYS, with the given thermal properties, and employing a 4-node thermal plane element with temperature as its dof. The step size used was 1 day (86400 s), with a total duration of 60 days (5184000 s). As mentioned in the example, a uniform temperature of 20 °C was applied to the entire soil area, and a temperature boundary condition of -15 °C was applied to the top of the model. The result of this analysis is shown in Figure 4.10, where the arrow on the right points to the 0 °C isotherm at a depth of 0.68 m, same as the analytical solution by Kreith et al. (2011), thus showing the ability of ANSYS to solve for this type of problem.

4.4.5 Temperature loading

For the temperature loads two identical models were used for each of the bridges: first, one transient heat transfer analysis and second, a structural analysis. The transient heat transfer analysis' results (heat distribution) were used as input for the structural analysis. The temperature

over time for each node is determined by the heat transfer analysis, this nodal temperature is then assigned to the corresponding node for the structural analysis as a loading condition. To account for the transient thermal effects density, specific heat and thermal conductivity were used as material properties. For the analyses a time step of one day (86400 s) was used. An initial uniform temperature of 12 °C was applied to the entire model, representing a time when the air temperature and soil temperature were approximately the same. This value (12 °C) represents an average ground temperature at approximately 4.7 m below the surface (bottom of the model) for this area of Wisconsin (WGNHS 2016). The thermal properties used in the analysis are shown in Table 4.4. To simulate the effect of changing air temperature on the system, temperatures ranging from -13 °C (8.6 °F) to 21 °C (70 °F) were used as boundary conditions for the outer areas of the model (top of deck, abutment walls, top of road).

To model the thermal behavior of a frozen soil and its corresponding phase change, the effects of latent heat (heat gain or loss) were considered by calculating the enthalpy of the soil-water system as a function of temperature (Figure 4.11) using Equation 4.3.

$$H = \rho \cdot c \cdot (273 + T) + L \cdot \theta_w \cdot \rho_w \quad (4.3)$$

where H is the enthalpy in J/m^3, ρ and ρ_w are the the densities of the soil and water respectively in kg/m^3, c is the specific heat of the soil in J/kg-°K (830 for dry/frozen soil, 1500 for wet/thaw soil – Farouki 1981; Thomas 1992), T is temperature in °C, L is the latent heat of water 334000 J/kg, and θ_w is the volumetric water content (0.3 for the foundation and 0.07 for the backfill).

For the structural part of the analysis, the soil's thermal expansion coefficient was set as a function of temperature (Figure 4.12). When the ambient temperature was below freezing point, the expansion coefficient was calculated using Equation 4.4. For temperatures above freezing a thermal expansion coefficient of $1 \cdot 10^{-5}$ °C^{-1} was used (Khalili et al. 2010).

$$\alpha = \frac{\epsilon_F}{T - T_{REF}} + \alpha_0 \quad (4.4)$$

where α is the thermal expansion coefficient, ε_F is the strain due to ice formation (frost heave), T is the temperature, T_{REF} is the reference temperature (12 °C), and α_0 is the linear thermal expansion coefficient for temperatures above 0 °C.

The strain due to frost heave (ε_F) was calculated using Equation 4.5, assuming a total volume of 1 m^3, a porosity of 0.33, desired saturation condition (0.9 for the foundation and 0.2 for the backfill), and deformation in just the vertical direction.

$$\epsilon_F = V_W \cdot 0.09 \quad (4.5)$$

where V_w is the volume of water, and 0.09 is the change in volume due to ice expansion (9%).

A complete presentation and description of the field measurements for this bridge is presented in Chapter 3. The measurements were taken using a total station, prism, and reflective targets mounted on the abutment walls, and were always made with respect to a reference point of known elevation assumed to not experience movement, and with respect to the first measurement, which was taken on a day with an average temperature of 17 °C. To reduce computer time just a few points from all the visits to the field were chosen to be modeled to obtain a general idea of the behavior of the structures at different temperatures. A total of 12 temperatures (approximately one month apart each) were used to represent an annual thermal cycle of the temperatures experienced by the structure. Field observations are then compared to nodal solutions from the finite element models, corresponding to nodes close to the location of some of the surveyed points (Figures 4.13-4.16). Figure 4.17 shows examples of the vertical deformation results for the temperature induced deformations when the air temperature was the coldest (-13 °C / 8.6 °F) and warmest (21 °C / 70 °F). An interpretation of the results is presented in the following section.

4.5 Modeling and Response Discussions

The results indicate that the deformations experienced by the system are related in some part to temperature changes, specially for the subfreezing temperatures, as the deformation from the numerical model shows a similar pattern to the field deformations. The up and down behavior of the different sections of the model was the result of the transient temperature effects over time. A period of a year of temperatures (12 points) was used to model the behavior, from Summer to Summer. As temperatures decrease and Summer transitions into Fall and Winter the soils contract. As the temperatures fall below zero and the water turns into ice it expands, causing the heaving as expected from the thermal expansion coefficient function (Equation 4.4, Figure 4.12). As temperatures rise from Winter to Spring and Summer the soil has a residual effect of the heaving as the expansion coefficient for temperatures below zero is larger (in magnitude) than for temperatures above zero and not all of the soil has thawed, thus it takes longer for the soil to feels the effect of the rising temperatures.

In the model the average day temperature was used during the analysis. This is important to consider because as Michal and Urban (2015) have shown that the deformation due to temperature changes usually expresses itself with a delay between 5 to 8 hours from the peak temperature. The field measurements may or may not be capturing this time delayed response, which could be a factor when comparing measurements over time and with the results from finite element analysis, thus adding to the discrepancy of the observed results and to the spread behavior of the field measurements.

Figures 4.10 to 4.13 show the comparison between the vertical field deformations and the results from the finite element model versus temperature. The results for the NE surveying points

are shown but other surveying points show similar patterns. In general, the different parts of the system experience frost heave when the temperatures fall below freezing, as shown also by the finite element model, indicating a response to the temperature changes experienced by the system. Not only do the soils heave but foundation and reinforced soil elements become stiffer and stronger as temperatures drop (Özgan et al. 2015; Qi et al. 2008; Wang and Liu 2015; Zhang and Michalowski 2015), which would make the effects of traffic load less significant, as the soils are less compressible due to ice-bonding.

In Chapter 3 a conceptual description is proposed, a hypothesis based on the observed data, of the response of the full system as follows. In addition to the frost heave when temperatures fall below zero, they propose the deformations as temperature increases to be due to thaw settlement, as the soil weakens due to a higher water content from ice melting, and changes in effective stresses as the water table lowers and soils become drier. As the water table lowers pore pressure decreases thus effective stress increase and the soils shrink/settle; as the pore space could have been increased due to water expansion when changing to ice, pushing the soil grains apart.

Other factors, such as moisture change and heterogeneity of the subsurface soils (specially the presence of fine-grained soils), can have also an effect on the deformations; as moisture increases the soils become weaker, becoming more prone to deformations (Moulton and Kula 1980; Moulton et al. 1985; Wahls 1990; Long et al. 1998; Kim et al. 2003; White et al. 2007; Li et al. 2013; Mitchell and Soga 2015).

The modeled soils were considered as homogeneous and linear-elastic for a couple of reasons. First, the subsurface exploration data shows predominantly coarse-grained soils, but also the data points are very sparse and localized, making it difficult to interpolate or extend the

presence of different layers. Second, the material parameters used in the analysis were taken from general sources or weak correlations (SPT to Young's modulus – Kulhawy and Mayne 1990; Bowles 1997). A more complex model, than the linear-elastic implemented here, would be more appropriate to model the soils, as soils are inherently non-linear and non-elastic, but the parameters used in any of these type of models require to be obtained through extensive field sampling and laboratory testing, which were not possible for this study. Since the scope of the analysis was to compare trends more than specifically match results, this was achieved by using the simpler linear-elastic model.

4.6 Conclusions

The analysis of the finite element modelling of the GRS-IBS bridge in south of Bloomer, WI allows drawing the following conclusions:

- Stiffness of the geosynthetic is a critical factor in the design of GRS structures, reducing the vertical and horizontal deformations as its stiffness increases, but having a larger impact on the horizontal deformations.
- The use of friction angle as material property for the backfill showed that larger deformations occur when low values are used, usually less than 30 degrees, which would suggest the system is in an unstable condition for the applied load.
- From the different loading cases applied here none of them seemed to cause high enough stresses in the deck, for this one to experience cracking, as the cracking stress for the deck was found to be 3 times greater than the maximum stress from the finite element models.

- The maximum deformations from the different loading cases also did not exceed the established threshold for differential settlement to be consider critical (> 1.3 cm).
- The bridge at Bloomer, and its foundation soil, has experienced deformations due in great part to environmental factors, especially temperature. As the water in the pore space freezes the soil will tend to expand due to frost heave. As ice melts and thaws the soil will experience settlement due to weakening at first, as water content increases, followed by increases in effective stresses as soils become drier.

Acknowledgments

We would like to thank Carl Martin (Engineering Physics – UW-Madison) for his help on the numerical modeling aspects of this research.

References

AASHTO (2012). *AASHTO LRFD Bridge Design Specifications*, American Association of State Highway and Transportation Officials, Washington, D. C.

Abu-Hejleh, N., Zornberg, J.G., Wang, T., and Watcharamonthein, J. (2002). "Monitored displacements of unique geosynthetic-reinforced soil bridge abutments." *Geosynth. Int.*, 9(1), 71-95.

ACI (2011). ACI 318-11 Building Code Requirements for Structural Concrete, American Concrete Institute.

Adams, M., Ketchart, K., Ruckman, A., DiMillio, A.F., Wu, J., and Satyanarayana, R. (1999). "Reinforced soil for bridge support applications on low-volume roads." *Transport. Res. Rec.*, 1652, 150-160.

Al-Azzawi, A.A. (2012). "Finite Element Analysis of Flexible Pavements Strenghted with

Geogrid." *ARPN J. Eng. App. Sci.*, 7(10), 1295-1299.

Belal, A., Nagy, N., and Elshesheny, A. (2015). "Numerical Evaluation of Bearing Capacity of Square Footing on Geosynthetic Reinforced Sand." *Proceedings of the International Conference on Civil, Structural and Transportation Engineering*, 1-9.

Bowles, J. (1997). *Foundation Analysis and Design*, McGraw-Hill Companies, Inc., New York.

Brosnan, D.A., Sanders, J.P., and Hart, S.A. (2011). "Application of thermal analysis in preservation and restoration of historic masonry materials." *J. Therm. Anal. Calorim.*, 106(1), 109-115.

Chadbourn, B.A., Luoma, J.A., Newcomb, D.E., and Voller, V.R. (1996). "Consideration of Hot-Mix Asphalt Thermal Properties During Compaction." *Quality Management of Hot-Mix Asphalt*, D. S. Decker, ed., American Society for Testing Materials.

Erickson, H., and Drescher, A. (2001). "The Use of Geosynthetics to Reinforce Low Volume Roads." *Report No. MN/RC – 2001-15*, Minessota Department of Transportation, St. Paul, Minnesota.

Farouki, O.T. (1981). "Thermal Properties of Soils." *Report No. CRREL Monograph 81-1*, United States Army Corps of Engineers, Hanover, New Hampshire.

Han, J., and Gabr, M.A. (2002). "Numerical Analysis of Geosynthetic-Reinforced and Pile-Supported Earth Platforms over Soft Soil." *J. Geotech. Geoenviron. Eng.*, 128(1), 44-53.

Helwany, M.B., and Wu, J.T.H. (1995). "A Numerical Model for Analyzing Long-Term Performance of Geosynthetic-Reinforced Soil Structures." *Geosynth. Int.*, 2(2), 429-453.

Helwany, S.M.B., Wu, J.T.H., and Froessl, B. (2003). "GRS bridge abutments - an effective means to alleviate bridge approach settlement." *Geotext. Geomembranes*, 21(3), 177-196.

Helwany, S.M.B., Wu, J.T.H., and Kitsabunnarat, A. (2007). "Simulating the Behavior of GRS

Bridge Abutments." *J. Geotech. Geoenviron. Eng.*, 133(10), 1229-1240.

Holtz, R.D., Kovacs, W.D., and Sheahan, T.C. (2011). *An introduction to geotechnical engineering*, Prentice Hall, New Jersey.

Huang, J., Han, J., and Oztoprak, S. (2009). "Coupled Mechanical and Hydraulic Modeling of Geosynthetic-Reinforced Column-Supported Embankments." *J. Geotech. Geoenviron. Eng.*, 135(8), 1011-1021.

INEOS Olefins & Polymers USA (2014). "Typical Engineering Properties of Polypropylene." <http://www.ineos.com/globalassets/ineos-group/businesses/ineos-olefins-and-polymers-usa/products/technical-information--patents/ineos-engineering-properties-of-pp.pdf>. (Nov. 5, 2015).

Keller, G.R., and Devin, S.C. (2003). "Geosynthetic-reinforced soil bridge abutments." *Transport. Res. Rec.*, 1819, 362-368.

Khalili, N., Uchaipichat, A., and Javadi, A.A. (2010). "Skeletal thermal expansion coefficient and thermo-hydro-mechanical constitutive relations for saturated homogeneous porous media." *Mech. Mater.*, 42(6), 593-598.

Kim, D.-S., Seo, W.-S., and Kim, M.-J. (2003). "Deformations characteristics of soils with variations of capillary pressure and water content." *Soils Found.*, 43(4), 71-79.

Kreith, F., Manglik, R.M., and Bohn, M.S. (2011). *Principles of Heat Transfer*, Cengage Learning.

Kulhawy, F.H., and Mayne, P.W. (1990). *Manual on Estimating Soil Properties For Foundation Design*, Electric Power Research Institute, Palo Alto, California.

Li, Q.-l., Ling, X.-z., Wang, L.-n., Zhang, F., Wang, J.-h., and Xu, P.-j. (2013). "Accumulative strain of clays in cold region under long-term low-level repeated cyclic loading:

Experimental evidence and accumulation model." *Cold Reg. Sci. Technol.*, 94, 45-52.

Ling, H.I., Tatsuoka, F., and Tateyama, M. (1995). "Simulating performance of GR-RW by finite-element procedure." *J. Geotech. Eng.*, 121(4), 330-340.

Liu, H., Wang, X., and Song, E. (2009). "Long-term behavior of GRS retaining walls with marginal backfill soils." *Geotext. Geomembranes*, 27(4), 295-307.

Long, J.H., Olson, S.M., Stark, T.D., and Samara, E.A. (1998). "Differential Movement at Embankment–Bridge Structure Interface in Illinois." *Transport. Res. Rec.*, 1633, 53-60.

Ma, W., Mu, Y., Wu, Q., Sun, Z., and Liu, Y. (2011). "Characteristics and mechanisms of embankment deformation along the Qinghai–Tibet Railway in permafrost regions." *Cold Reg. Sci. Technol.*, 67(3), 178-186.

Mamlouk, M.S., Witczak, M.W., Kaloush, K.E., and Hasan, N. (2005). "Determination of thermal properties of asphalt mixtures." *J. Test. Eval.*, 33(2), 118-126.

Michal, O., and Urban, R. (2015). "Temperature effects on the bridge structure during the all-day monitoring." *Geoinformatics FCE CTU*, 14(1), 79.

Ming, F., and Li, D.-q. (2016). "A model of migration potential for moisture migration during soil freezing." *Cold Reg. Sci. Technol.*, 124, 87-94.

Ming, F., Li, D.Q., and Zhang, K. (2012). "Theoretical study on thaw settlement of saturated frozen soil." *2012 International Conference on Civil, Architectural and Hydraulic Engineering, ICCAHE 2012*, Trans Tech Publications, 155-162.

Mitchell, J.K., and Soga, K. (2005). *Fundamentals of Soil Behavior*, John Wiley & Sons, Inc., Hoboken, New Jersey.

Mohamed, K., Abouzakhm, M., and Elias, M. (2011). "Applications and Performance of Geosynthetic-Reinforced Soil Abutments on Soft Subsurface Soil Conditions." *Transport.*

Res. Rec., 2212, 74-81.

Moulton, L.K., GangaRao, H.V.S., and Halverson, G.T. (1985). "Tolerable movement criteria for highway bridges." *Report No. FHWA/RD-85/107*, Federal Highway Administration, U.S. Department of Transportation, Washington, DC.

Moulton, L.K., and Kula, J.R. (1980). "Bridge Movements and Their Effects." *Public Roads*, 44(2), 62-75.

Narayanan, S.P., and Sirajuddin, M. (2013). "Properties of Brick Masonry for FE modeling." *Am. J. Eng. Res.*, 1, 6-11.

Özgan, E., Serin, S., Ertürk, S., and Vural, I. (2015). "Effects of Freezing and Thawing on the Consolidation Settlement of Soils." *Soil Mech. Found. Eng.*, 52(5), 247-253.

Pelte, T., Pierson, P., and Gourc, J.P. (1994). "Thermal Analysis of Geomembranes Exposed to Solar Radiation." *Geosynth. Int.*, 1(1), 21-44.

Poulos, H.G., Booker, J.R., and Ring, J.G. (1972). "Simplified calculation of embankment deformations." *Soils Found.*, 12(4), 1-17.

Qi, J., Ma, W., and Song, C. (2008). "Influence of freeze–thaw on engineering properties of a silty soil." *Cold Reg. Sci. Technol.*, 53(3), 397-404.

Razmi, J., Ladani, L., and Aggour, S.M. (2014). "Finite element simulation of pile behaviour under thermo-mechanical loading in integral abutment bridges." *Struct. Infrastruct. Eng.*, 10(5), 643-653.

Singh, R.M., and Bouazza, A. (2013). "Thermal conductivity of geosynthetics." *Geotext. Geomembranes*, 39, 1-8.

Siriwardane, H., Gondle, R., Kutuk, B., and Ingram, R. (2008). "Experimental investigation and numerical analysis of reinforced geologic media." *12th International Conference on*

Computer Methods and Advances in Geomechanics 2008, International Association for Computer Methods and Advances in Geomechanics, 4369-4376.

Skinner, G.D., and Rowe, R.K. (2003). "Design and behaviour of geosynthetic-reinforced soil walls constructed on yielding foundations." *Geosynth. Int.*, 10(6), 200-214.

Skinner, G.D., and Rowe, R.K. (2005). "Design and behaviour of a geosynthetic reinforced retaining wall and bridge abutment on a yielding foundation." *Geotext. Geomembranes*, 23(3), 234-260.

Syverson, K.M. (2007). "Pleistocene Geology of Chippewa County, Wisconsin." Wisconsin Geological and Natural History Survey.

Tarefder, R.A., Zaman, A.M., and Uddin, W. (2010). "Determining hardness and elastic modulus of asphalt by nanoindentation." *Int. J. Geomech.*, 10(3), 106-116.

Thomas, L.C. (1992). *Heat Transfer*, Prentice Hall, New Jersey.

Viswanadham, B.V.S., and König, D. (2009). "Centrifuge modeling of geotextile-reinforced slopes subjected to differential settlements." *Geotext. Geomembranes*, 27(2), 77-88.

Wahls, H.E. (1990). "NCHRP Synthesis of Highway Practice 159: Design and Construction of Bridge Approaches." National Cooperative Highway Research Program, Transportation Research Board, National Research Council, Washington, D.C.

Wang, S., and Liu, F. (2015). "A Hypoplasticity-Based Method for Estimating Thaw Consolidation of Frozen Sand." *Geotech. Geol. Eng.*, 33(5), 1307-1320.

Wathugala, G.W., Huang, B., and Pal, S. (1996). "Numerical Simulation of Geosynthetic-Reinforced Flexible Pavements." *Transport. Res. Rec.*, 1534, 58-65.

Weidenfeller, B., Höfer, M., and Schilling, F.R. (2004). "Thermal conductivity, thermal diffusivity, and specific heat capacity of particle filled polypropylene." *Composites Part A*,

35(4), 423-429.

WGNHS (2016). "Geophysical logs available by request from the Wisconsin Geological and Natural History Survey data collections." WGNHS (Wisconsin Geological and Natural History Survey), Madison, WI.

White, D.J., Mekkawy, M.M., Sritharan, S., and Suleiman, M.T. (2007). "“Underlying” Causes for Settlement of Bridge Approach Pavement Systems." *J. Perform. Constr. Facil.*, 21(4), 273-282.

WisDOT (2015). "Bridge Manual." Wisconsin Department of Transportation.

Zhang, Y., and Michalowski, R. (2015). "Thermal-Hydro-Mechanical Analysis of Frost Heave and Thaw Settlement." *J. Geotech. Geoenviron. Eng.*, 141(7), 04015027.

Tables

Table 4.1. Embankment properties for the case h/H=0.6

Property	Value
Young's modulus [MPa]	70
Poisson's ratio [-]	0.3
Unit weight [kN/m^3]	19
Final height [m]	5
Lift height [m]	3
Base length [m]	8.66
Slope angle [°]	30

Table 4.2. Material properties used in the GRS-IBS model.

Section	Young's modulus [MPa]	Poisson's ratio
Road (Asphalt) [1]	$2 \cdot 10^3$	0.2
Deck (Concrete) [2]	$25 \cdot 10^3$	0.2
Geosynthetic [3]	500	0.1
Walls (Masonry) [4]	600	0.15
Backfill [5]	70	0.3
Foundation [6]	40	0.3

[1] From Tarefder et al. (2010)

[2] From Razmi et al (2014)

[3] Young's modulus of geosynthetic used in the field, Poisson's ratio from Wathugala et al. (1996)

[4] From Narayanan and Sirajuddin (2013)

[5] Value for dense sands from Bowles (1997)

[6] From SPT correlations (Kulhawy and Mayne 1990; Bowles 1997) and typical Poisson's ratio for soils

Table 4.3. Summary of the results for the different loading cases.

Load case	Vertical deformation [cm]	Horizontal deformation [cm]	Deviatoric stress [MPa]
Uniform	0.249	0.048	1.00
Non-uniform	0.110	0.020	0.37
Induced differential settlement SE + uniform	0.356	0.228	1.00
Induced differential settlement NE + uniform	0.424	0.222	1.00
Truck load SE-NW	0.131	0.040	0.38
Truck load SE-NE	0.196	0.049	0.33
Truck load NE-SW close to the center	0.201	0.034	1.06
Truck load NE-SW close to the center with settlement on NE	0.317	0.165	1.08

Table 4.4. Material properties used for the temperature loading models.

Section	Density [kg/m^3]	Specific heat [J/(kg °K)]	Thermal conductivity [W/(m °K)]	Thermal expansion coefficient [1/°K]
Road (Asphalt)	2100 [a]	920 [g]	0.75 [a]	$4 \cdot 10^{-5}$ §
Deck (Concrete)	2300 [a]	880 [a]	1.2 [a]	10^{-5} †
Geosynthetic	910 [f]	1580 [e]	0.4 [b]	$1.5 \cdot 10^{-5}$ ^
Walls (Masonry)	1700 [a]	837 [a]	0.65 [a]	$6 \cdot 10^{-6}$ *
Backfill	1937 [d]	830-1500 [a, c]	0.7 [a]	$-4.2 \cdot 10^{-4}$ to 10^{-5} ‡
Foundation	1937 [d]	830-1500 [a, c]	0.7 [a]	$-1.9 \cdot 10^{-3}$ to 10^{-5} ‡

[a] From Thomas (1992)

[b] From Singh and Bouazza (2013)

[c] From Farouki (1981)

[d] Based on unit weight value of 19 kN/m^3 fro sand from Bowles (1997)

[e] From Weidenfeller et al. (2004)

[f] From INEOS (2014)

[g] Chadbourn et al. (1996)

§ From Mamlouk et al. (2005)

† From Razmi et al (2014)

^ Modified after Pelte et al. (1994)

* From Brosnan et al. (2011)

‡ From Khalili et al. (2010) and Equation 4.4 in this document

Figures

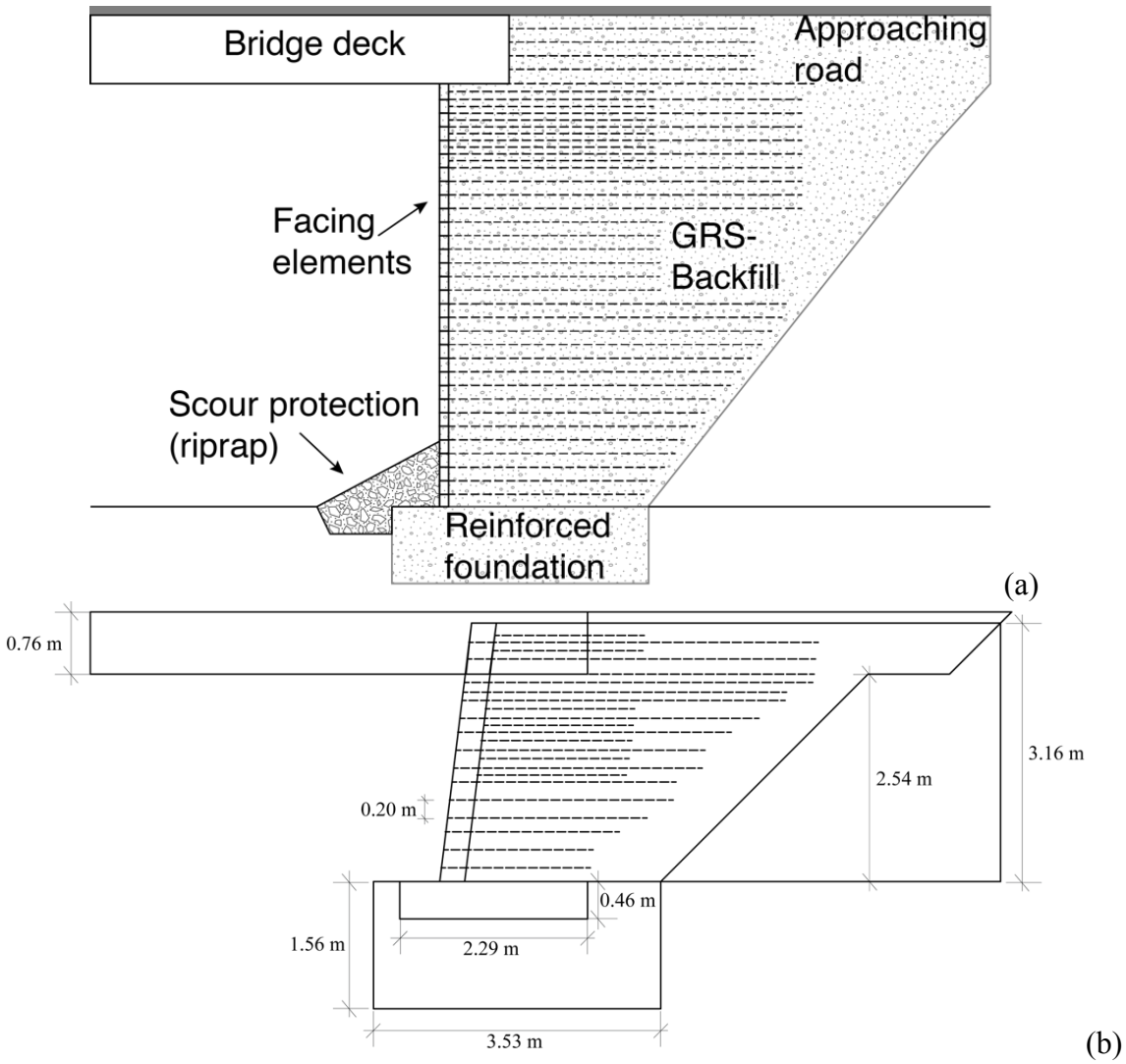

Figure 4.1. (a) Typical cross-section of a Geosynthetic Reinforced Soil-Integrated Bridge System (GRS-IBS). (b) Dimensions of the GRS-IBS at Bloomer, WI.

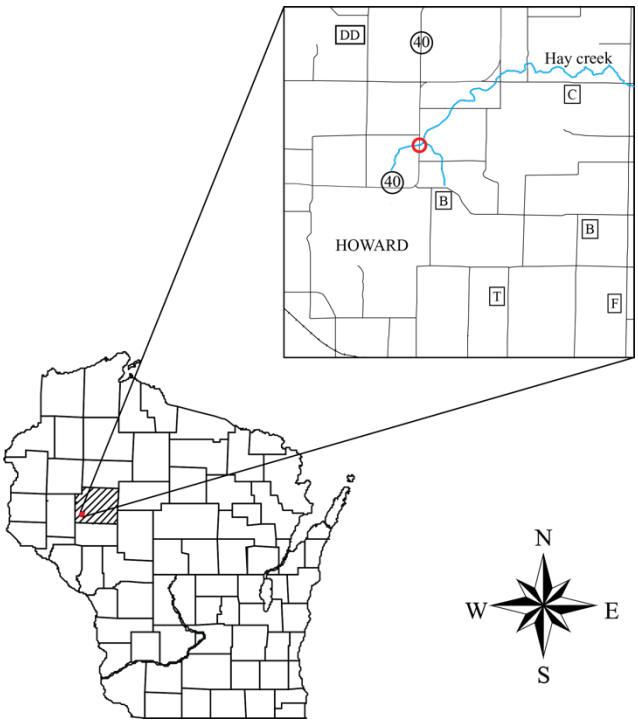

(a)

(b)

Figure 4.2. (a) Location of the GRS-IBS bridge. The red circle indicates the location of the bridge. (b) Picture of the GRS-IBS bridge.

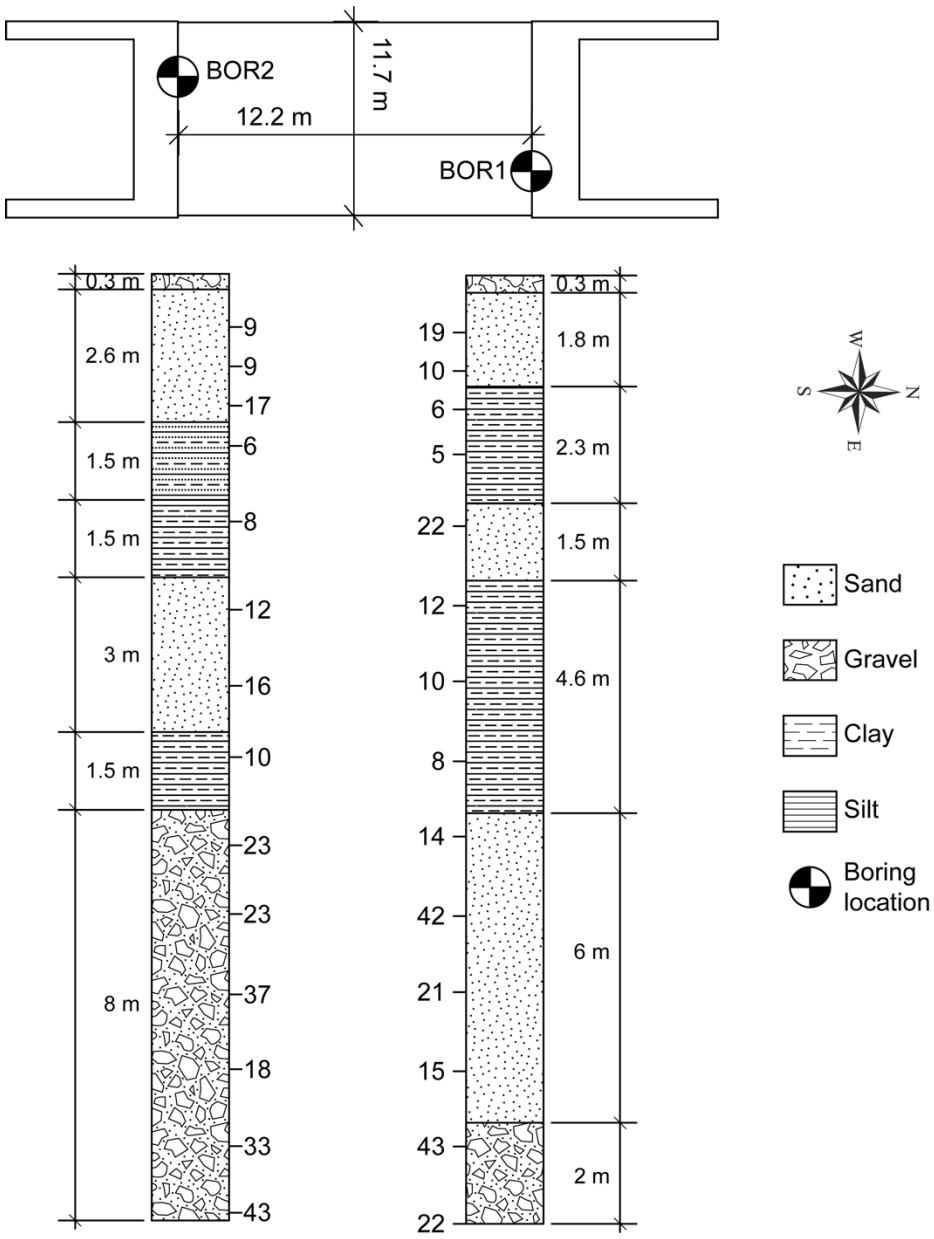

Figure 4.3. Subsurface exploration data for the GRS-IBS bridge at Bloomer

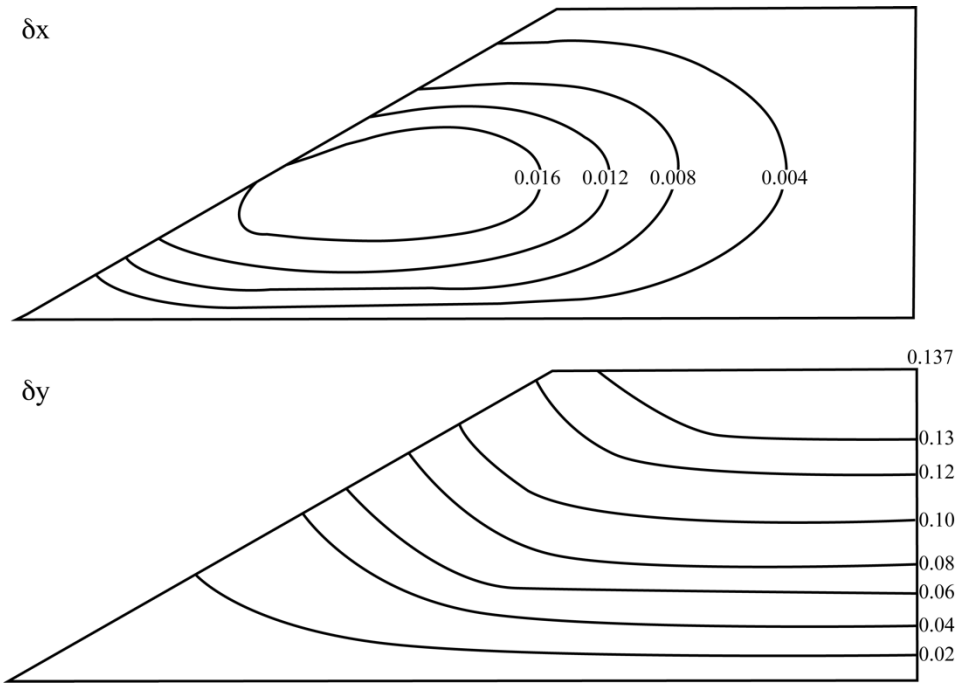

Figure 4.4. Dimensionless solutions for horizontal and vertical displacements for the case where h/H=0.6 (Modified after Poulos et al. 1972).

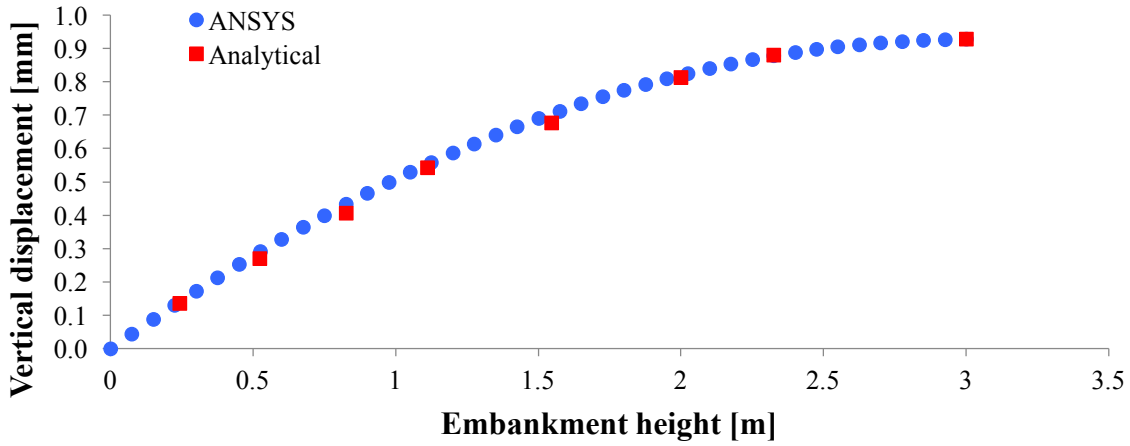

(a)

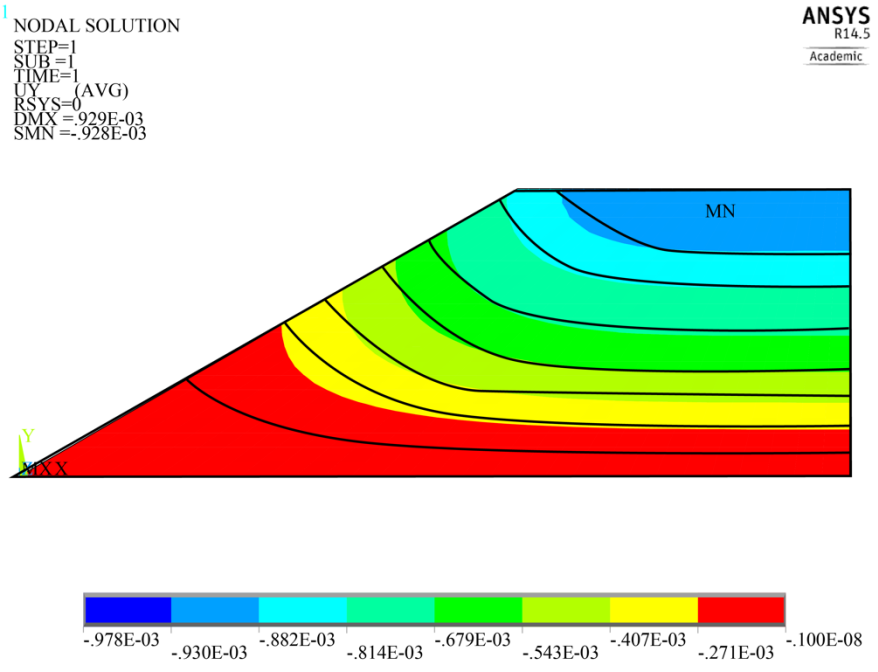

(b)

Figure 4.5. (a) Vertical displacement plot comparing the analytical and finite element nodal solutions along the middle of the embankment (right boundary), vertical edge. (b) Vertical displacement contour plot from ANSYS. The black lines correspond to the contours from the analytical solution.

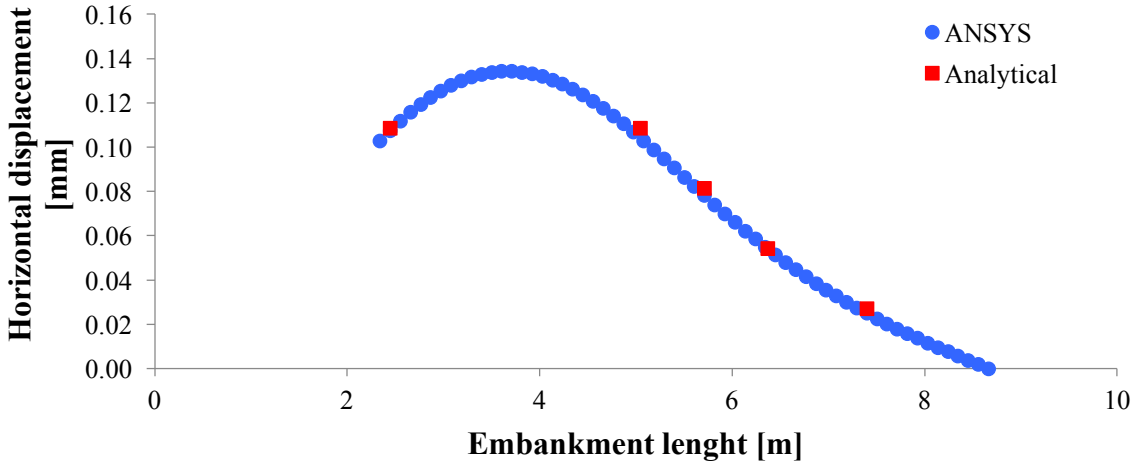

(a)

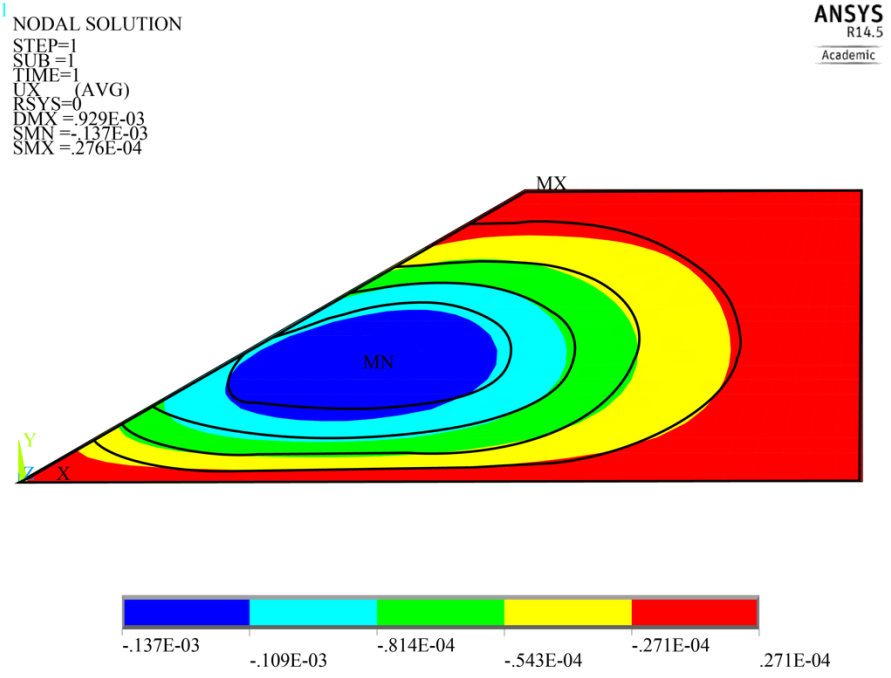

(b)

Figure 4.6. (a) Horizontal displacement plot comparing the analytical and finite element nodal solutions at mid-height of the embankment. Horizontal displacement contour plot from ANSYS. (b) The black lines correspond to the contours from the analytical solution.

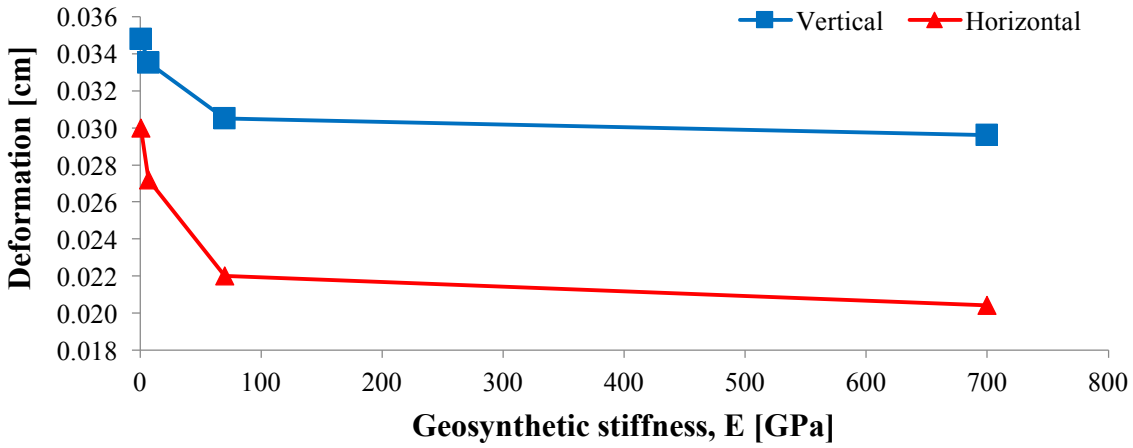

(a)

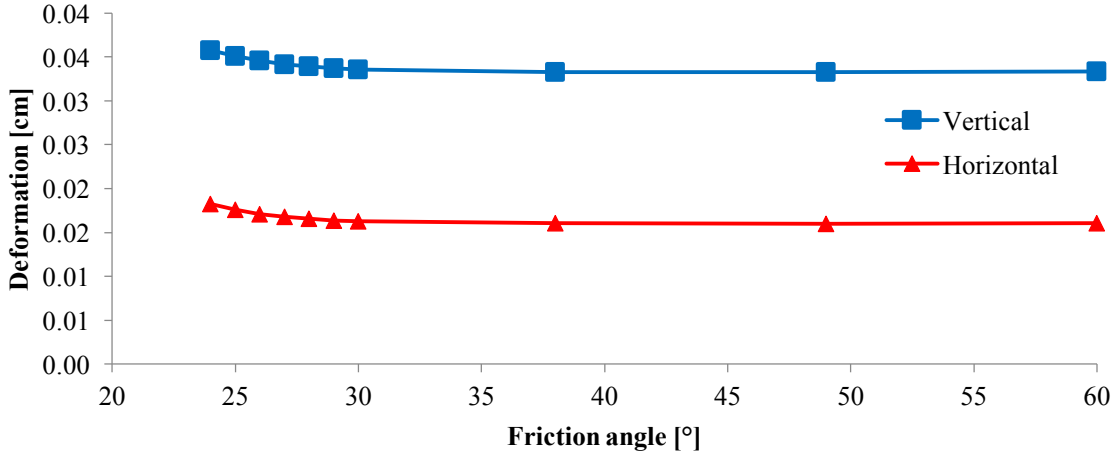

(b)

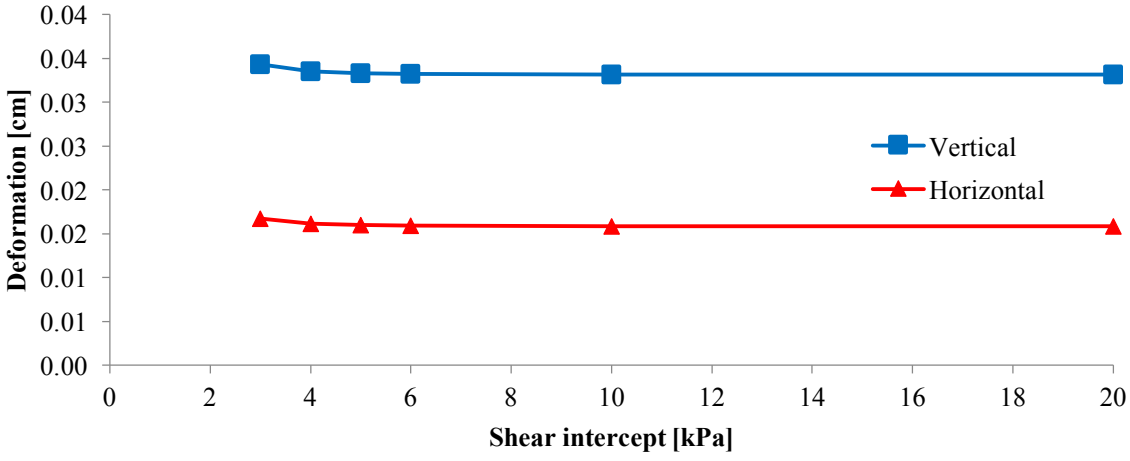

(c)

Figure 4.7. (a) Deformation as function of geosynthetic stiffness, with a friction coefficient of 0.5. (b) Deformation as a function of backfill's friction angle. (c) Deformation as a function of backfill's shear intercept.

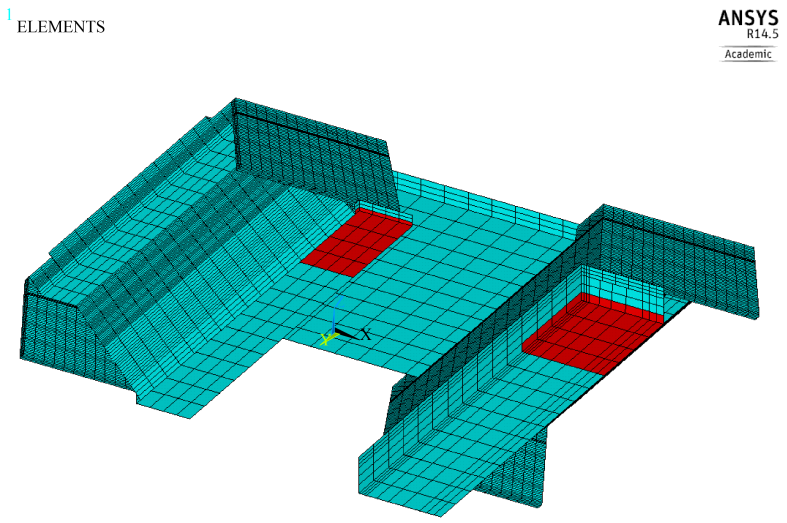

(a)

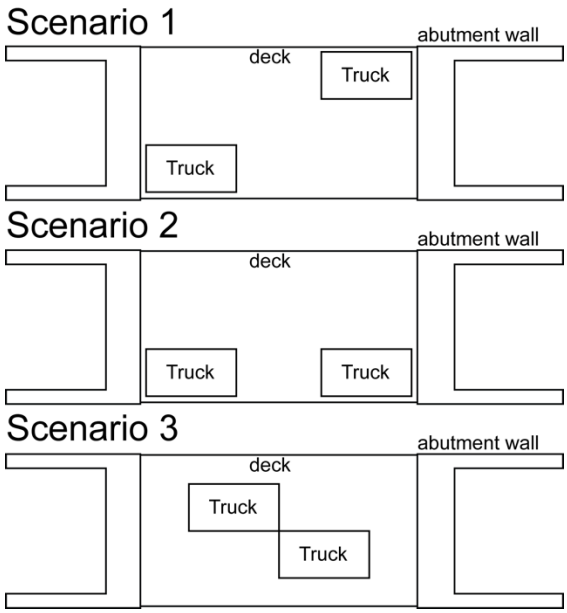

(b)

Figure 4.8. (a) Location of "killed" elements (red elements) to simulate differential settlement. (b) Sketch of the location of the analyzed truck loads. Scenario 1: Opposing corner, SE-NW. Scenario 2: Same side corner, SE-NE. Scenario 3: NE-SW close to the center.

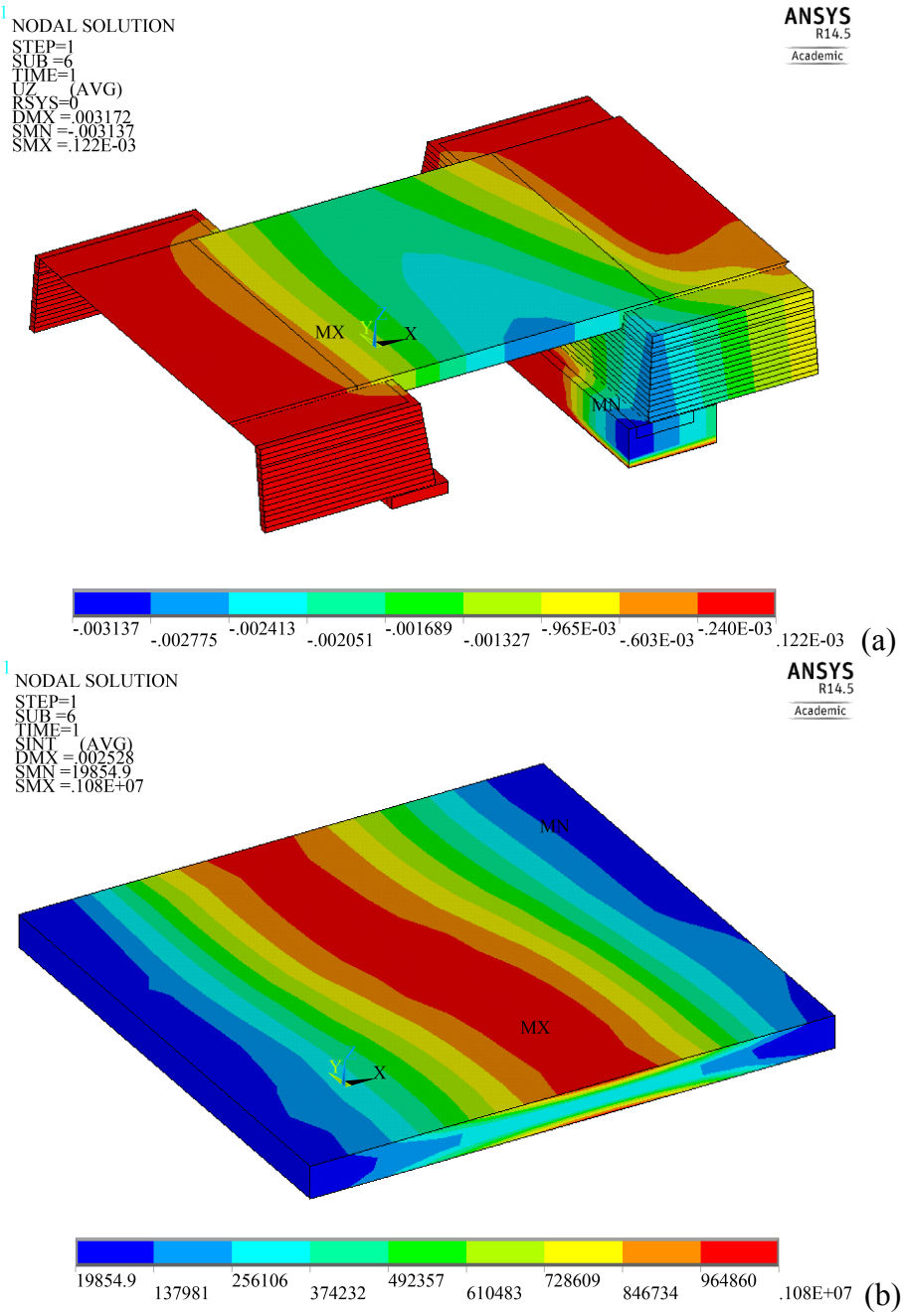

Figure 4.9. (a) Vertical displacement and (b) deviatoric stress finite element analysis results for the most critical service loading case: truck load on NE-SW close to the center with induced settlement on NE corner.

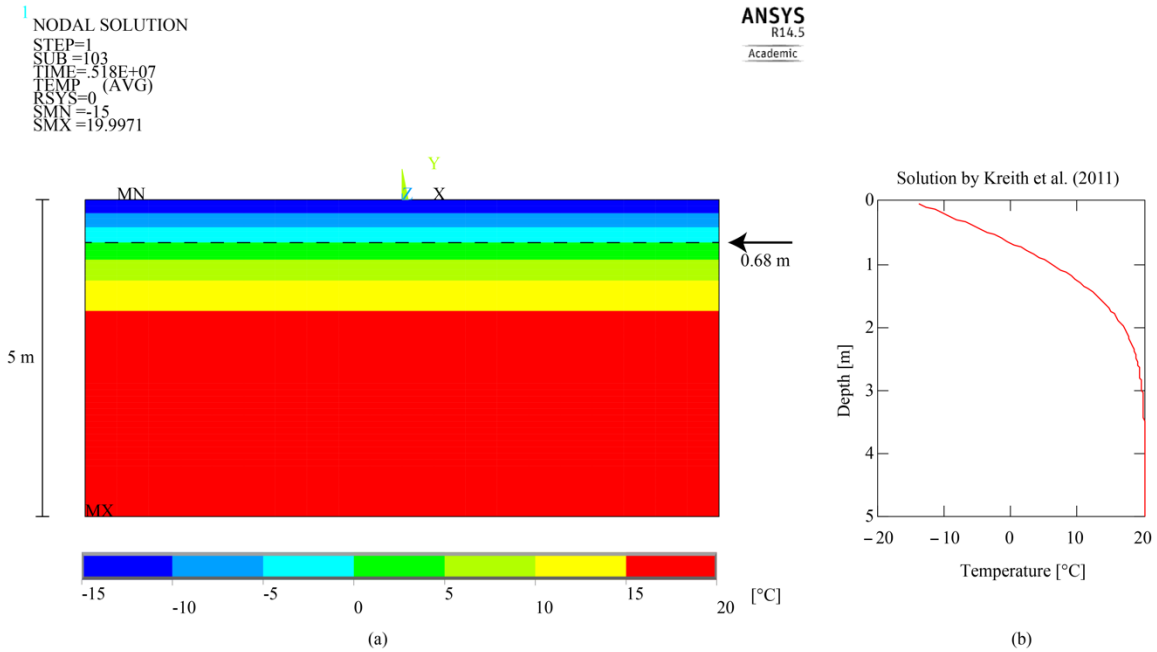

Figure 4.10. (a) Transient heat transfer model results for example 2.11 from Kreith et al. (2011). The arrow on the right and black dashed line represent the 0 °C isotherm at 0.68 m below the ground surface, same as the analytical solution. (b) Solution by Kreith et al. (2011) as function of depth.

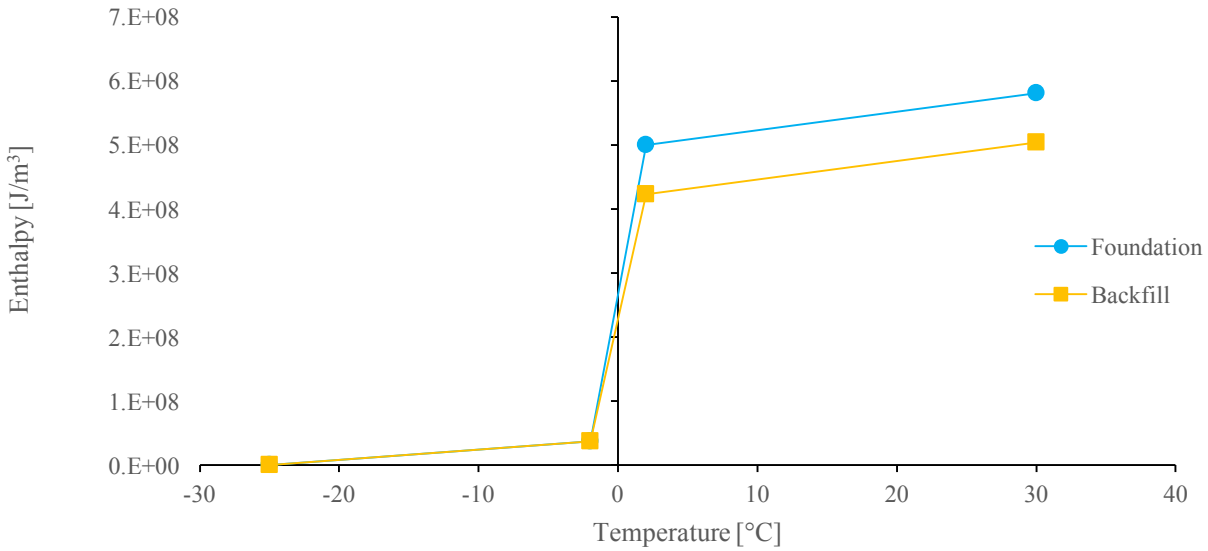

Figure 4.11. Enthalpy as function of temperature.

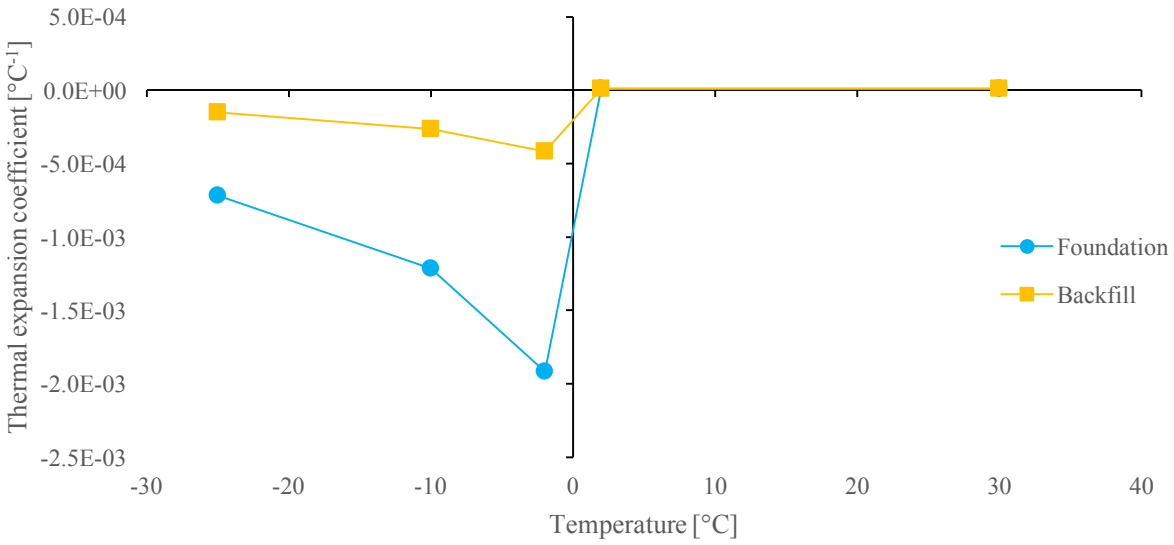

Figure 4.12. Thermal expansion coefficient as function of temperature.

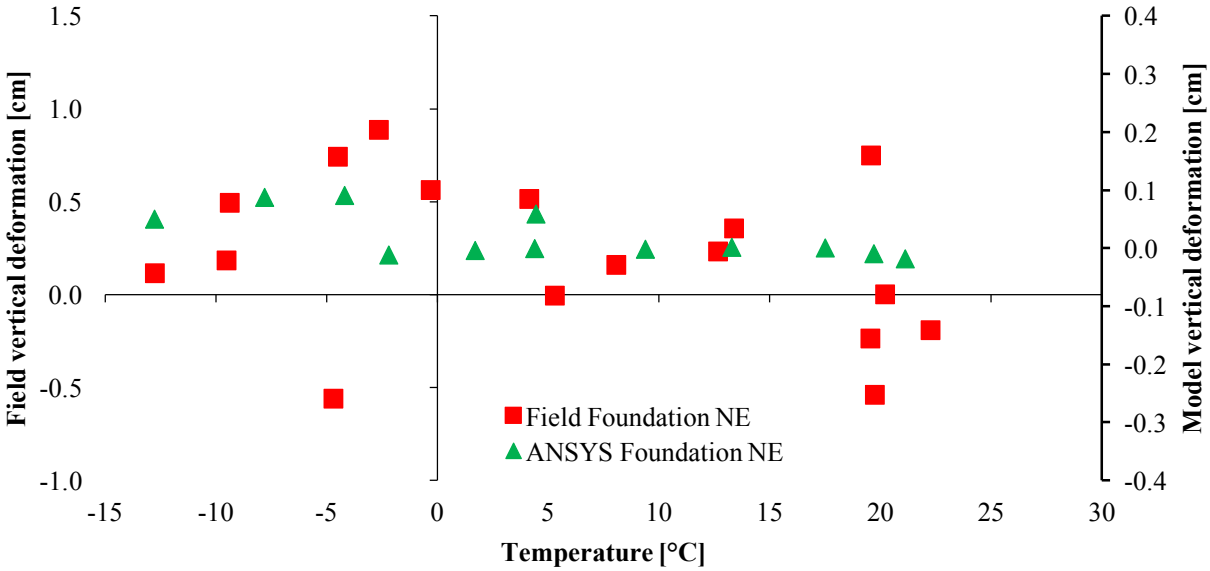

Figure 4.13. Comparison between field measurements and finite element model results for the NE and NW settlement plate (foundation).

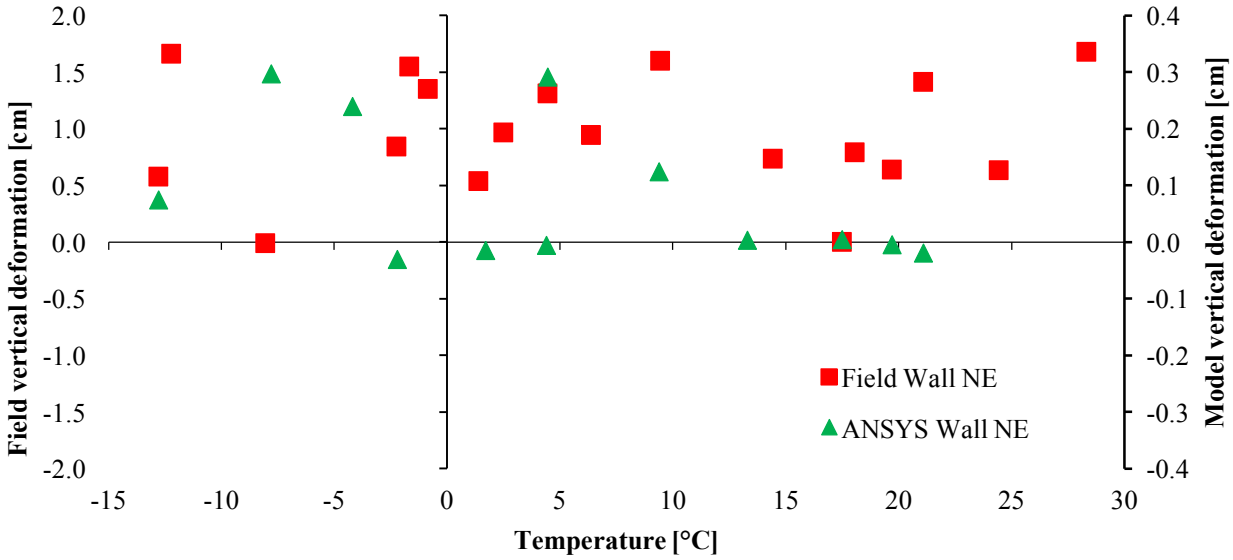

Figure 4.14. Comparison between field measurements and finite element model results for the NE and NW wall.

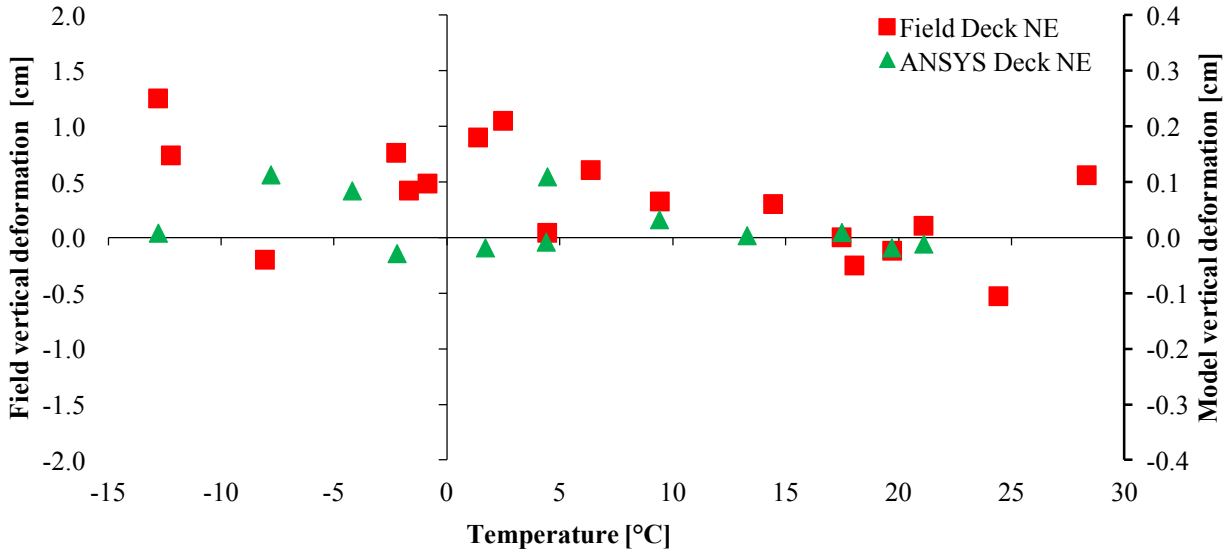

Figure 4.15. Comparison between field measurements and finite element model results for the NE and NW deck.

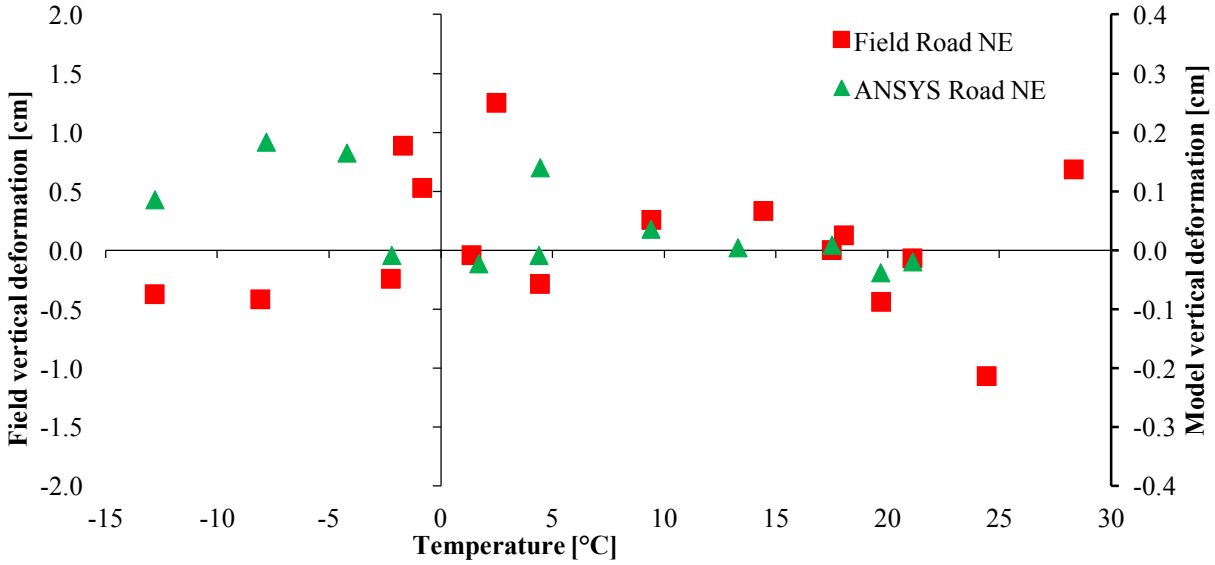

Figure 4.16. Comparison between field measurements and finite element model results for the NE and NW road.

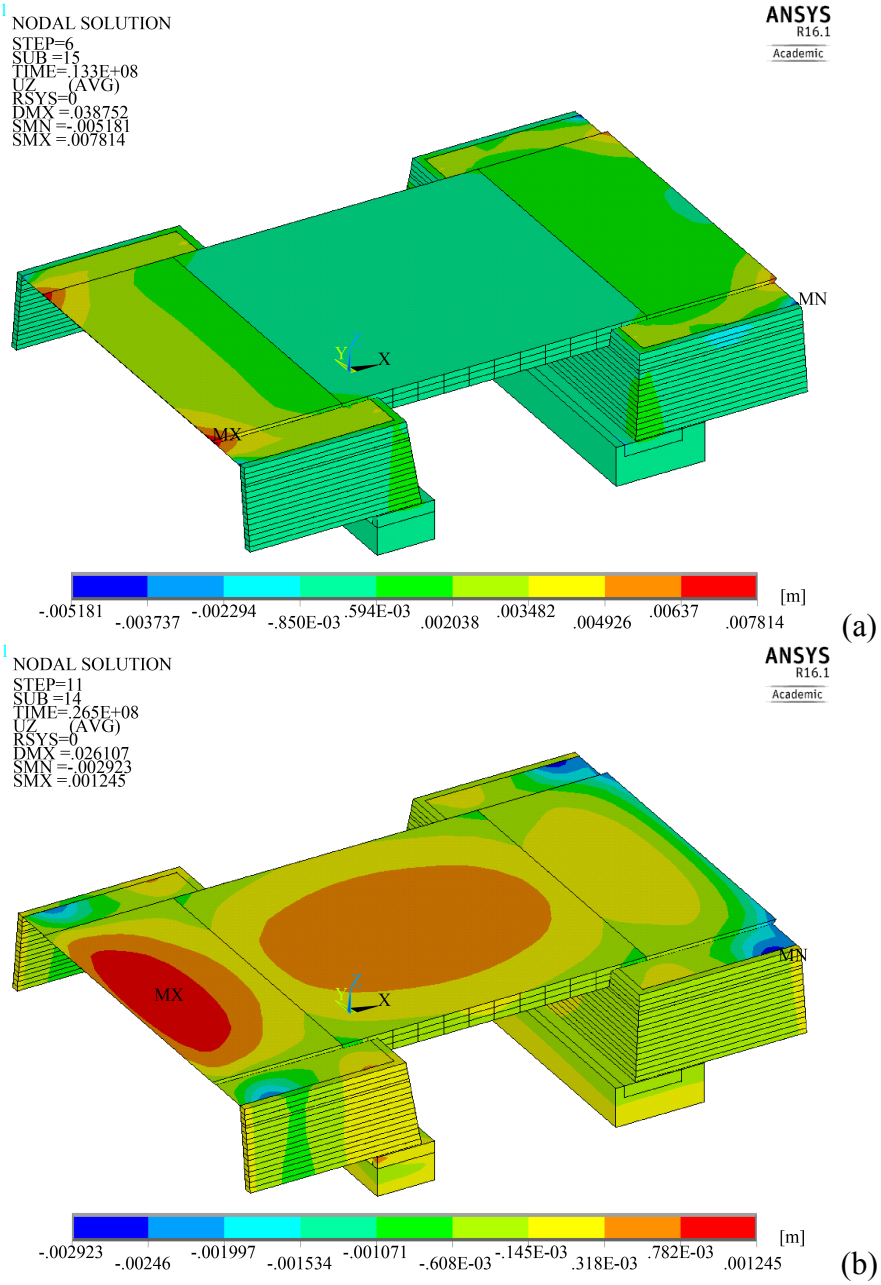

Figure 4.17. Finite element analysis results (vertical displacement) for the temperatures induced deformations for the cases were air temperature was (a) coldest at-13 °C and (b) warmest at 21 °C.

CHAPTER 5: Summary

In this thesis are presented the results from studies considering the effect of different loading conditions on bridges with different foundation types, environmental conditions, and subsurface conditions. Monitoring of the deformations over time and numerical modeling of the different structures were performed to determine how the different loads affect the behavior of these structures.

From the field monitoring and finite element modelling of the deep foundation bridges on H51 the following conclusions can be made:

- Bear Tree bridge seems to be the one affected by both traffic loads and temperature loads, as this bridge is being supported by the shortest piles, giving place to larger deformations due to service loads.
- The three bridges show a deformation pattern that can be linked or explained by the changes in temperature between measurements, as one of the major factors affecting the behavior of the bridges.
- The pile length could be a factor affecting the deformation due to temperature changes, as the longer piles would experience a larger volumetric change for the same temperature change than shorter piles.
- Other factors such as moisture changes and presence of fine-grained soils could explain deformations that are not fully explained by the temperature changes. The difficulty to account for both of these in the field measurements and the finite element model results, can be a reason for the behavior of some of the recorded deformations. Factors such as creep and shrinkage of concrete can have an effect on the deformations of the system.

- The assumption that the reference point is static and not affected over time might not be realistic, this combined with other several factors can add up to errors while taking field measurements, thus affecting the results from the surveying campaign.

From the field monitoring of the GRS-IBS bridge in Bloomer the following conclusions can be made:

- The bridge at Bloomer has experienced deformations due predominantly to environmental factors, such as temperature and water content changes, as these factors have been known to affect the properties of the soils (stiffness, compressibility, etc.).
- During winter when temperatures fall below freezing, the soils freeze and experience heaving, transferring this effect to the structure. The deformations show a general upward trend, as the cumulative effect of frost heave seems to be greater than settlement from thawing.
- Settlement can also be affected by a decline in the pore pressure, resulting in an increase of the effective stresses.
- Differential settlement has occurred between the approaching road and deck, the main reason for this being probably the lack of the joint-sealing layer over the structure, as water is believed to infiltrate into the backfill, giving room for erosion and the generation of ice lenses.
- Soil composition plays a significant factor on the soil's response to freezing and thawing, as the laboratory test showed, a soil with higher content of coarse-grained particles does not seem to be affected as much as a soil with higher content of fine-grained particles, as the soil with higher fine-grained content experiences larger deformations.

The analysis of the finite element modelling of the GRS-IBS bridge in south of Bloomer, WI allows drawing the following conclusions:

- Stiffness of the geosynthetic is a critical factor in the design of GRS structures, reducing the vertical and horizontal deformations as its stiffness increases, but having a larger impact on the horizontal deformations.
- The use of friction angle as material property for the backfill showed that larger deformations occur when low values are used, usually less than 30 degrees, which would suggest the system is in an unstable condition for the applied load.
- From the different loading cases applied here none of them seemed to cause high enough stresses in the deck, for this one to experience cracking, as the cracking stress for the deck was found to be 3 times greater than the maximum stress from the finite element models.
- The maximum deformations from the different loading cases also did not exceed the stablished threshold for differential settlement to be consider critical (> 1.3 cm).
- The bridge at Bloomer, and its foundation soil, has experienced deformations due in great part to environmental factors, specially temperature. As the water in the pore space freezes the soil will tend to expand due to frost heave. As ice melts and thaws the soil will experience settlement due to weakening at first, as water content increases, followed by increases in effective stresses as soils become drier.

In general, and from all the studies presented here, the deformation experienced by the structures and results from the numerical models follow a trend in relation with temperature and environmental changes and not a steady deformation due to service loads, indicating that the

behavior of these structures is being controlled by these environmental loading conditions more than the service loading conditions.

Appendices

Appendix A - Deep foundation bridges monitoring results

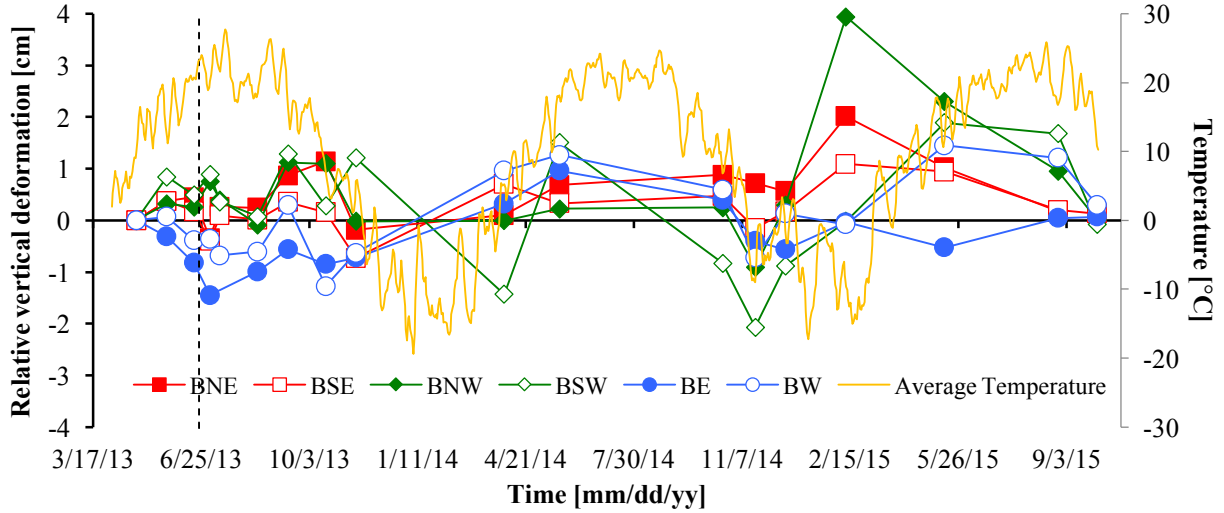

Figure A.1. Bridge over Bear Tree Road. Relative vertical deformation on the deck with respect to the reference point. Positive values correspond to upward movement. Vertical dashed line corresponds to the opening date to traffic.

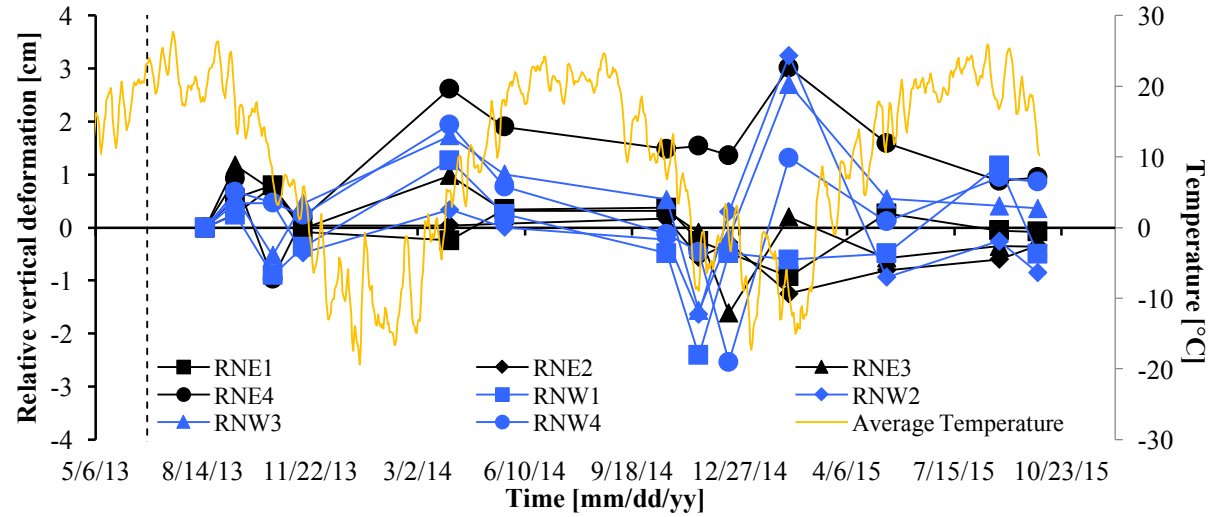

Figure A.2. Bridge over Bear Tree Road. Relative vertical deformation on the north approaching road with respect to the reference point. Positive values correspond to upward movement. Vertical dashed line corresponds to the opening date to traffic.

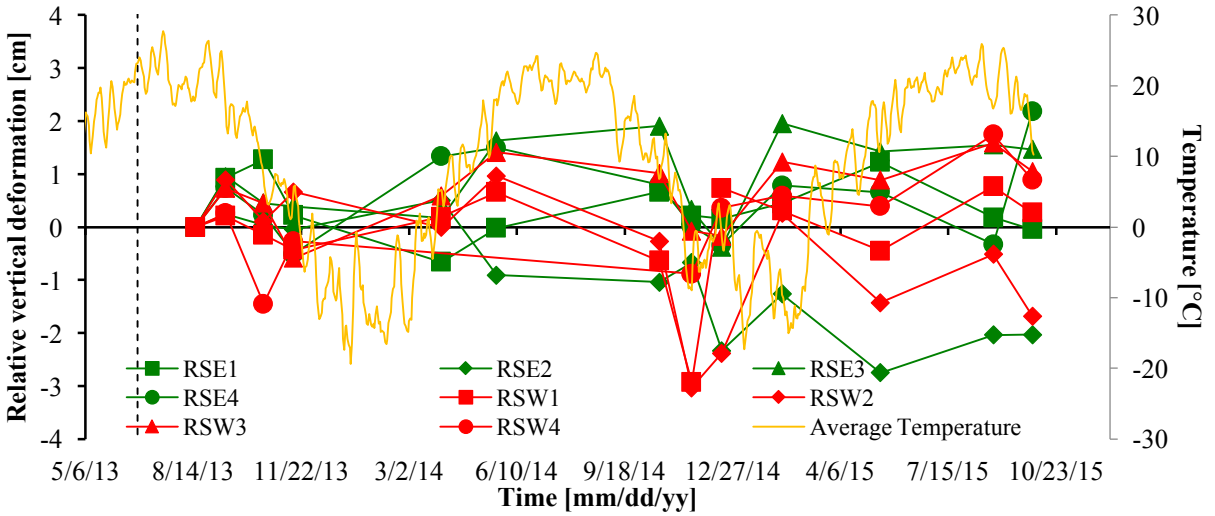

Figure A.3. Bridge over Bear Tree Road. Relative vertical deformation on the south approaching road with respect to the reference point. Positive values correspond to upward movement. Vertical dashed line corresponds to the opening date to traffic.

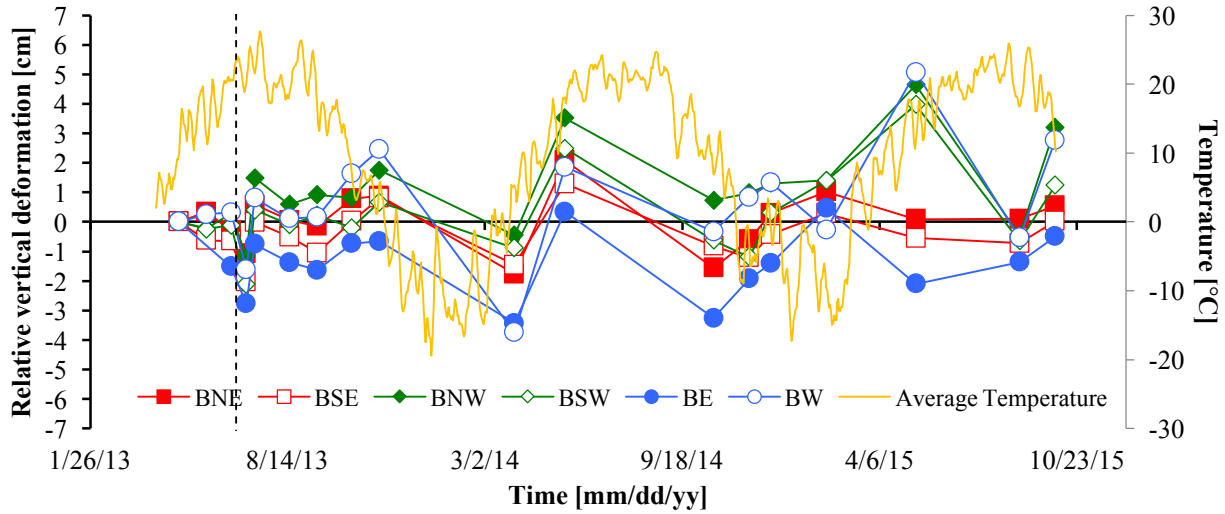

Figure A.4. Bridge over Windsor Road. Relative vertical deformation on the deck with respect to the reference point. Positive values correspond to upward movement. Vertical dashed line corresponds to the opening date to traffic.

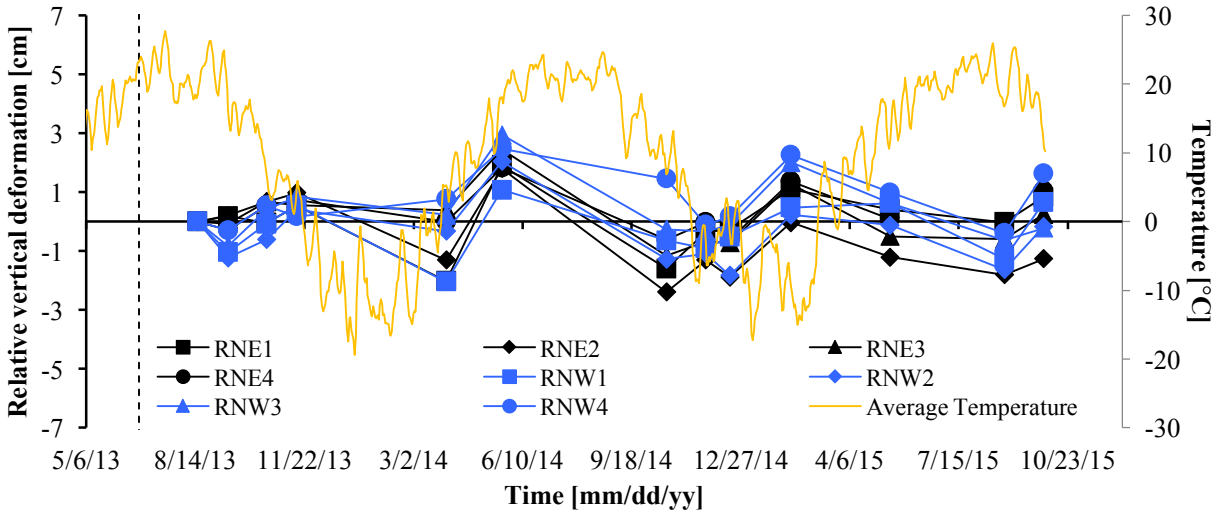

Figure A.5. Bridge over Windsor Road. Relative vertical deformation on the north approaching road with respect to the reference point. Positive values correspond to upward movement. Vertical dashed line corresponds to the opening date to traffic.

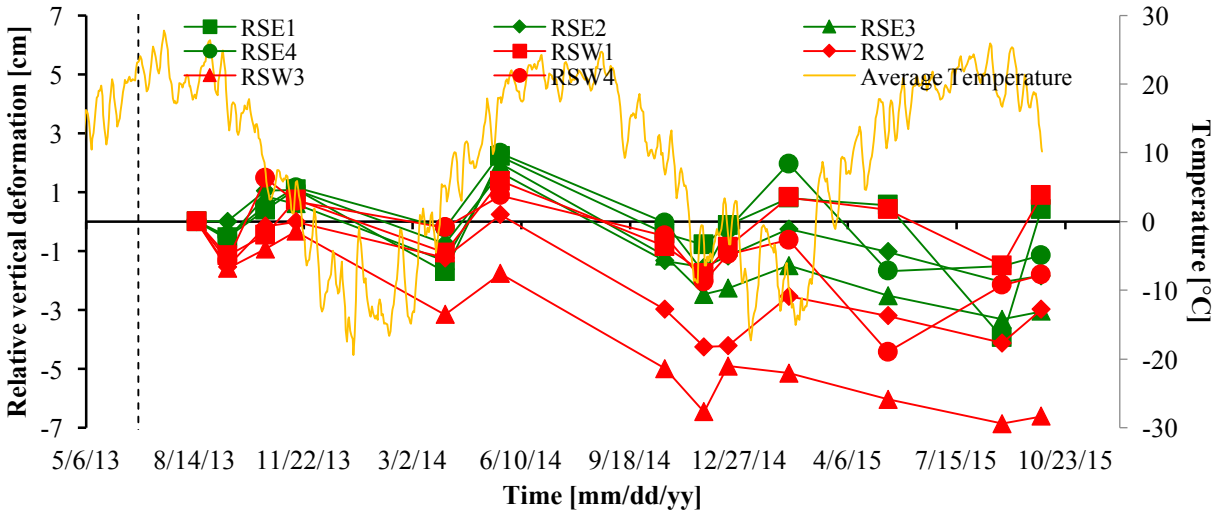

Figure A.6. Bridge over Windsor Road. Relative vertical deformation on the south approaching road with respect to the reference point. Positive values correspond to upward movement. Vertical dashed line corresponds to the opening date to traffic.

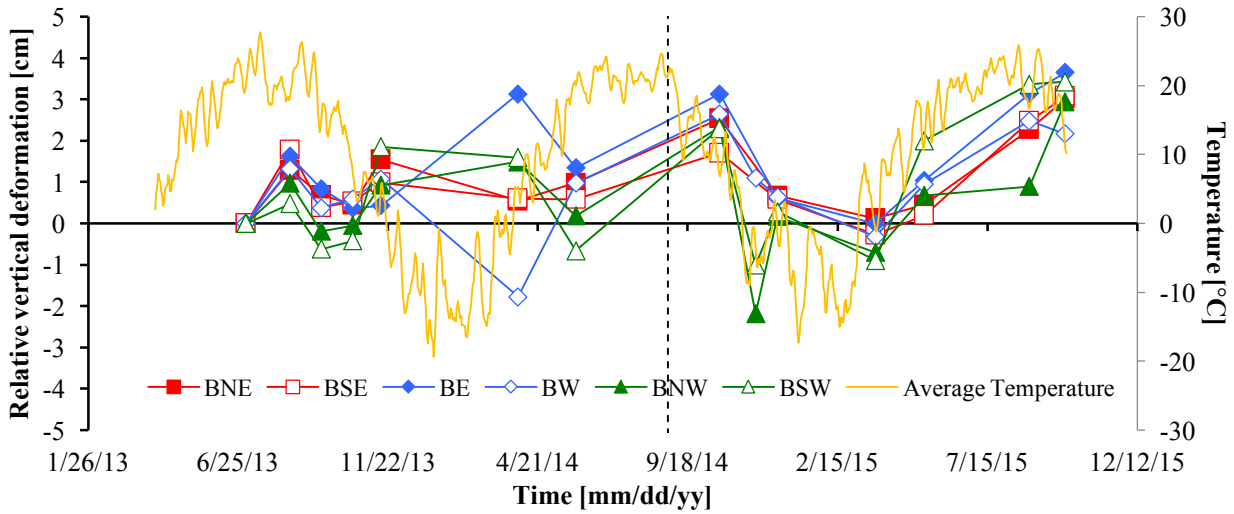

Figure A.7. Bridge over Vinburn Road. Relative vertical deformation on the deck with respect to the reference point. Positive values correspond to upward movement. Vertical dashed line corresponds to the opening date to traffic.

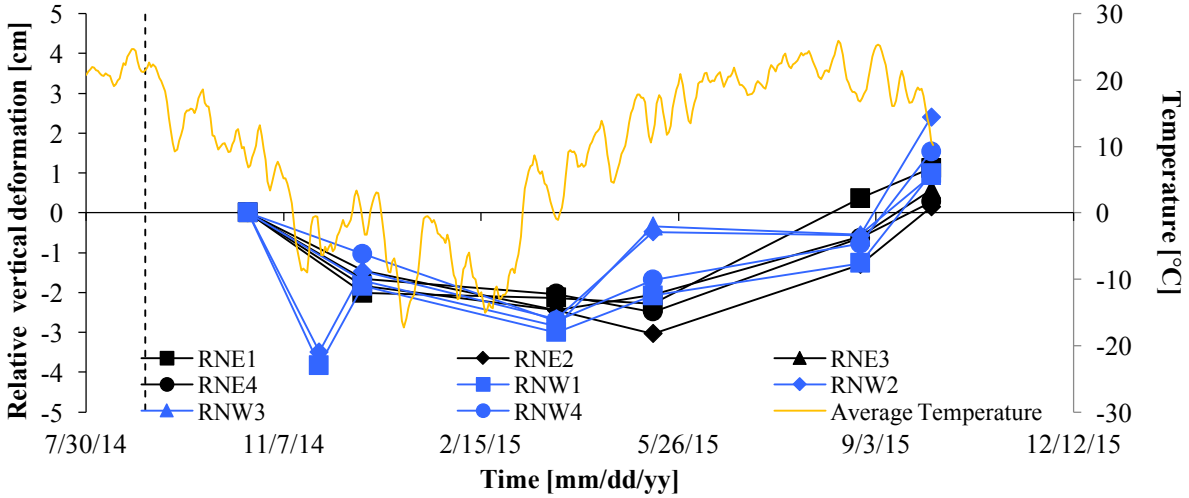

Figure A.8. Bridge over Vinburn Road. Relative vertical deformation on the north approaching road with respect to the reference point. Positive values correspond to upward movement. Vertical dashed line corresponds to the opening date to traffic.

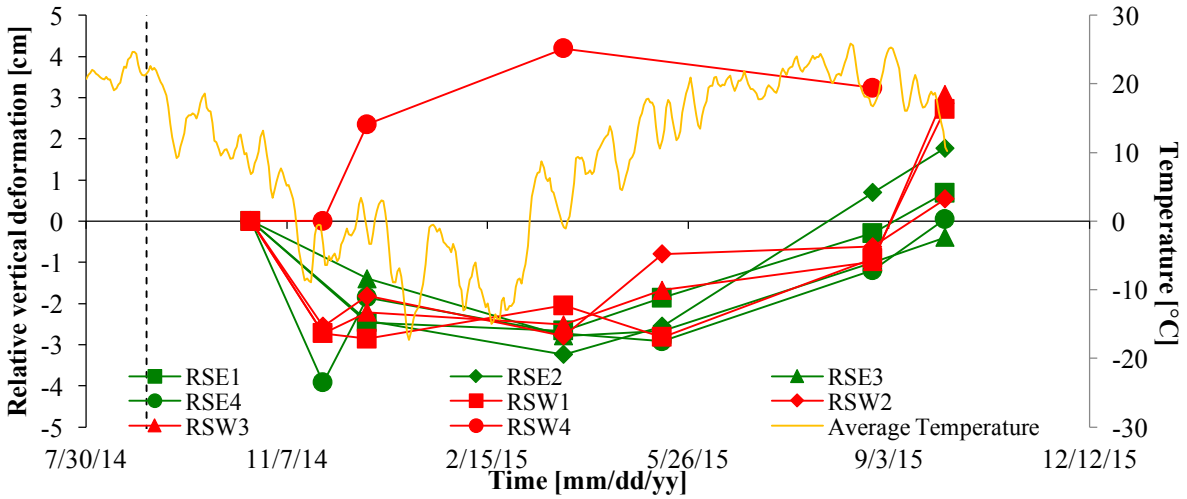

Figure A.9. Bridge over Vinburn Road. Relative vertical deformation on the south approaching road with respect to the reference point. Positive values correspond to upward movement. Vertical dashed line corresponds to the opening date to traffic.

Appendix B - Deep foundation bridges numerical modeling results

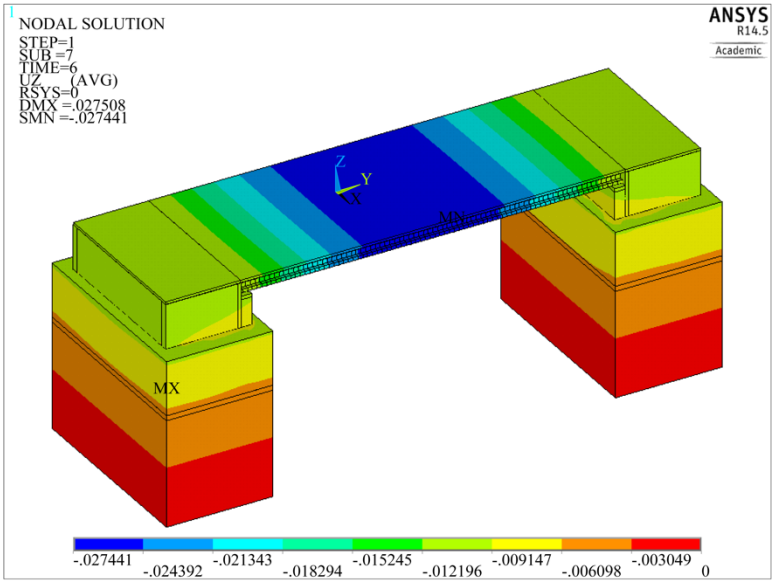

Figure B.1 Bridge over Bear Tree Road vertical deformation finite element results, in meters.

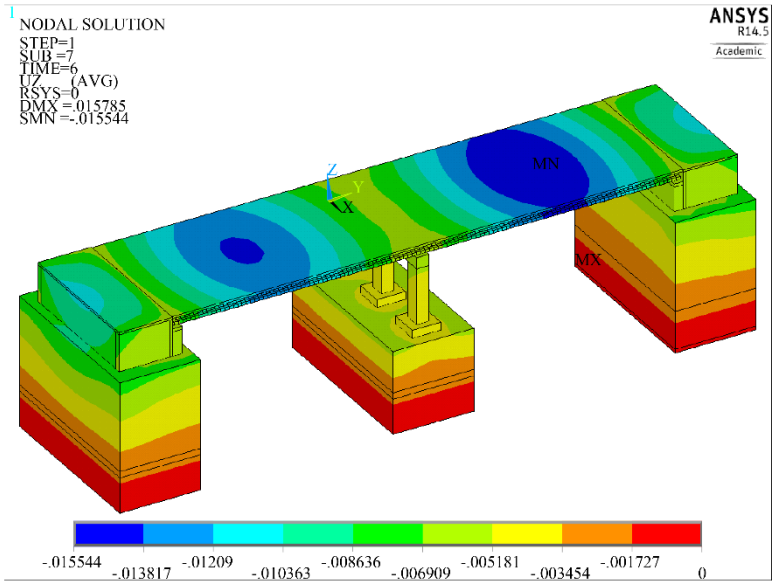

Figure B.2 Bridge over Windsor Road vertical deformation finite element results, in meters.

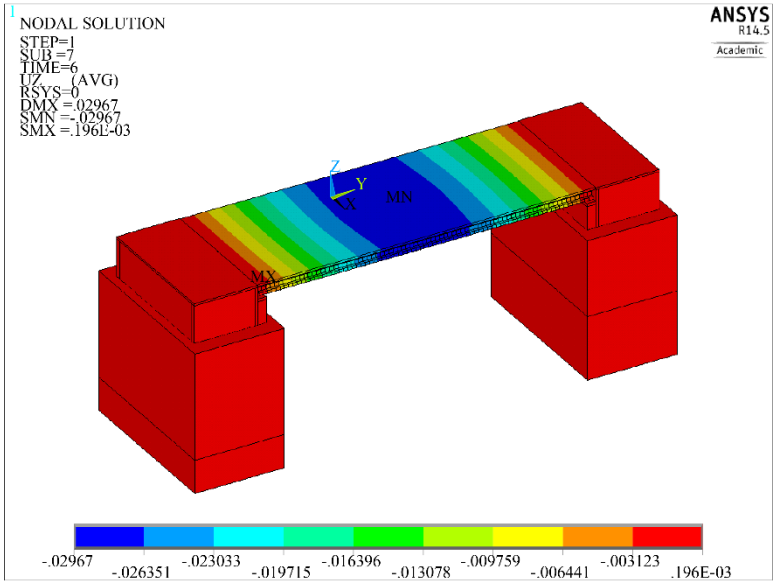

Figure B.3 Bridge over Vinburn Road vertical deformation finite element results, in meters.

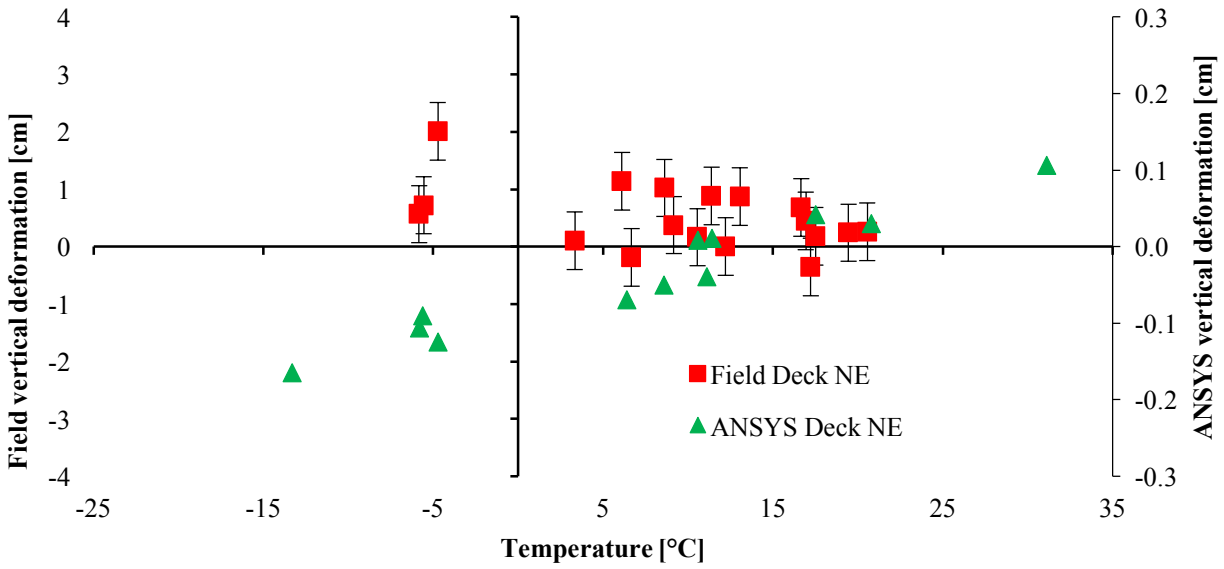

Figure B.4. Bridge over Bear Tree Road. Vertical deformation comparison between field measurements and finite element model results for the NE deck. Error bars are +- 0.5 cm instrument accuracy.

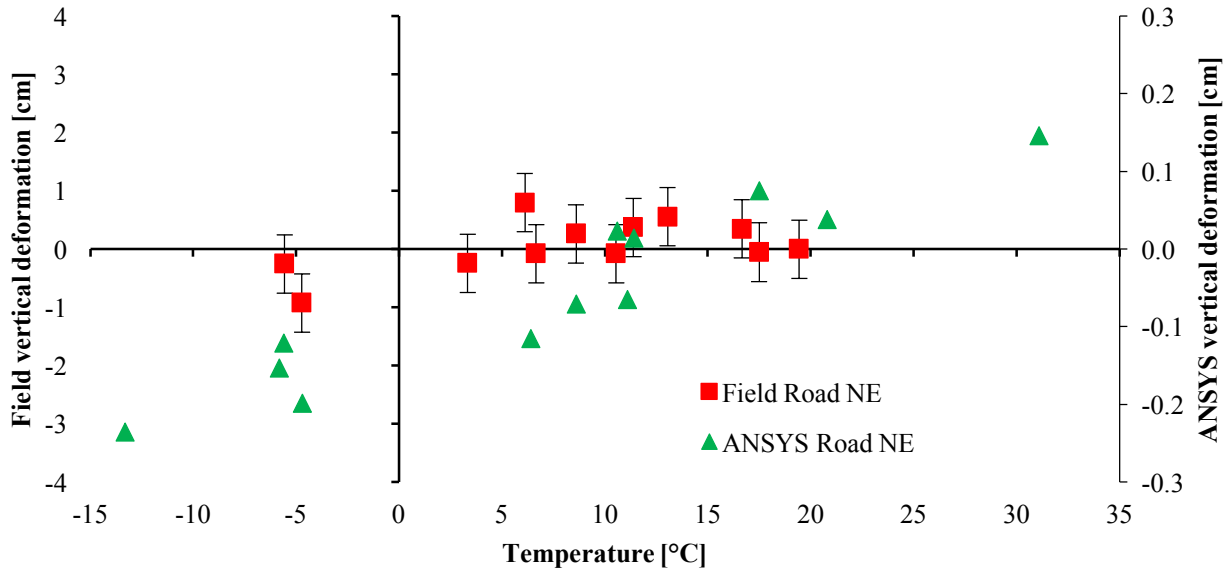

Figure B.5. Bridge over Bear Tree Road. Vertical deformation comparison between field measurements and finite element model results for the NE road. Error bars are +- 0.5 cm instrument accuracy.

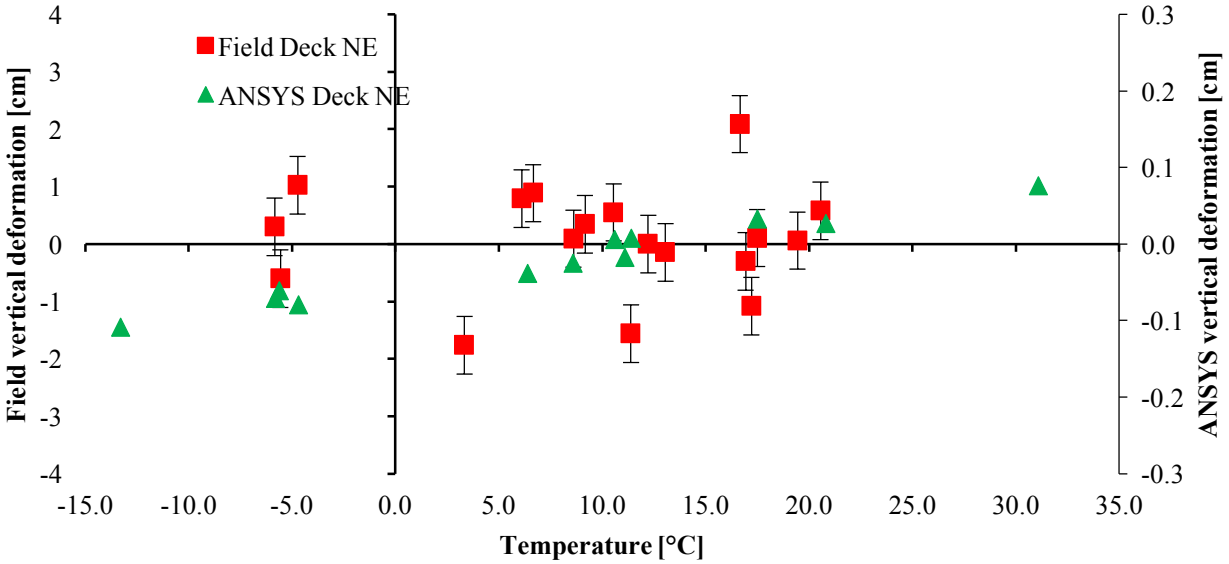

Figure B.6. Bridge over Windsor Road. Vertical deformation comparison between field measurements and finite element model results for the NE deck. Error bars are +- 0.5 cm instrument accuracy.

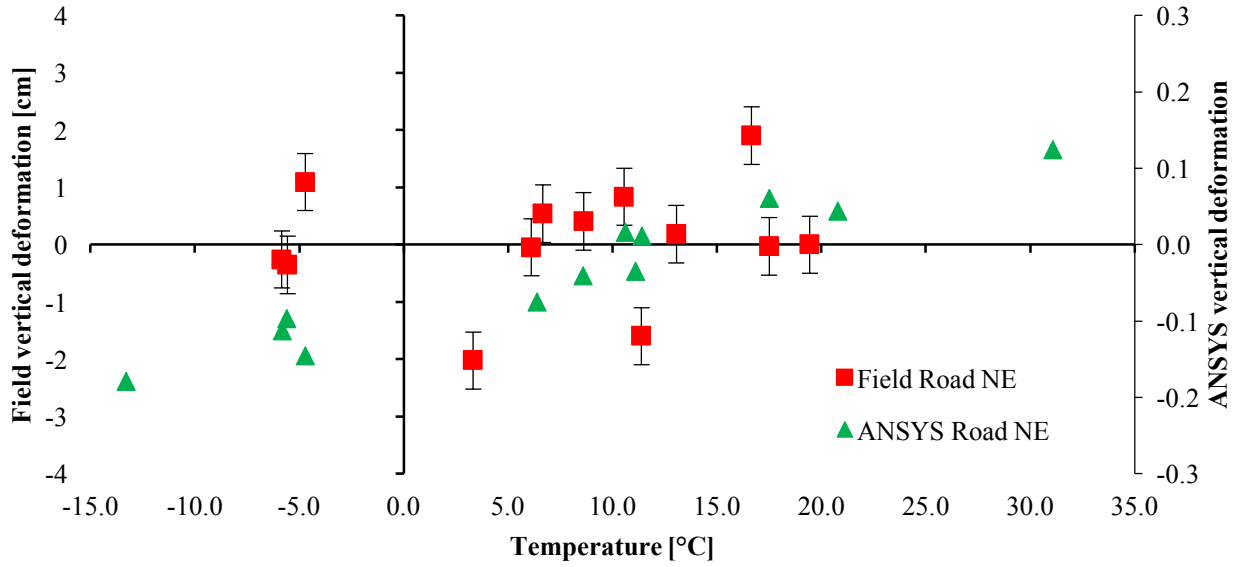

Figure B.7. Bridge over Windsor Road. Vertical deformation comparison between field measurements and finite element model results for the NE road. Error bars are +- 0.5 cm instrument accuracy.

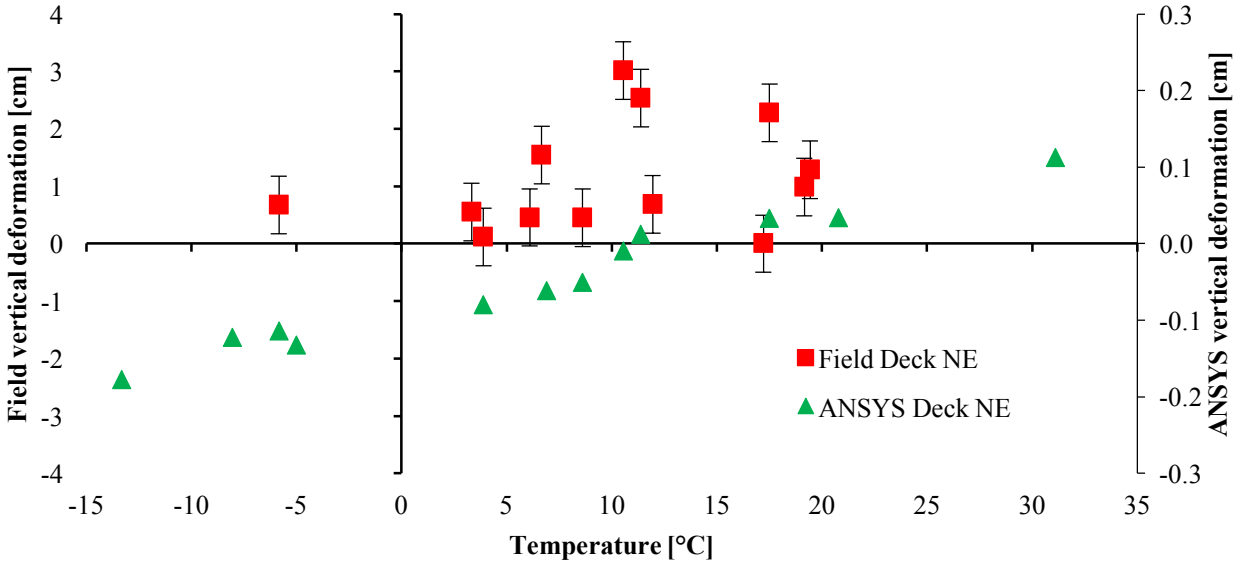

Figure B.8. Bridge over Vinburn Road. Vertical deformation comparison between field measurements and finite element model results for the NE deck. Error bars are +- 0.5 cm instrument accuracy.

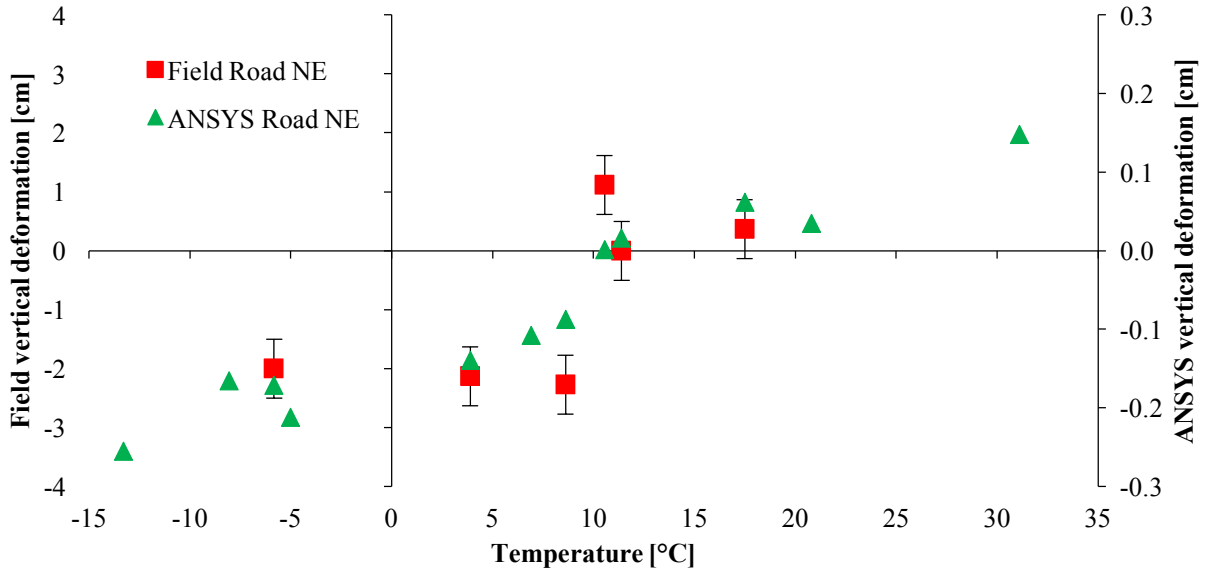

Figure B.9. Bridge over Vinburn Road. Vertical deformation comparison between field measurements and finite element model results for the NE road. Error bars are +- 0.5 cm instrument accuracy.

Appendix C - GRS-IBS monitoring results

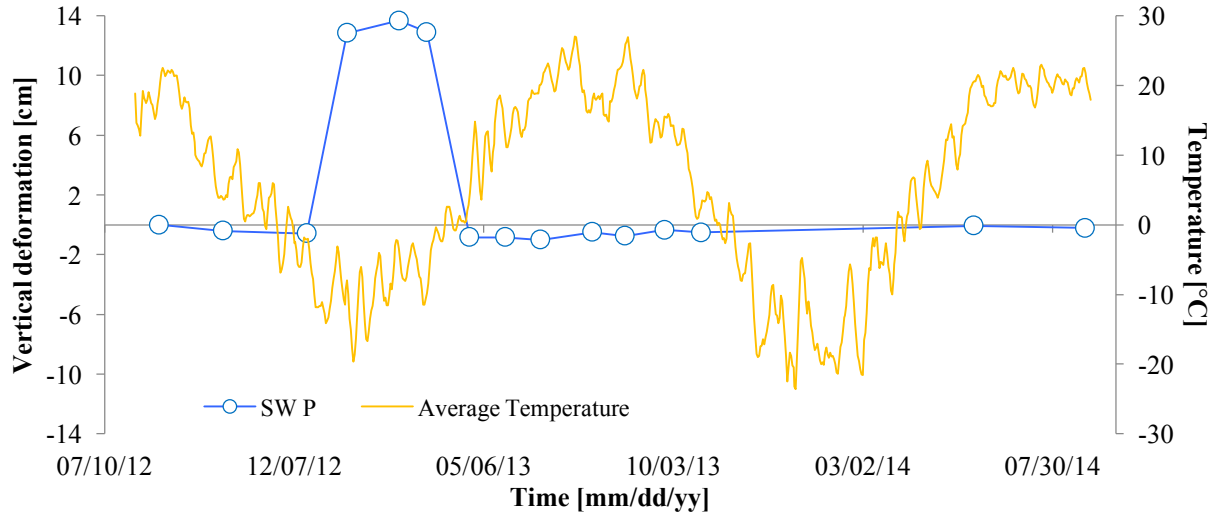

Figure D.1 Relative vertical deformation on the southwest (SW P) settlement plate with respect to the reference point. Positive values correspond to upward movement. The large deformation recorded from January to May of 2013 is considered to be accumulation of ice and/or snow inside the pipe used to reach the settlement plate.

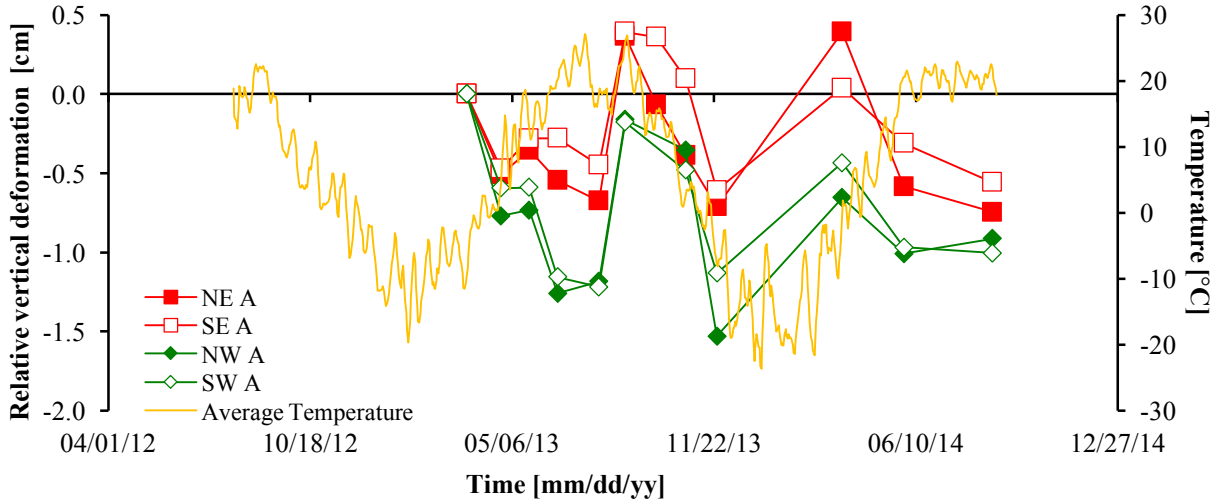

Figure D.2. Relative vertical deformation on top of the abutment walls' corners with respect to the reference point. Negative values correspond to downward movement.

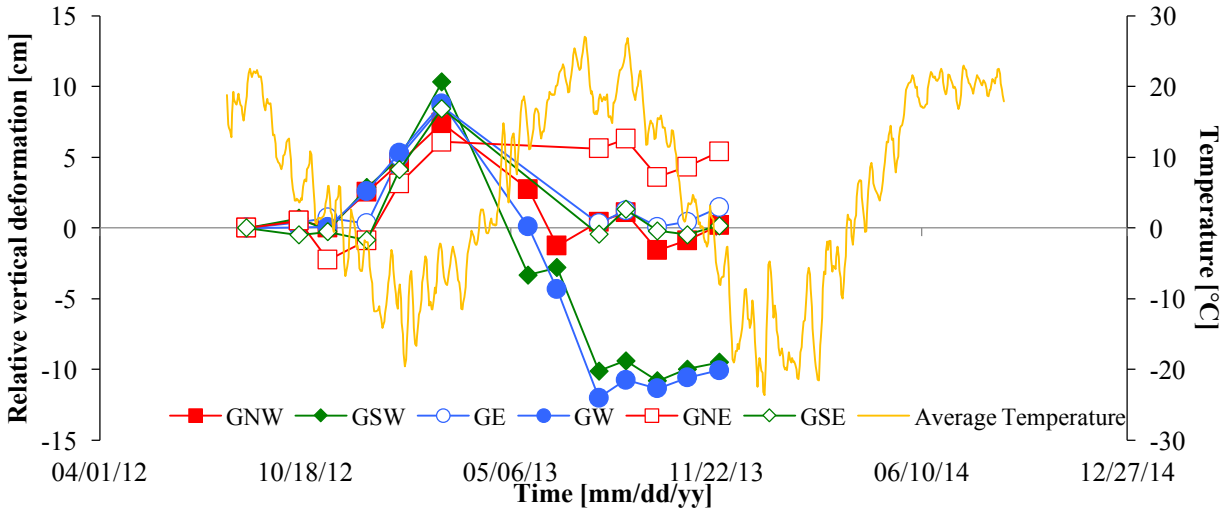

Figure D.3. Relative vertical deformation of surveying points on the creek with respect to the reference point. No data were collected either because of snow cover or because the creek was flooded. Positive values correspond to upward movement.

Appendix D - GRS-IBS numerical modeling results

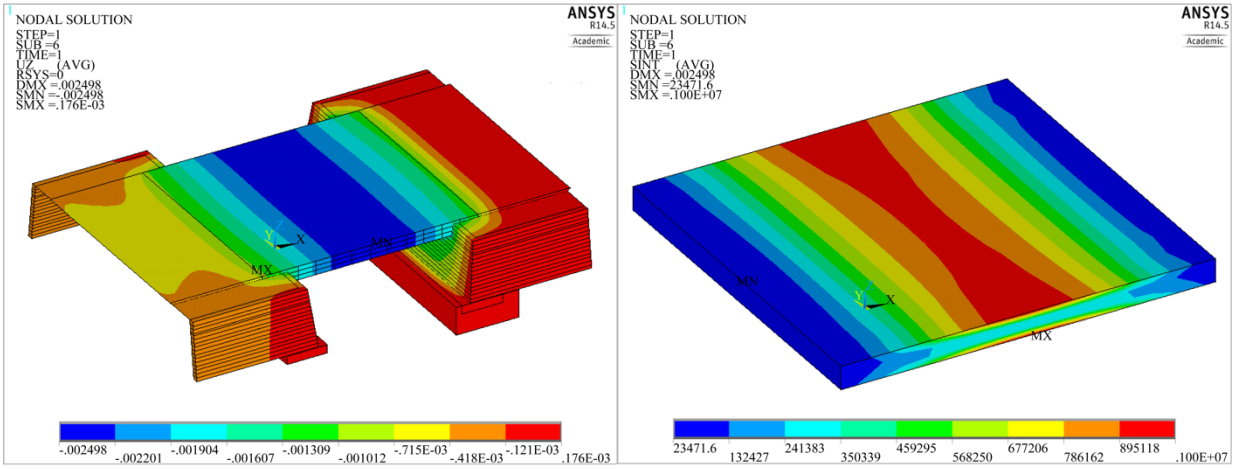

Figure D.1. Vertical deformation (left) and deviatoric stress (right) results for the uniform loading case, in meters and Pascals, respectively.

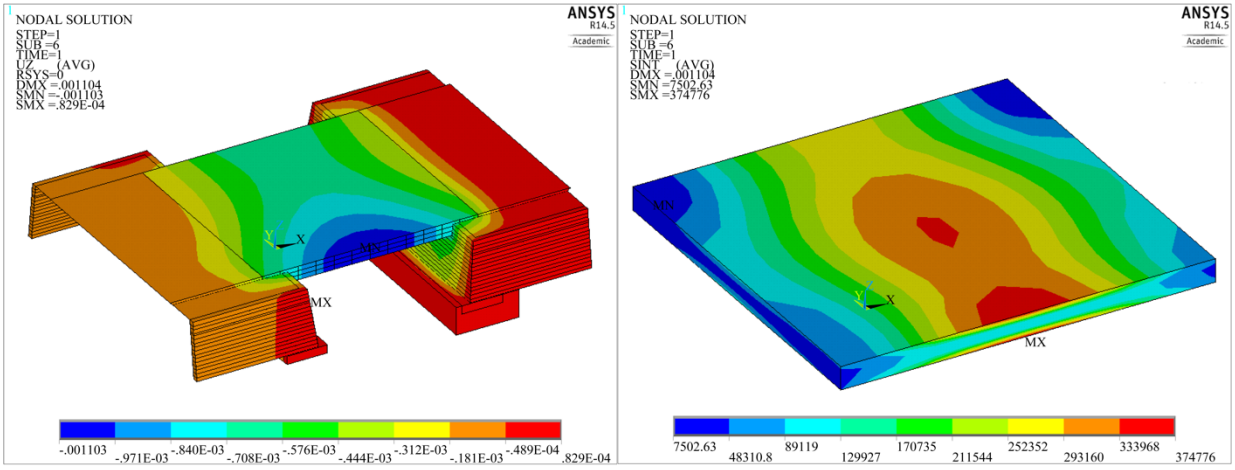

Figure D.2. Vertical deformation (left) and deviatoric stress (right) results for the non-uniform loading case, in meters and Pascals, respectively.

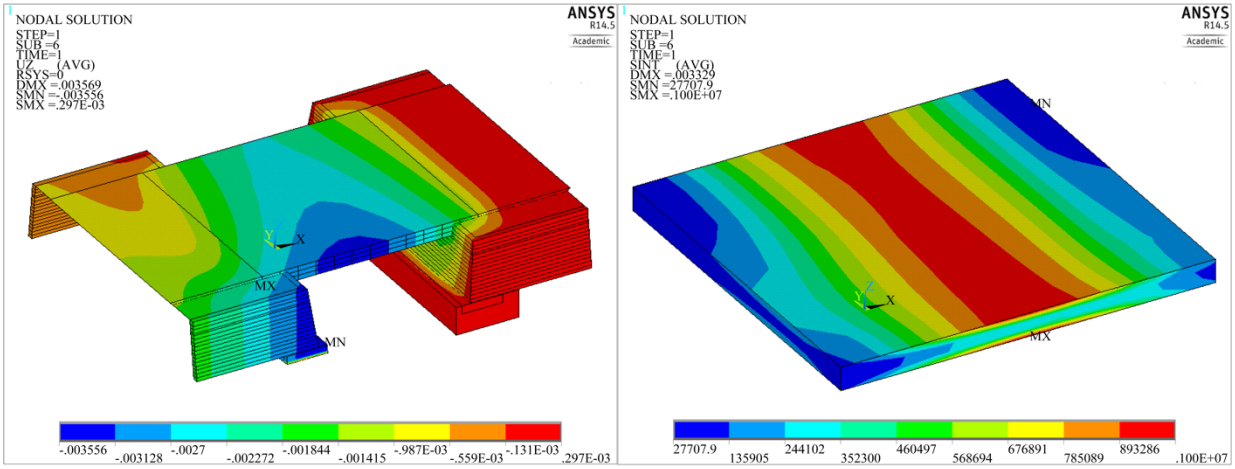

Figure D.3. Vertical deformation (left) and deviatoric stress (right) results for the South-East corner induced settlement loading case, in meters and Pascals, respectively.

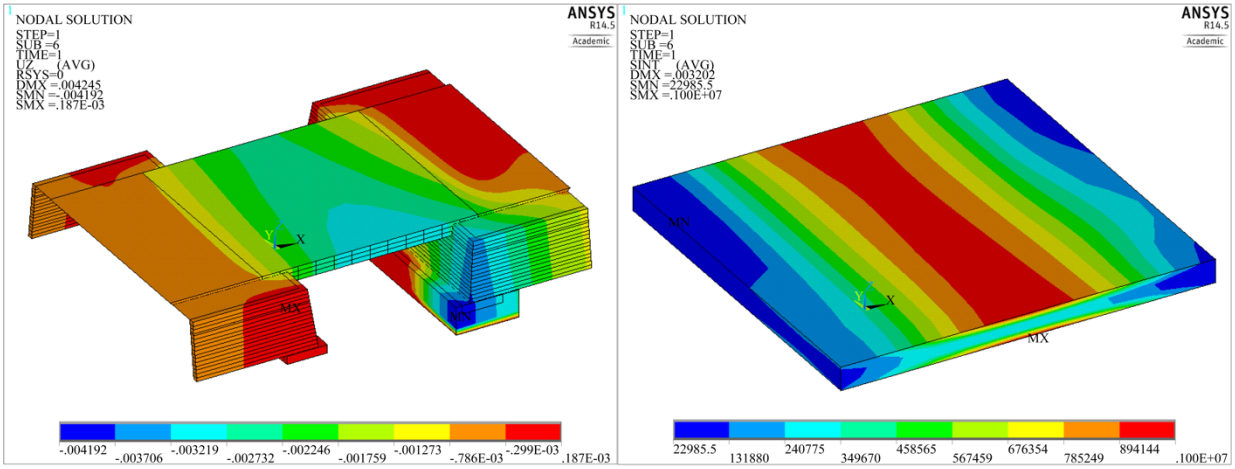

Figure D.4. Vertical deformation (left) and deviatoric stress (right) results for the North-East corner induced settlement loading case, in meters and Pascals, respectively.

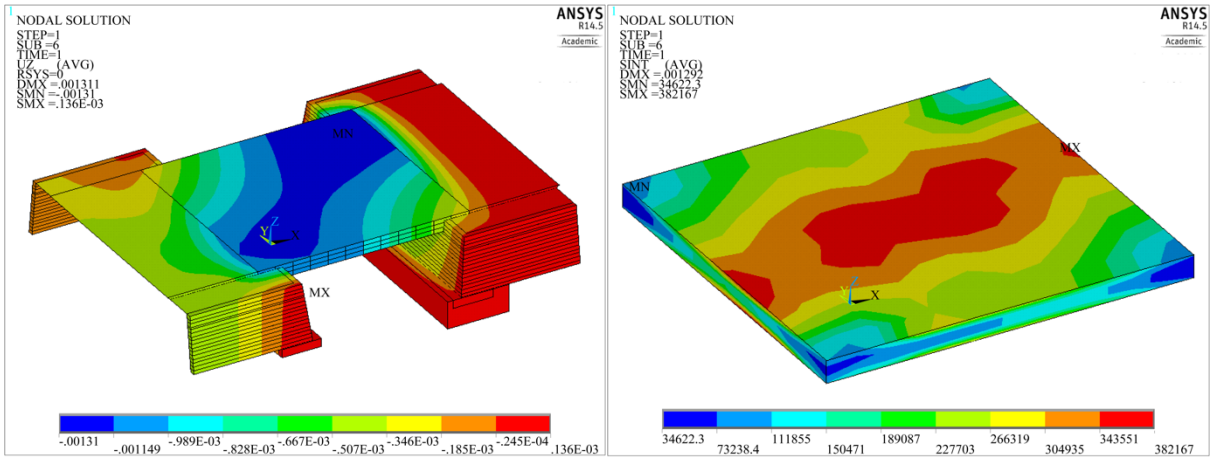

Figure D.5. Vertical deformation (left) and deviatoric stress (right) results for the truck loads on opposing corners, in meters and Pascals, respectively.

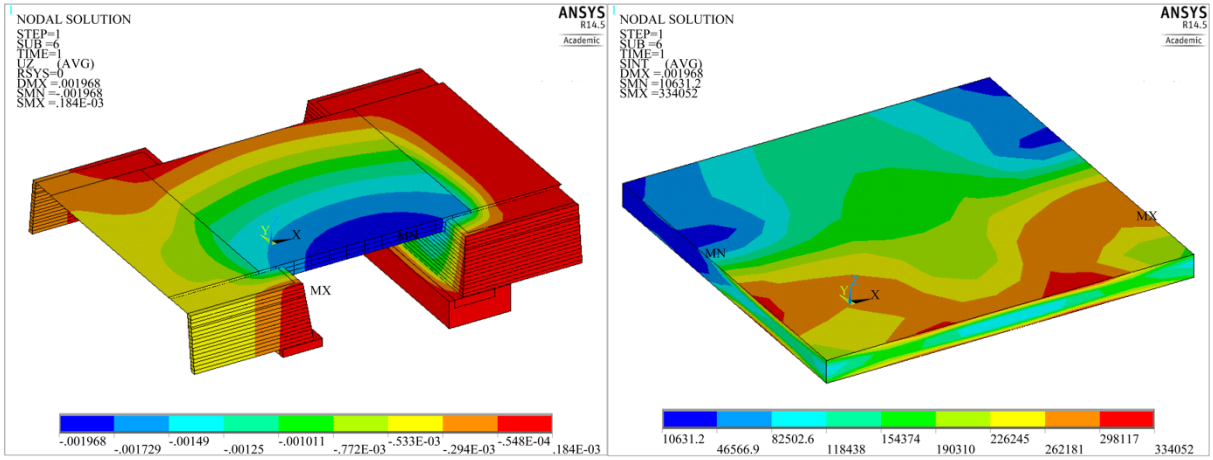

Figure D.6. Vertical deformation (left) and deviatoric stress (right) results for the truck loads on same side, in meters and Pascals, respectively.

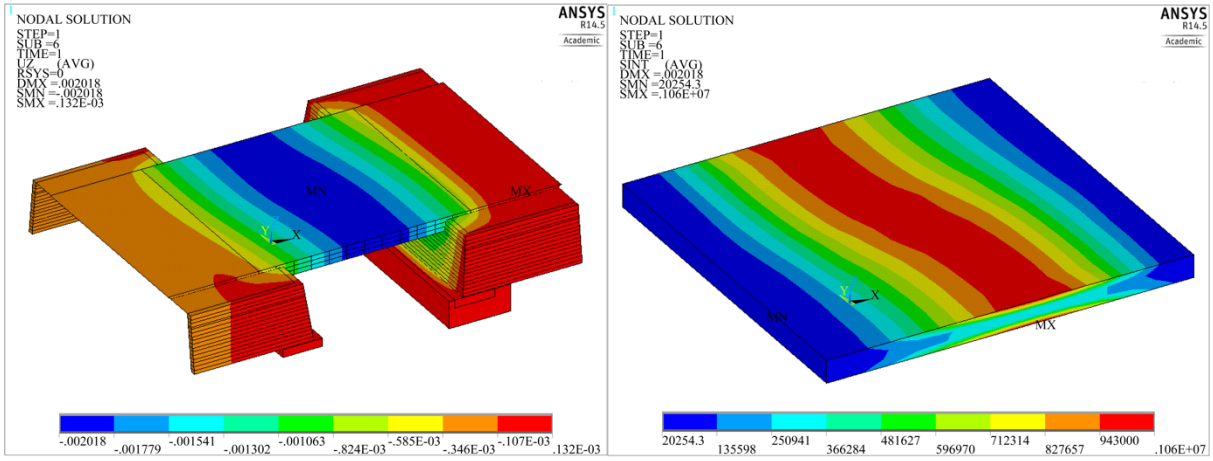

Figure D.7. Vertical deformation (left) and deviatoric stress (right) results for the truck loads close to the center, in meters and Pascals, respectively.